**Universität für Bodenkultur Wien**
University of Natural Resources
and Applied Life Sciences, Vienna

# Establishment of a comprehensive analytical platform for the implementation of advanced process monitoring and control of cell-culture processes

## Dissertation

zur Erlangung des Doktorgrades an der Universität für Bodenkultur Wien

**Department of Biotechnology (DBT)**

Vorstand: Reingard Grabherr, Ao.Univ.Prof. Dipl.-Ing. Dr.rer.nat.

Betreuer: Gerald Striedner, Assoc.Prof. Dipl.-Ing. Dr.rer.nat

Karola Vorauer-Uhl, Ao.Univ.Prof. Dipl.-Ing. Dr.nat.techn

Eingereicht von **Bernhard Sissolak, Dipl.-Ing. Ing**.

Vienna, February 2020

For my father, Dr. Manfred Sissolak

*25.10.1956 †9.05.2018

# Statutory Declaration

I declare that I have authored this thesis independently, that I have not used other than the declared sources/resources, and that I have explicitly marked all material which has been quoted either literally or by content from the used sources.

Vienna, _____ _____

Date Signature

# Eidesstattliche Erklärung

Ich erkläre an Eides statt, dass ich die vorliegende Arbeit selbstständig verfasst, andere als die angegebenen Quellen/Hilfsmittel nicht benutzt, und die den benutzten Quellen wörtlich und inhaltlich entnommenen Stellen als solche kenntlich gemacht habe.

Wien, _____ _____

Datum Unterschrift

# Acknowledgements

I want to express my deepest gratitude to my parents, Daniela and Manfred, who always showed great interest into my work and constantly supported me with my study. Thank you for encouraging me to start my career in the field of biotechnology back then. It is truly sad that my father cannot witness this moment anymore.

Kerstin, you are on my side now for more than one third of my life. Just a big thank you for enduring all the things happened along the way and your endless support in the last four and a half years. Luzia and Frederik, thank you for being the cutest and best excuse for not finalizing my thesis any sooner.

I am especially grateful for having such a great supervisory team, many thanks to Gerald Striedner, Karola Vorauer-Uhl and Wolfgang Sommeregger. Combining the distinct worlds of bioprocessing and analytics would not have been possible without your help.

A big shout out to Gerald Berghammer who made this project and, with it, my PhD possible.

I want also express thanks to all the other people who were substantial involved in making the publications possible. Thanks to Nataša Sarić, Christian Zabik, Nico Lingg, Gabi Lhota, Mark Dürkop and in particular thanks to Magdalena Pappenreiter, Benjamin Bayer and Jakob Wallner for their contributions.

I also want to acknowledge all the other people who worked together with the PATPlant core team and made my life here at BOKU much more joyful. Thank you Sabine Necina, Markus Luchner, Martin Fellner, Florian Bacher, Verena Eder, Roland Alt, Patrick Scheidl, Raphael Große, Pablo Pino-Grace, Daniel Komuczki, Petra Polak, Estella Veigl, Katarina Kljajic, Clemens Kainprecht, and of course, the rest of the working group of Striedner.

# Zusammenfassung

Einer der größten Herausforderungen in der biopharmazeutischen Industrie ist es eine konstante Produktqualität in Zellkulturprozessen zu gewährleisten. Die Zellen werden stark von ihrer Umgebung beeinflusst und selbst kleinste Variationen können zu markanten Qualitätsabweichungen führen. Die Anwendung einer fortgeschrittenen Prozessüberwachung und -regelung kann die Prozessführung flexibler gestalten. Eine solche würde adaptiv auf Veränderungen reagieren und somit die Produktqualität auf einen konstant hohen Level halten. Dafür wird allerdings grundlegendes Prozessverständnis und –wissen über die kritischen Prozessparameter und Produktqualitätsattribute benötigt, welche nur mittels einer geeigneten analytischen Plattform generiert werden können.

Das Ziel dieser Dissertation war es eine solche analytische Plattform für einen Chinese Hamster Ovary (CHO) Zellkulturprozess, welche einen industrierelevanten monoklonalen Antikörper (mAb) produziert, zu etablieren. Dabei wurden Methoden zur Bestimmung von zell- (Zelllyse; zellspezifische Substrate- und Sauerstoffaufnahmerate) und produktrelevanten Eigenschaften (Ladungsverteilung; Mannosylierung und Fucosylierung von mAbs) entwickelt, welche eine zeitnahe und robuste Messung dieser wichtigen Attribute in einem Zellkultur Prozess ermöglichen. Die hier vorliegende Arbeit präsentiert auch deren Anwendung und deren Relevanz, hinsichtlich der Etablierung einer fortgeschrittenen Prozessüberwachung und –regelung, anhand von simulierten als auch realen Prozessen.

# Abstract

Achieving consistently high-quality output in cell-culture processes is a major challenge in biopharmaceutical manufacturing of monoclonal antibodies (mAbs), since the outcome is highly susceptible to environmental factors and input materials. Only with utilization of an advanced process monitoring and control tool the process becomes flexible enough to react to variations and set control actions against it. However, this requires an appropriate analytical platform to generate in-depth process understanding and knowledge about linkage of the critical process parameters (CPPs) and critical quality attributes (CQAs).

This work focuses on the establishment of an appropriate analytical platform for a Chinese hamster ovary (CHO) cell-culture process recombinantly producing industrially relevant mAb. It presents the development of mathematical and analytical methods for accurate and precise determination of cell-related (cell lysis; oxygen-uptake rate; substrate-uptake rate) and product-related attributes (charge variant distribution; glycosylation). Their applicability is exemplified by particular cases, and their importance for advanced process monitoring and control is elucidated.

This thesis presents an analytical perspective on the implementation step and shows that an appropriate analytical platform is the basis for realization of advanced process-monitoring-and-control regimes in cell-culture processes.

# Table of Contents

# 1 Introduction

## 1.1 From Quality by Testing to Advanced Process Monitoring and Control

Recombinantly produced monoclonal antibodies (mAbs) are invaluable for the biopharmaceutical industry. Since the first mAb (Orthoclone OKT3) was approved in 1985 [1], they have become an important factor in the market [2]. Over recent decades, the approval rate of mAbs has increased steadily. Between 2015 and 2018, 53% of all new approvals by the Food and Drug Administration (FDA) or the European Medicine Agency (EMA) in the biopharmaceutical sector were mAb-based products, accounting for around 65% of total sales in this industry [3]. Currently, seven of the top ten best-selling biopharmaceutical products are mAbs. Worldwide sales reached around 100 billion US$ in 2017, and it is estimated that these will grow to $160 billion by 2022. The majority of those products (over 60%) are produced in Chinese hamster ovary (CHO) cells [4].

Almost all currently approved processes in the biopharmaceutical industry are likely to have necessitated extensive product quality testing. This is because manufacturers must comply with strict regulatory requirements and also work according to rigorous, self-imposed guidelines in order to ensure that their products are safe for patients. Hence, the production of biopharmaceuticals is performed in a very conservative way. Processing is fixed, and no flexibility is permitted.

Precious little information is available (or none at all) during the process in terms of cell performance, product-formation and -quality. The bioprocess is usually only monitored using well-established sensors (for instance, pH or dissolved oxygen and temperature). These few process parameters are set to a certain value and are tightly controlled throughout the process. Interestingly, although the process seems to be tightly controlled, outcomes in terms

of product quantity and quality can be highly variable due to complex interactions between cell physiology and the surrounding environment [5]. At the end of the bioprocess, the product is purified, and quality attributes are tested to ensure that the product meets relevant efficacy and safety criteria, and can be released onto the market (Quality by Testing approach).

This approach is unfavourable for innovation and leaves almost no room for process adaptation. Such processes can be regarded as a black box system, where the user has limited knowledge of its mechanism (Figure 1) [5]–[7]. Hence, this results in a rigid process that is unlikely to produce the product of interest in a consistently high quality.

In 2004, the FDA, therefore, launched the process analytical technology (PAT) initiative [8] to push the industry towards implementation of a so-called Quality by Design (QbD) framework.

The idea of achieving consistently high product quality via the QbD approach had already emerged in the 1980s, described by J.M. Juran [9], who proposed that QbD must be an iterative process consisting of three building blocks:

- Quality planning
- Quality control
- Quality improvement.

Through these criteria, existing knowledge is used to plan processes in such a way as to achieve an optimized risk-benefit ratio for the desired product quality (quality planning). Throughout the process, quality is controlled via process analysers (quality control), and information retrieved from these is used to improve the process and reduce expenditure even further (quality improvement).

The FDA’s intention was to enable manufacturers to establish more flexible and agile processes with an enlarged operational space. Process variations can be tolerated to a larger extent since the effect on product quality is known. Due to implementation of sophisticated process analysers, decisions about product releases can be scheduled earlier in the process

chain (Figure 1). Reduction of batch failures, faster product release and reduced costs in the generation of high-quality output are the major advantages of this approach.

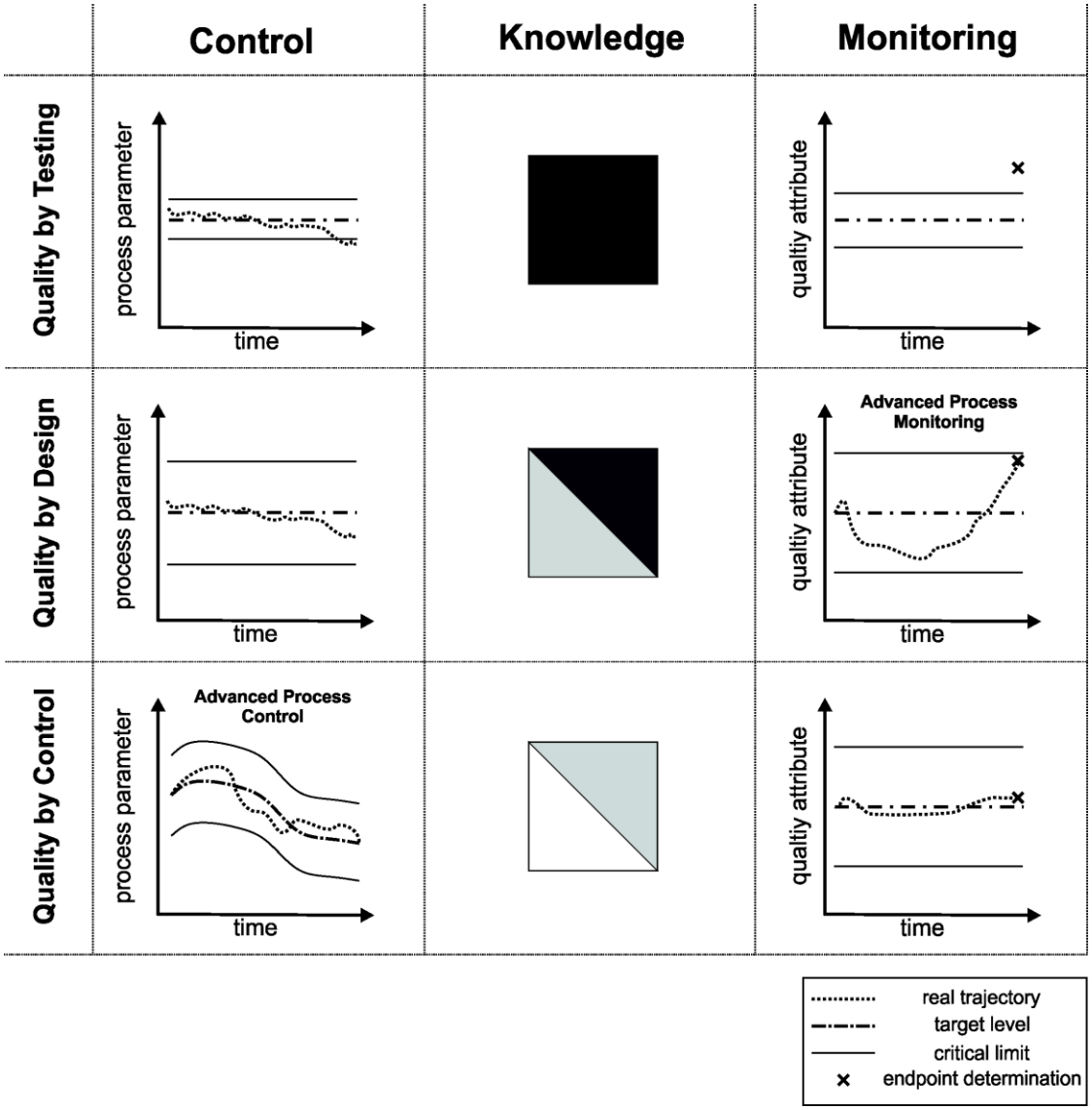


***Figure 1****: A schematic comparison of the three different methodologies (QbT, QbD & QbC), in terms of process control, process knowledge and process monitoring. In QbT, the process is a black box. The underlying mechanism of this process is not yet understood. In QbD, the CPPs and CQAs are identified. The mechanism of this process is partly known. In QbC, the process is well known and the underlying mechanism well understood.*

In principle, QbD is about identifying critical process parameters (CPPs) and critical quality attributes (CQAs), linking them together via black box or grey box models (and, on rare occasions, white box models) for the purpose of implementing an advanced online monitoring tool. In a black box model, limited information about the mechanism is available. Mathematical

description of the connection between input and output variables might not necessarily have a scientific meaning. In grey box models, the link between output and input variables is partly based on sound science. Similarly, in white box models, the link is based on a scientifically valid function.

However, QbD, in particular, does not take the control perspective into account. Due to possible lot-to-lot variations in the raw materials used for cell cultures, consistently high quality output is often not achieved [10]–[12].

The Quality by Control (QbC) approach seeks to fill this gap. In QbC, one of the main challenges is the establishment of advanced process control (APC) regimes [13], [14]. Established process models (for instance, hybrid models [15]) capture the process dynamics and are used to quantitatively forecast the outcome of the system [16]. Feedback loops are installed to ensure that the model is frequently updated. Accordingly, the process can react to input and process variations, and can set control actions against these. Hence, the upstream process becomes more flexible and results in continuously high-quality output (**Figure 1**).

Nowadays, the Quality by Design concept is common knowledge within the biopharmaceutical industry [17]. As of 15 years ago, the regulatory authorities had already started emphasizing and promoting the QbD and PAT approach, with the goal of enhancing innovations in process development in order to reduce manufacturing costs. However, the concept has not yet been fully implemented in many biopharmaceutical companies for various reasons [17], [18]. QbD/QbC implementation is a troublesome task, and the issues that arise generally fall into one of the four categories listed below.

- Variable/parameter identification: describing the impact of CPPs and CQAs alone is not sufficient. It is essential that identified CPPs and CQAs can be monitored and are controllable.
- Process setup: an appropriate experimental setup and sampling plan is required to generate the data required for robust process models for online monitoring and control purposes.

- Data generation: utilization of appropriate analytical methods to determine the dynamics of CQAs and CPPs is necessary. Time-consuming and complex methods can lead to an enormous workload and further costs.
- Process software: in the absence of a sophisticated software solution, capable of controlling, monitoring and running the process in situ, implementation of QbD/QbC is not possible.

Hence, the sought-after paradigm shift from a parameter-controlled process (conventional) to a performance and product quality-controlled process (advanced) is still not achieved.

## 1.2 Implementation of advanced process monitoring and control

Implementation of advanced process monitoring and control requires considerable effort. To establish a control algorithm for the desired product or performance-related variable, a link must first be established to a controllable parameter. Existing knowledge and available literature are usually used to set up a risk analysis to define the appropriate design space [19]. A series of experiments is subsequently performed within this particular design space to capture the response of the product and/or process-related variable to variations in the independent input parameters.

Several methodologies can be used to design the experimental setup. For instance, to describe a two-dimensional space, a full factorial (or Doehlert design) can be used [20], [21]. After conducting all the experiments, the response can be mathematically described. For noise reduction, retrieved data are often pre- and/or post-processed. The process information obtained is then used to establish models and algorithms for prediction and control of the desired target variable.

For a one-dimensional design space, this can easily be performed and results in simple solutions, preferably linear ones like the equation below (Eq. 1).

$$\frac{dX}{dt} = f(P) = k * P \quad (1)$$

The change in measured outcome for desired target variable X over time is a function of controllable parameter P. Parameter k describes the rate of this function. Hence, if k is positive, a higher P results in higher output of X per measure of time. Rates like k comprise the information about a bioprocess. For instance, for cell-culture cultivation, this would be the substrate-uptake rate, the growth rate, the protein production rate and many others.

But a biological process such as Chinese hamster ovary (CHO) cell cultivation can be regarded as a multidimensional system with several layers [22]–[24]. Outcome X is not influenced by controllable parameter P alone. Moreover, variables A and B also affect outcome X, and it becomes even more complex if variable B exhibits a hidden dependency associated with parameter P and variable C (Figure 2). Hence, to describe X as function of B, the dependency of B on P and C must also be known. In this respect, the solution becomes more difficult, and outcome X is now described as per the equation below (Eq. 2).

$$\frac{dX}{dt} = f(A, B, P) = g(P)\, h(A)\, i(B(P, C)) \quad (2)$$

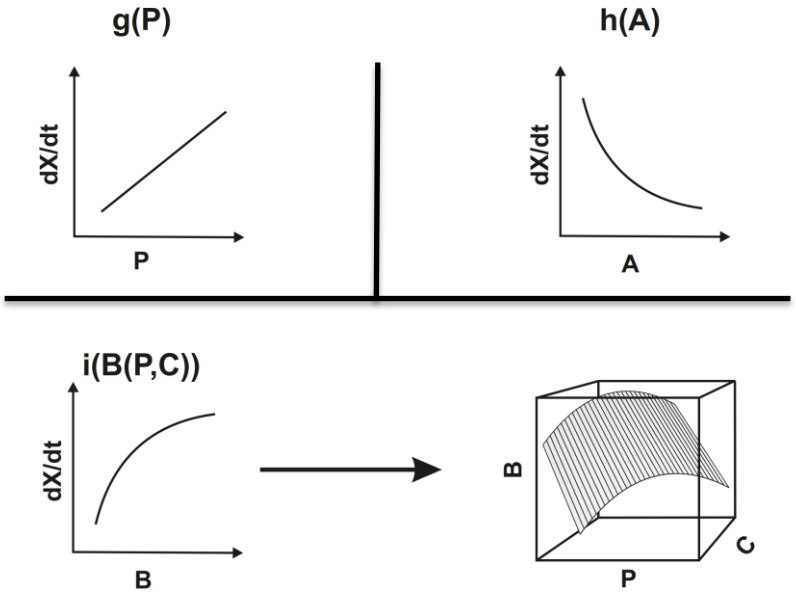


***Figure 2****: Three examples of possible functions influencing outcome X. The upper-left and upper-right examples show the change in X over time as a linear function of P and as a nonlinear dependency on parameter A. Hence, outcome X is directly dependent on parameters P and A. The lower panel exemplifies a typical hidden dependency. It seems that X exhibits a nonlinear dependency on B. In reality, B is a function of parameters P and C.*

Establishing an advanced monitoring and control algorithm for a cell-culture cultivation process which taking the entire metabolism into account is, therefore, hardly feasible [25] because there are only a few adjustable parameters available, and everything must be identified in relation to these. Simplification of the correlation is, therefore, desirable so that what remains, in the best-case scenario, is outcome X expressed as a function of the single controllable parameter P.

## 1.3 Establishing an appropriate analytical platform

For implementation of advanced process monitoring and control in the above-mentioned process, it is particularly important that parameter P and variables A and C are controlled or, if control is not possible, at least monitored. For this purpose, accurate and precise data on these variables are a necessity.

A suitable analytical platform is, therefore, the key requirement for implementation of advanced process monitoring and control. The term “analytical platform” combines all sorts of methods and techniques, which are used to measure, determine, monitor and evaluate certain variables over the time course of a bioprocess. It should provide values for this particularly important variable as accurately and precisely as possible in the shortest time possible.

It is important to understand that every experiment required to capture the desired design space substantially increases the number of analyses. Analysis should, therefore, be fast but also accurate and reliable. If not, it will create a bottleneck, impeding implementation of advanced process monitoring and control in the bioprocess. Determination of the related product species can either be performed directly in the supernatant matrix, or the mAb can be captured and purified prior to analysis. Both strategies have advantages and disadvantages, which need to be thoroughly evaluated, although analyses of the supernatant are always preferable to an *a priori* sample purification step, as is commonly performed with Protein A chromatography. This not only reduces the amount of laborious work but also decreases the risk of an incorrect set of data. *A priori* sample purification can induce unwanted effects and

eventually generate misleading data during the process. For instance, it has been reported that IgG associated with chromatin elements tends, under elution conditions, to aggregate and cross-link to a larger extent with host-cell proteins [26]. In another study, it was shown that oxidation of methionine residues can induce a conformation change and thereby decreases the affinity with Protein A, resulting in loss of IgG [27].

However, the surrounding environment of the analyte and potential disturbing matrix effects on analytical results also need to be considered during method development. In mammalian fed-batch cultivation, the matrix changes throughout the entire process. Obviously, a sample taken on the day of harvesting will contain significantly more impurities (cell debris, antibody fragments and aggregates, host-cell protein, DNA, etc.) than a sample from the day of inoculation.

The analytical platform must also be able to provide in-depth information about the dynamics of the process. In principle, the above-mentioned rate *k* represents the process knowledge. During process development, it is, therefore, of particular importance to retrieve such rates as accurately and precisely as possible. Several mathematical solutions are available to compute these rates. Due to its simplicity, simple stepwise integral estimation is often the method of choice [28]–[31], but more complex algorithms, such as the Gaußian distribution or cubic smoothing spline functions, are better at coping with noise [32]–[35].

Capturing process dynamics increases the analytical workload even more, since the trajectory of the parameter over the time course of the process must be described. In this regard, more samples are needed, and more analyses must be performed. Hence, it is invaluable to design and establish the analytical platform in accordance with the implementation purpose. It is important to create a balance between the information content needed and the resulting analytical effort. Accordingly, the analytical platform represents the basis for implementation of advanced process monitoring and control.

## 1.4 Characterization of cell-related attributes

### 1.4.1 Cell lysis quantification and host-cell proteins

Cell death can occur passively (necrosis) or can be programmed (apoptosis and autophagy) and is mostly caused due to nutrient deprivation, external forces or accumulation of toxic metabolites in the cell environment [36]. Via necrosis, the inner content of a cell is directly released into the environment. In programmed cell death, cell compartments or apoptotic bodies remain intact until an external force breaks them apart. Accordingly, dead as well as living cells can undergo lysis, but the main fraction of lysed cells derives from the living population [37].

Cell lysis is always accompanied by release into the supernatant of cell contents such as host-cell proteins (HCPs) and deoxyribonucleic acid (DNA). HCP exhibits the largest contribution to this (up to 70wt%). However, the protein amount per cell can be wide-ranging and can be dependent on the size of the cell. Between 200 and 500 pg/cell have been reported for mammalian cell lines [23], [38]–[40]. Although lysed cells are usually in a minority compared to the total cell count, they are the major source of impurities.

HCP is considered to be a critical quality attribute and must be below a certain threshold in the final drug formulation (<100 ppm) [41]. Hence, the subsequent downstream operation units must be effective in clearance of this component. However, the wide-ranging characteristics of HCPs make purification steps more challenging, since certain types of HCP do not differ significantly from the product in terms of size, isoelectric point (pI) and hydrophobicity [42]. A low amount of HCP in the supernatant is, therefore, generally preferable to facilitate subsequent downstream processing.

State-of-the-art cell lysis markers are DNA or the activity of lactate dehydrogenase (LDH) [43]. Others are rarely used as the measurement of cell debris or viscosity change is more common in microbiological fermentation processes [44], [45]. Use of residual protein content (RPC) as a lysis marker has recently been reported [46].

However, disregarding cell lysis falsifies process- and performance-related attributes [37], [46], [47]. For example, the term “viability” is typically used as a process performance indicator and as a harvest criterion, and is defined as follows (Eq. 3):

$$Via_{app} = \frac{VCC}{TCC} \tag{3}$$

where apparent viability ($Via_{app}$) is described as the ratio of viable cell concentration (VCC) to the total cell concentration (TCC). TCC is the sum of viable and dead cells. If cell lysis is considered, viability should be defined as follows (Eq. 4):

$$Via = \frac{VCC}{TCC+LCC} \tag{4}$$

where *LCC* describes the lysed cell concentration. Since lysed cells can derive from a living as well as a dead cell, LCC can be described as a function of TCC (Eq. 5); hence,

$$\frac{dLCC}{dt} = k\,TCC \tag{5}$$

*k* represents the cell lysis rate, the percentage of cells which undergo lysis per hour in relation to the total number of cells. The more and the longer cells are available in the system, the more lysed cells will emerge.

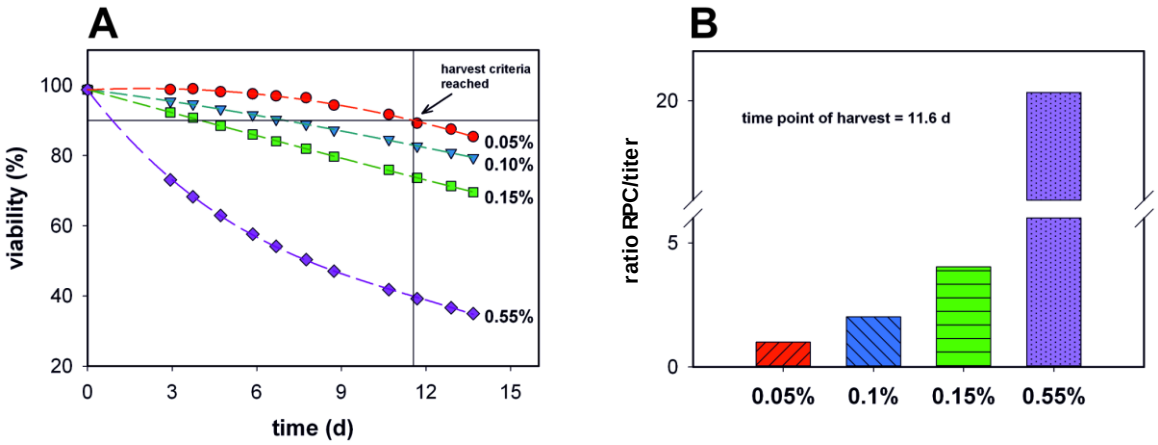


***Figure 3**: (A) depicts changes in the viability pattern at different cell lysis rates (from 0.05% up to 0.55%). (B) depicts the ratio of RPC to titer at the harvest time point at different cell lysis rates. Experimental data indicate a 0.05%/h lysis rate in our study. The entire 0.05% dataset depicts real experimental data. Accordingly, for 0.10%, 0.15% and 0.55%, the values of residual protein content (RPC) were recalculated (350 pg RPC per lysed cell).*

In our study, a constant cell lysis rate of 0.05%/h was calculated [46]. If this rate were to increase, the viability trend would become significantly different (see Figure 3A).

Disregarding cell lysis not only affects the viability pattern but is also significant in terms of the outcome of the process. Obviously, for the same example at the same harvest time point, the impurity level will increase the higher the cell lysis rate is (Figure 3B). Hence, utilization of $Via_{app}$ as a harvest criterion erroneously suggests a similarity between the processes where there is none.

### 1.4.2 Oxygen-uptake rate as a process monitoring tool

Most glucose is usually converted to $CO_2$ during the citric acid cycle under the premise of building nicotinamide adenine dinucleotide (NADH). NADH is further recycled/oxidized in mitochondria via oxidative phosphorylation under the premise of building energy for the cells, adenosine triphosphate (ATP). Oxygen is one of the key substrates, and utilization of this boosts energy production [48]. One important performance parameter for mammalian cell-culture cultivation is, therefore, the oxygen-uptake rate (OUR), given in mol per cell per day. OUR provides in-depth information on the bioprocess. Several studies have shown that OUR can be linked to the biomass in cultures [49], [50] or to glucose consumption [51]. A recently published study reports that in combination with a permittivity probe, even metabolic transitions are detectable [52].

Three different methods are commonly used to determine OUR: the dynamic technique, global mass balance and stationary liquid mass balance. Since the dynamic method uses oxygen pulses to measure specific oxygen-uptake rate ($qO_2$), it is impracticable for use in an advanced process-monitoring-and-control regime. The physical-chemical perturbations introduced can lead to cell stress and distortion of the process performance [49], [53].

The global mass balance is a non-intrusive method. Here, in a steady state, OUR is defined as follows (Eq. 6):

$$OUR = uf_{in}\ O_{2,in}\% - uf_{out}\ O_{2,out}\% \qquad (6)$$

where $uf_{in}$ and $uf_{out}$ describe the flow rate, and $O_{2,in}\%$ and $O_{2,out}\%$ describe the oxygen concentration into and out of the system. For this mass balance equation, precise and

accurate measurements of the off-gas are necessary. Nevertheless, for large-scale cultivations or high cell-density cultures (as is existent in a perfusion system), the accuracy of off-gas analysers is not the limiting factor anymore [48].

The stationary liquid mass balance technique utilizes the fact that oxygen must be transferred from the gas phase to the liquid phase to guarantee optimal process performance. This is described via the oxygen transfer rate (OTR) and is defined as follows (Eq. 7):

$$OTR = k_L a\ (c^* - c) \tag{7}$$

where $c$ is the oxygen concentration in the supernatant, and $c^*$ is the maximum oxygen saturation. The term $k_L a$ describes the mass transfer rate of this phase transition and is dependent on several parameters, for instance, the type of stirrer, stirrer speed, air-flow rate, bubble size and coalescence, media viscosity, media composition and the partial pressure of oxygen. Methodologies for the determination of $k_L a$ for bioreactors have been reviewed elsewhere [54]. Furthermore, changes in dissolved oxygen concentration (DO) are dependent on the amount of oxygen consumed by cells and transferred into the liquid phase (Eq. 8); hence,

$$\frac{dDO}{dt} = OTR - OUR \tag{8}$$

DO is usually kept constant throughout the cell cultivation process. Accordingly, dDO/dt equals zero, and the equation is simplified to OTR equals OUR. In this case, OUR is driven by the concentration gradient and the term $k_L a$. Since DO is routinely measured and the oxygen concentration is known, the concentration gradient can be calculated. Due to the changing environment over the time course of the fed-batch process, oxygen mass transfer also varies. The stationary liquid mass transfer technique, therefore, requires knowledge of the bioreactor geometry and desired operational space.

OUR represents an efficient, simple and easy-to-use process monitoring tool, which has already been shown to be usable for an advanced process control regime [49], [51]. Nevertheless, it does not represent a state-of-the-art method for a mammalian cell-culture

process. Under the expectations of continuous improvements in process control, OUR determination via dynamic $k_La$ should be favoured over alternative approaches.

## 1.5 Characterization of product-related attributes

### 1.5.1 Heterogeneity of monoclonal antibodies

The immunoglobulin G (IgG) isotype is the most commonly produced monoclonal antibody in the biopharmaceutical industry. It is a dimer linked via a disulphide bridge bond, and it consists of two light- and two heavy-chain subunits. IgG is divided into a constant region and a variable region. The antigen-binding site exhibits complementary determining regions (CDRs) present in the variable regions and is highly specified for a certain type of antigen. The constant region is highly conserved and mediates unique effector functions, like antibody-dependent cellular cytotoxicity (ADCC) or complement-dependent cytotoxicity (CDC). IgG is a large (150 kDA) complex molecule. To achieve desired functionality, IgG has to be precisely assembled by the cell. During the assembly process, the protein has to undergo a vast number of modifications, which all contribute to the overall number of variations and the heterogeneity of the product. On the one hand, they are essential to the product characteristics of relevant therapeutic applications, but on the other hand, such modifications can occasionally also have unwanted impacts on product quality attributes and can negatively affect efficacy and safety. Thus, any alteration in the machinery of modifications which does not comply with set requirements must be primarily considered as a potentially hazardous change in product characteristics [55], [56].

These modifications can be subdivided into the following types: co-translational modifications (CTMs), post-translational modifications (PTMs) and chemical modifications (CMs). In general, CTMs take place when the polypeptide chain is released into the endoplasmatic reticulum (ER), and such CTMs include initial folding of the heavy and light chains, attachment of the high-mannose oligosaccharides (N-linked glycosylation) and any

other modifications occurring during synthesis [57]. PTMs are closely related to the Golgi apparatus. Glycosylation processing, O-linked glycosylation and proteolytic cleavage are typical PTMs [58]. CMs can be intra- as well as extracellular and may not be related to any enzymatic process. Any modification which falls into the category of protein aging should be considered as a CM, for example, glycation, cyclization of glutamine to pyroglutamic acid at the N-terminal sequence, deamidation of asparagine and glutamine residues or the oxidation of exposed methionine residues [56].

During production, the protein undergoes numerous modifications. Thus, the product will exhibit inherent natural heterogeneity. Hence, setting up control algorithms to maintain consistent product quality throughput the process is a difficult and sophisticated challenge. Correct assessment of the product's quality and dynamics is necessary in order to establish such process control models.

### 1.5.2 Charge variants of IgG

IgG consists of several acidic, basic and neutral amino acids. Due to the tertiary and quaternary structure of the protein, its surface exhibits several charged patches (Figure 4). The electrostatic appearance of the entire protein in a solution is based on the sum of the patches (the net surface charge). For instance, if the protein appears neutral, the sum of all the patches is also neutral, and this is called the isoelectric point of a protein (pI). Electrostatic characteristics depend on the amino acid sequence, the tertiary and quaternary structure of the protein and any modification that changes the structural conformity of the protein.

The charge variant patterns of IgG are divided into the main, acidic and basic species. In theory, the main fraction is defined as the correctly processed molecule, and this normally appears as the peak with the largest area [59]. It exhibits, for instance, a correct glycosylation pattern, complete C-terminal lysine clipping and no protein-aging effects (such as deamidation or glycation etc.). In reality, the main fraction will still exhibit different modifications which are not in accordance with the theoretical classification [60]. However, the natural heterogeneity

that occurs during a bioprocess results in a distinct charge distribution pattern [61] – the unique fingerprint of the respective protein.

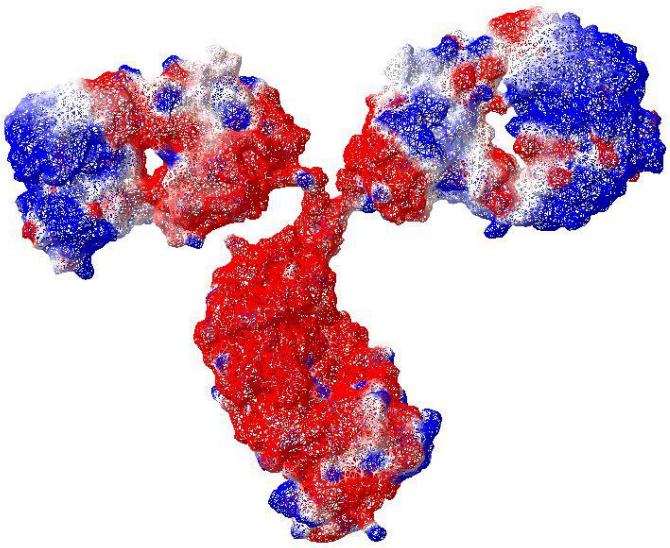

***Figure 4****: Electrostatic potential of IgG in water at a pH of 7 and at 20°C. Surfaces with a red appearance represent acidic patches; blue indicates basic; and white indicates neutral.*

Determination of charge variants is usually done via ion exchange chromatography (IEX), (imaged) capillary isoelectric focusing (iCIEF) or isoelectric focusing gel electrophoresis (IEF) [61], [62]. However, IEX appears to be the gold standard [59]–[63], with separation of individual charge variants commonly achieved by salt gradients. Alternatively, pH gradients would be advantageous due to the improved resolution characteristics and their applicability for a variety of mAbs [64], [65]. We were even able to demonstrate that for application of IEX with a pH gradient, no *a priori* purification is needed, so direct injection of a crude supernatant is possible [66].

In recent decades, charge heterogeneity of IgG has become a more important research objective in antibody drug development. The possibility of capturing certain protein modifications or the investigation of single variants and their role in the product quality attributes of IgG have been part of several research projects. Still, it remains an open question whether charge heterogeneity is as important as other quality attributes, and this is due to two reasons [60], [61], [67]–[69]. Firstly, evident modifications are not all critical [60], [68] or considered to be as not critical for this particular protein. For instance, glycation (a non-

enzymatic reaction in which a reactive sugar binds to a peptide rest) is usually grouped in the category of less-critical modifications [59], [70]. However, the criticalness of glycation depends on how accessible the amino acid sites are and where they are located. Moreover, glycation tends to build advanced glycated end products (AGEs) and is likely to enhance aggregation behaviour; both characteristics are grouped as critical quality attributes [71].

Secondly, the fact that there is a nicely separated peak in an IEX chromatogram does not, in itself, imply that it consists of an IgG species with only a single modification [60], [72]. Accordingly, there is a lack of techniques that can efficiently separate large quantities of single charged species in order to test their immunogenicity. This results in an increased likelihood of false assumptions being made about the criticality of single modifications [72]. A recent example of this is the C-terminal lysine clipping of IgG, which was considered to be a non-critical modification [59]. Nevertheless, a recent study reported that complete C-terminal lysine clipping, in fact, results in maximal complement activation and increased cytotoxicity potential [73], and the researchers claimed that previous studies actually had an issue with separating the single species correctly.

However, charge heterogeneity is a promising fingerprint technique for process monitoring purposes and is a suitable tool for the implementation of an advanced process-monitoring-and-control regime. Any variation in the charge distribution pattern can expose a performance-related issue and might even hint at an undesirable modification. Detecting these early in the process chain helps with identification of possible process implications, enabling an appropriate and timely response to be made.

### 1.5.3 Galactosylation and fucosylation of IgG

Glycosylation is a complex but variable mechanism, which mainly occurs within two compartments of the cell (the Golgi apparatus and endoplasmic reticulum), and it is managed by glycosyltransferases and glycosyl hydrolases. This process undergoes several metabolic and enzymatic reactions. All of these are dependent on environmental conditions and/or co-factors. Since differences in the glycan patterns affect immunogenicity, serum half-life and

safety, the glycosylation pattern of IgG is indisputably one of the most important product quality criteria. The impact of glycan structure variations on the structure, function, pharmacokinetics and pharmacodynamics of the protein has already been extensively reviewed elsewhere [74]–[76]. Basically, each important therapeutic IgG currently sold on the biopharmaceutical market is N-glycosylated, and the glycan structure forms a biantennary assembly [77].

This structure can be found in a conserved asparagine residue (Asn 297) in the CH2 domain of the Fc region. In a complex and non-sialylated glycan type (no sialic acid residue), the carbohydrate galactose remains as the terminal sugar. The attachment of galactose to the glycan structure happens in the Golgi apparatus and is mediated by the galactosyl transferase [77]. Three different IgG moieties can be existent during a production process, a di-, mono- or non-galactosylated IgG (G2, G1 and G0 type, respectively).

The galactosylation of Fc-N glycans is important for regulation of antibody effector functions (increased potential to induce CDC) [77], [78]. Interestingly, most of the Fc-N glycans in serum from healthy human subjects are galactose-terminated (around 50%) [79]. In patients with autoimmune disorders such as rheumatoid arthritis, an aberrant proportion of glycovariants is often shifted towards non-galactosylated moieties [80], [81].

However, galactosylation is influenced by various media components, such as manganese, uridine, galactose and ammonia. Ammonia, for instance, is a by-product generated during the cultivation process. It shifts the internal pH towards alkaline conditions, which results in a decrease of galactosyl transferase enzymatic activity [82]. Process parameters such as the culture’s pH and dissolved oxygen are also suspected to impact on the galactosylation level [83].

The core fucose content (fucose bound to the innermost N-acetylglucosamine of the glycan structure) is another important attribute. In contrast to galactosylation, the more that IgG antibodies have no fucose bound to the core of the glycan structure (afucosilated), the better. The presence of core fucose leads to steric hindrance, which significantly affects binding to the FcγRIII receptor and, in addition, ADCC activity [84].

According to the published literature, few components and parameters affect the enzymatic activity of fucosyltransferase or reduce the enzyme substrate guanosine triphosphate (GTP). For instance, substituting fucose with an analogue such as 2F-PerAcFuc in the cell-culture media has been found to lead to a significantly reduced level without increasing other unwanted glycan species [82]. Osmolality has been found to have a substantial influence on the magnitude of fucosylation. This is independent of the scale used and supplementing compounds, and is attributed to reduced gene expression of the involved enzymes at a low osmolality [85]. In another recently published study, soluble $CO_2$ was found to affect afucosylation [86], which is mainly attributed to the fact that it reduced the cell's internal pH.

However, at first sight, it seems that controlling and maintaining the right glycosylation pattern of mAbs is easily feasible, and much is known about process parameters affecting the glycosylation pattern. Still, the right analytical methods and process models must be put in place, and this remains a challenge [87].

Mass spectrometry is mainly used for the determination of these glycan structures. Multiplexing and high-throughput techniques are available, which are especially useful for screening purposes [88] but require considerable expertise and/or a lot of labour. Lectin-based microarrays could, therefore, be a promising alternative if the glycan structure of the reference protein is basically known [89]. In two recently published studies, the well-established biolayer interferometry platform (BLI) was utilized as a lectin-based array for determination of the sialyation [90], fucosylation and galactosylation content [91]. Due to the microplate devices, the BLI facilitates analysis of many samples in parallel, determining a large variety of glycan moieties. The ranking-based outcome is sufficient for assessing the glycan deviations/divergences and the impact on process variations. Such a lectin-based method reduces the workload, enables automation and is cost efficient. In addition, data allocation is simpler compared to MS techniques and, therefore, of particular interest for the implementation of advanced process monitoring and control.

# 2 Objectives

The main objective of this thesis was to establish an appropriate analytical platform for the implementation of advanced process monitoring and control in a mammalian fed-batch process. This objective was further divided into three major working packages as follows:

1) Establishing a cell-culture cultivation process

   The focus was on single-cell cloning, media adaptation and design of the experimental setup. This was performed for two cell lines, each producing a different industrially relevant monoclonal antibody. Test runs were performed in a shake flask, and the process was eventually scaled up to a 15 L reactor.

2) Establishing appropriate analytical methods for capturing process dynamics

   In this phase, a broad analytical platform was established and the important parameters identified. For this purpose, analytical methods were developed which were able to provide in-depth information content but with a reduced analytical workload.

3) Evaluation of the dataset and generating process models

   In this package, analytical values were set in the context of actual bioprocess characteristics in order to generate in-depth process knowledge. In this way, the measured analytes were linked to one or more process parameters, preferably via linear models and preferably to parameters that were actually controllable.

# 3 Results and Discussion

## 3.1 Publications

Along with this thesis, one mini-review and five original research papers have been published. Whereas the mini-review (Publication #1) explained the theoretical nature of advanced process control of mammalian cell cultures, the original research article presented methodologies and approaches for retrieving key features of the bioprocess and exemplified their applicability in simulated as well as real cases (Publications #2–#6). Below, each publication is briefly explained, and the most important findings are highlighted.

*Publication #1:*

W. Sommeregger, **B. Sissolak**, K. Kandra, M. von Stosch, M. Mayer, and G. Striedner, “Quality by control: Towards model predictive control of mammalian cell culture bioprocesses,” *Biotechnol. J.*, p. 1600546, 2017.

*Publication #2:*

B. Bayer, **B. Sissolak**, M. Duerkop, M. von Stosch, and G. Striedner, “The shortcomings of accurate rate estimations in cultivation processes and a solution for precise and robust process modeling,” *Bioprocess Biosyst. Eng.*, 2019. https://doi.org/10.1007/s00449-019-02214-6

*Publication #3:*

M. Pappenreiter, **B. Sissolak**, and W. Sommeregger, “Oxygen Uptake Rate Soft-Sensing via Dynamic k L a Computation: Cell Volume and Metabolic Transition Prediction in Mammalian Bioprocesses,” *Front. Bioeng. Biotechnol.,* vol. 7, pp. 1–16, 2019.

*Publication #4:*

**B. Sissolak**, C. Zabik, N. Saric, W. Sommeregger, K. Vorauer-Uhl, and G. Striedner,

"Application of the Bradford Assay for Cell Lysis Quantification: Residual Protein Content in Cell Culture Supernatants," *Biotechnol. J.*, vol. 14, no. 7, 2019.

*Publication #5:*

**B. Sissolak**, N. Lingg, W. Sommeregger, G. Striedner, and K. Vorauer-Uhl, "Impact of mammalian cell culture conditions on monoclonal antibody charge heterogeneity: an accessory monitoring tool for process development," *J. Ind. Microbiol. Biotechnol.*, vol. 46, no. 8, pp. 1167–1178, 2019.

*Publication #6:*

J. Wallner, B. Sissolak, W. Sommeregger, N. Lingg, G. Striedner, and K. Vorauer-Uhl, "Lectin bio-layer interferometry for assessing product quality of Fc- glycosylated immunoglobulin G," *Biotechnol. Prog.*, vol. 35, no. 5, pp. 1–9, 2019.

## 3.2 Towards Quality by Control

The terms QbD and PAT imply development of more flexible processes where CPPs are identified and the impact on CQAs is described. In this respect, publication #1 goes one step further and illuminates QbD and PAT from a control engineering perspective. This mini-review proposes a roadmap (Figure 5) identifying key methodologies for implementation of APC in a mammalian cell-culture fed-batch process.

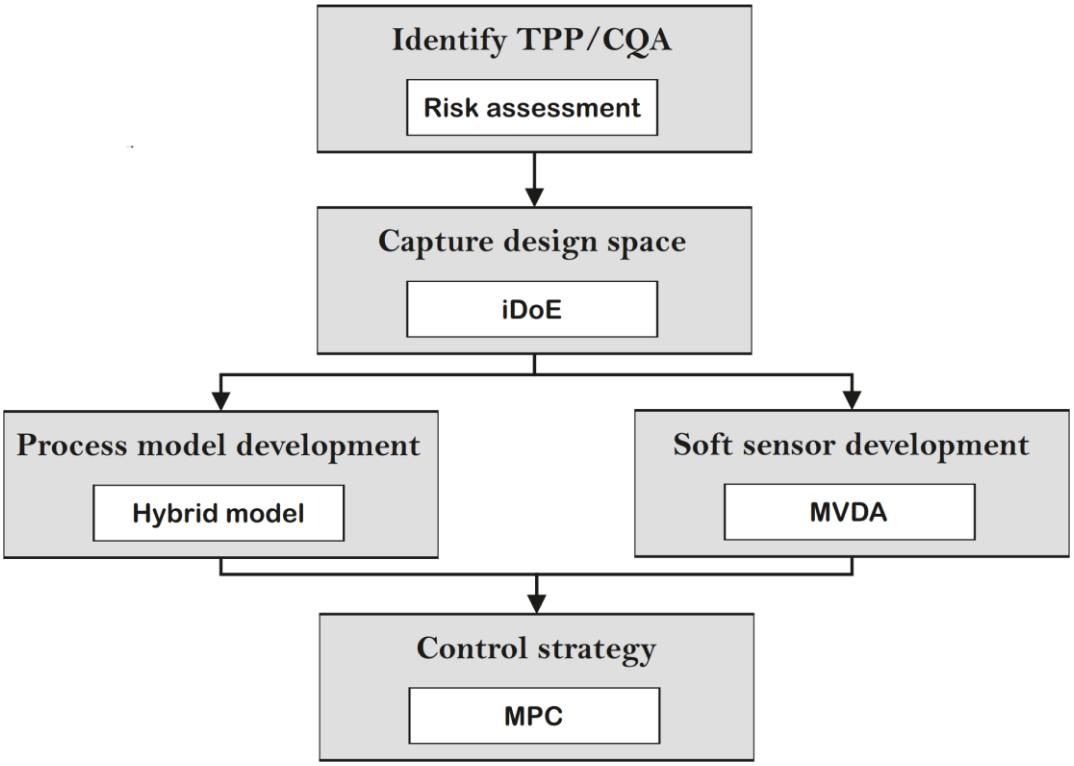


***Figure 5**: Proposed roadmap for implementation of quality by design and control in the mammalian bioprocess. (Taken from reference [13].)*

A solid APC regime can react to input variations, predict the future outcome and set control actions in order to maintain consistently high-quality output. Quality is now not only built in by design but is also entirely controlled throughput the process (Quality by Control; QbC). For this purpose, process models and soft sensors need to be developed which must be accompanied by a sophisticated and appropriate analytical platform that returns key figures as accurately and precisely as possible.

## 3.3 Utilization of a cubic smoothing spline function for rate estimations

Growth, product and substrate rates are particularly important key figures for gaining process understanding and for modelling. Rates are retrieved via the following mass balance equation (Eq. 9):

$$\frac{d(I_{S,X,P,M}V)}{dt} = qI_{S,X,P,M}\ xV + \ u_f I_{S,X,P,M} \quad (9)$$

where *I* stands for the respective substance (substrate (S), biomass (X), product (P) or metabolite (M)); *qI* stands for a cell-specific consumption or production rate; *x* stands for the biomass concentration; *V* stands for the reactor volume; and $u_f$ stands for the feeding rate. According to Eq. 9, the change in substrate (*S*), biomass (*X*), titer (*P*) or metabolite (*M*) in a bioreactor is dependent on consumption ($q\ I_{S,X,P,M}\ x\ V$) and the feeding term ($u_f\ I_{S,X,P,M}$).

The real trajectory of these parameters (*S, X, P and M*) is usually hidden beneath random noise, which provokes huge variances in the calculated rates. Even a minor variation in the feeding term can have a substantial impact on the preciseness of the rates. Publication #2 elucidated a mathematical methodology for accurate and precise calculation of rates. For this purpose, several bioprocesses were simulated at different levels of noise (up to 12.5% coefficient of variation) and with different sampling frequencies. Two different methodologies had been utilized to calculate the rates: the commonly used integral stepwise approach and a cubic smoothing spline function. This study can show that the latter approach was superior for the entire experimental setup and reduced variations to a satisfactory level.

The cubic smoothing spline approach enables precise evaluation of processes without applying any pre- and/or post-smoothing methods, even when the data are packed with noise (see Figure 6).

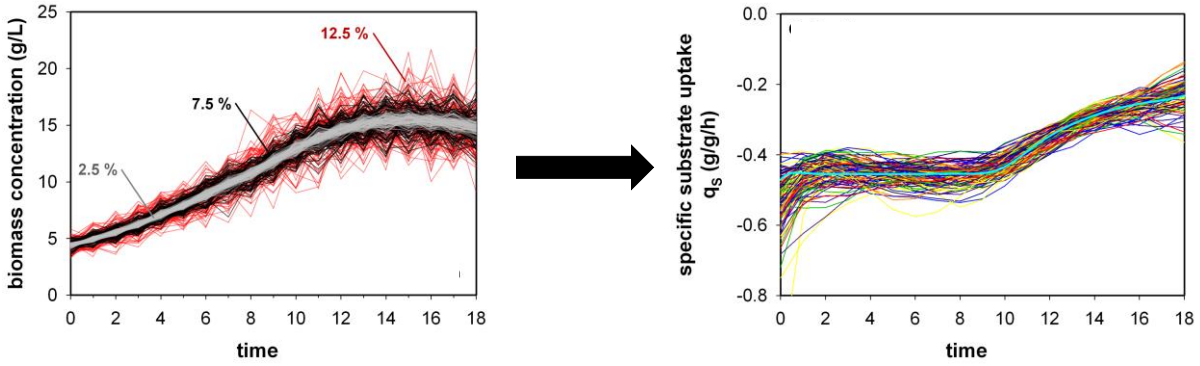


***Figure 6**: Estimation of specific substrate-uptake rate ($q_S$) via the cubic smoothing spline function. The left-plot shows input: simulated bioprocesses (n = 100) depicted at different levels of noise (2.5%, 7.5% and 12.5% coefficient of variation in the biomass determination). The right plot shows output: specific substrate-uptake rate calculated via the cubic smoothing spline approach. Data are shown for bioprocesses with an error of 12.5% CV and an additional 1% variance in the feed term (n = 100). The cubic smoothing spline approach results in very precise rate estimation. (Taken from reference [35].)*

## 3.4 Oxygen-uptake rate and soft sensing of metabolic transitions

Implementation of an APC regime requires process analysers, which are capable of real-time monitoring of CPPs and CQAs. In publication #3, we developed a soft sensor for online monitoring of wet biomass and for identifying metabolic transitions in real time. In principle, this sensor is solely based on process understanding and knowledge. For this, the bioreactor was thoroughly characterized to describe the oxygen mass transfer rate ($k_La$) as a function of stirrer speed, and the flow rate of process air and $CO_2$. By ascertaining the trajectory of the $k_La$ over the time course of the process, the OUR could be estimated. Moreover, we could show that the OUR was linked to biomass in the system and to the metabolic state of the cells (Figure 7). A clear transition to less oxygen consumption was evident. This transition was closely related to the aspartate-to-glutamate ratio and to alanine production, indicating a possible truncated citric acid cycle.

This study showed that the OUR soft sensor is a powerful advanced online monitoring tool, which allows an insight to be gained into the state of the cell culture. Furthermore, this

will enable advanced process control regimes to be set up to maintain the metabolic state of cells and keep the cell-culture performance at a high level.

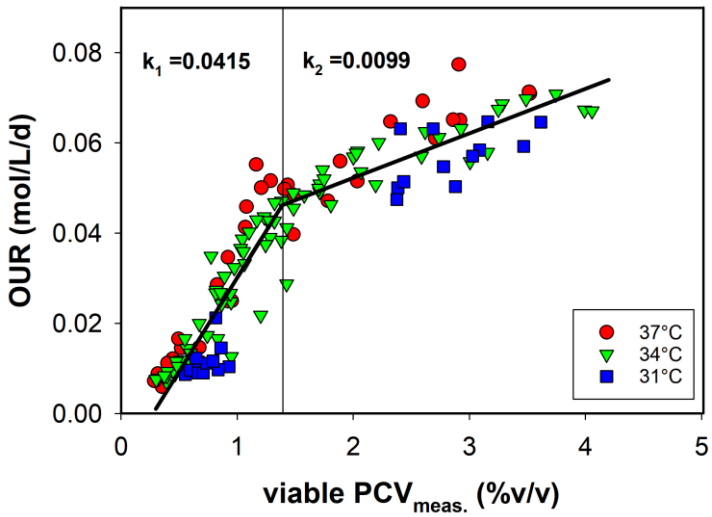


***Figure 7**: OUR as a function of the viable biomass, depicted as packed cell volume (PCV).The change in metabolic transition is depicted via the vertical line at around 1.4 PCV. After the metabolic transition, the cells reduced their oxygen consumption from 0.04 to 0.01 mol per cell volume per d. (Taken from reference [52].)*

## 3.5 Residual protein content as a cell lysis indicator

Another important CPP can be cell lysis, since it contributes to a great extent to the total amount of host-cell proteins and DNA. Publication #4 describes a method for indirect determination of cell lysis via determination of total protein with Coomassie Brilliant Blue (CBB) dye, compared to the commonly used approach involving determination of DNA via Pico Green. This CBB method utilizes the simple relationship shown below (Eq. 10), whereby

$$AU_{total} = AU_{Blank} + AU_{RPC} + AU_{IgG} \quad (10)$$

The total measured absorbance ($AU_{total}$) is the sum of the absorbance caused by mAb concentration ($AU_{IgG}$), the residual protein content concentration ($AU_{RPC}$) and the surrounding matrix ($AU_{Blank}$). For this purpose, the absorbance characteristics of mAb and the host-cell protein must be known first (Figure 8).

In one long-term study, this method was proven to be more reliable and accurate than quantifying cell lysis via DNA. Moreover, the DNA content of cells changed with the phase of

the cell cycle. This falsified the cell lysis estimate for the low temperature process, where the cells mainly remained in the G1/G0 phase.

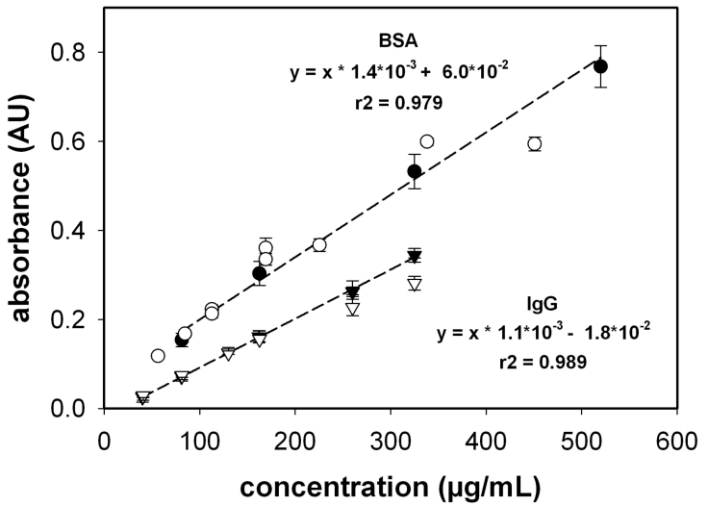


***Figure 8**: Calibration curves for BSA (black circle), the host-cell protein standard (white circle), reference IgG (black triangle) and recombinant-produced mAb (white triangle). The host-cell protein standard was made via lysing a certain number of cells from the non-producing host-cell line. The mAb and residual protein content exhibits distinct absorbance characteristics. (Taken from reference [46].)*

Conclusively, this easy-to-apply method provides important process data, which can be further used for the establishment of advanced process monitoring tools and control regimes. This study elucidated that RPC is a potential key process indicator for mammalian cell-culture processes.

## 3.6 mAb charge variant formation during a fed-batch process

Publication #5 presented a method for determining the charge variant distribution of a monoclonal antibody from crude supernatants. No impurities were likely to distort the analysis, and the emerged peaks were only due to mAb heterogeneity (Figure 9). The method was further applied in a case study which identified the impact on product quality caused by process temperature and glucose addition in the feed.

The basic variant formation could be described as a function of process temperature. The acidic variant formation followed a second-order reaction kinetic, showing a dependency for

the titer and the glucose concentration. Glycation (the non-enzymatic binding of a reactive sugar to a peptide rest) was identified as being one of the biggest contributors to this acidic peak formation.

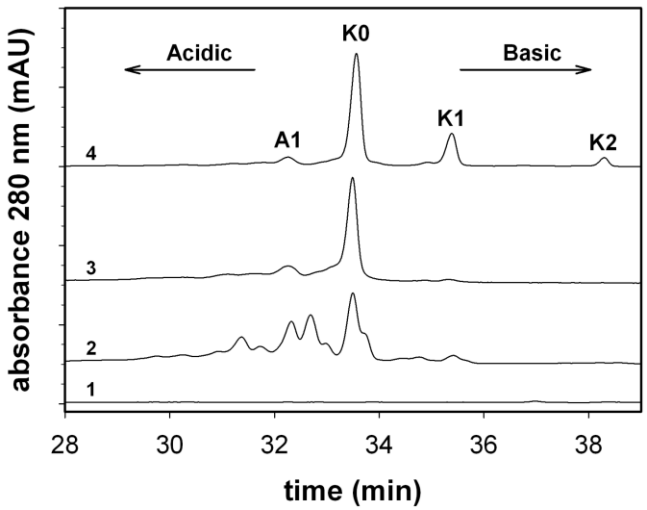


***Figure 9****: Charge variant distribution measured via ion exchange chromatography using a linear pH gradient. 1: Direct injection of supernatant derived from the non-producing host-cell line. 2: Direct injection of supernatant derived from the cell line producing mAb of interest. 3: Protein A purified mAb from the same supernatant. 4: Adalimumab reference material.*

This study presented a robust method, which allows important CQAs to be determined *a priori* without the need for a purification step, making this tool such an interesting fingerprinting technique, especially useful for implementation of an APC regime in mammalian cell-culture processes.

## 3.7 A lectin-based bio-layer interferometry method for detection of galactosylation and mannosylation of mAbs

Another important CQA is undoubtably the glycosylation pattern of mAbs. Publication #6 addresses this topic, particularly the determination of mannosylation and galactosylation of mAbs. This study presents a method based on a lectin-binding assay for identification of end-terminal mannose or galactose in the Fc region of the protein.

This method was established on a platform device, which is well known and commonly used in the industry for protein titer and kinetic analysis. The results were in good agreement with the mass spectrometry data (Figure 10). Moreover, the paper exemplifies the applicability of this approach in a case study, where ammonia production was identified as a critical process parameter affecting the galactosylation content.

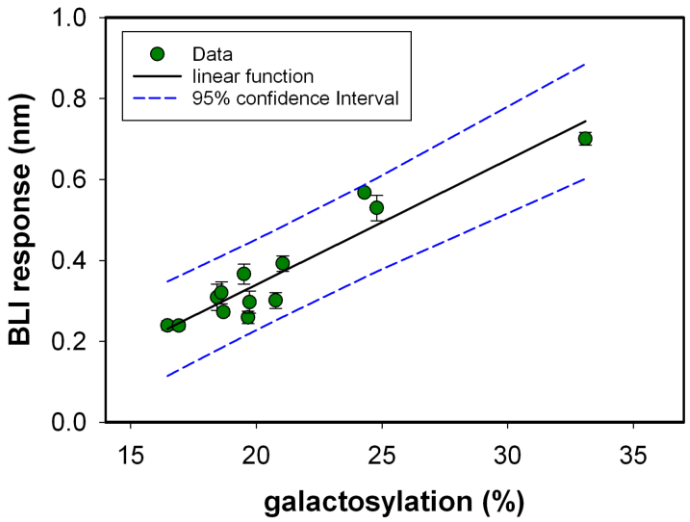


***Figure 10**: Lectin-based biolayer-interferometry-method response as a function of the galactosylation content measured via mass spectrometry (MS). (Taken from reference* [91]*.)*

# 4 Conclusion

Since mAbs are complex molecules which have to meet specific and detailed requirements to ensure efficacy and safety for patients [92], the production process is sophisticated, time-consuming and expensive [93]–[96]. In economic terms, the typical key process drivers are productivity, batch success rates and duration, as well as raw material costs [97]. In the context of cell-culture processes, consistently high-quality output is especially important from an economical point of view. However, the genetic heterogeneity of cells [98], [99], slight differences in media composition (due to lot-to-lot variations), process conditions and/or metabolite concentrations have a substantial impact on the quality of the desired product [98], [100]. Advanced process monitoring and control generates a more flexible process, which can actually react to deviations in order to maintain consistently high-quality output.

A proper and sophisticated analytical platform that comprehensively covers the wide-ranging aspects of cell- and product-related characteristics is a necessity for implementation of an advanced process monitoring and control regime in a mammalian fed-batch process. Nevertheless, the establishment of such an analytical platform can be a very challenging and overwhelming task, since several distinct requirements must be fulfilled for each method:

- Provision of insight into the dynamics of the processes;
- Keeping the analytical burden at a low level;
- Returning accurate and precise key figures;
- Determining key figures as quickly as possible.

Clearly, not all of these requirements can be achieved at once, and there must be a trade-off against each of them. For instance, although accurate and precise determination of a certain key figure might be possible using a more sophisticated and time-consuming method, a less-complicated method might be used to capture complex process dynamics, since the number of samples will increase significantly and elevate the analytical burden.

However, the link between CPPs and CQAs must be well understood and known to be capable of controlling the process properly. This requires data, and a huge number of samples need to be analysed to acquire this information. For example, over the course of this thesis, about 22,000 single analytes alone (off- and online analyses) were determined to capture the desired design space and dynamics of the process. It is, therefore, important to be aware which and how many analyses are actually needed to describe the process thoroughly. This will decrease the analytical burden and prevent the analytical platform from creating a bottleneck during the implementation step.

In this respect, decisions about sampling frequency are of particular importance. A high frequency does not necessarily mean additional information. On the contrary, unnecessary samples introduce noise into the data, which can then hide certain information. However, sampling frequency is commonly determined on the basis of intuition and experience. This can lead to huge quantities of samples which provide no additional information. For example, during this thesis, it became apparent that a large number of samples is not necessarily a prerequisite for gaining the same amount of information. Hence, identifying the optimal sampling frequency for particular key figures can reduce analytical workload and costs.

However, determining key figures via offline analytical approaches usually takes time. This is especially true if product quality attributes are determined. It is obvious that the higher the analytical effort, the greater will be the delay before the actual process evaluation and decision-making processes for future activities can take place. High-end and sophisticated analytical approaches need experts who can implement the methods and evaluate the data (as is the case, for instance, with spectroscopic methods). Thus, it is important to invest time developing methods for analytical approaches that are capable of detecting important key figures as accurately and precisely as possible within a reasonable amount of time. The methods of choice should be simple to apply and either return concrete values or have algorithms in place that can automatically evaluate the key figures of interest.

# 5 List of Figures

# 6 References


[1] S. L. Smith, “Ten years of Orthoclone OKT3,” *J. Transpl. Coord.*, vol. 6, no. 3, pp. 109–121, 1996.

[2] D. M. Ecker, S. D. Jones, and H. L. Levine, “The therapeutic monoclonal antibody market,” *MAbs*, vol. 7, no. 1, pp. 9–14, 2015.

[3] G. Walsh, “Biopharmaceutical benchmarks 2018,” *Nat. Biotechnol.*, vol. 24, no. 7, pp. 769–76, 2018.

[4] A. L. Grilo and A. Mantalaris, “The Increasingly Human and Profitable Monoclonal Antibody Market.,” *Trends Biotechnol.*, vol. 37, no. 1, pp. 9–16, 2019.

[5] G. Grampp and S. Ramanan, “Managing unexpected events in the manufacturing of biologic medicines,” *BioDrugs*, vol. 27, no. 4, pp. 305–316, 2013.

[6] B. Hassett, B. Fitzpatrick, E. Singh, E. Mahgoub, J. O’Brien, and S. M. Vicik, “Manufacturing history of etanercept (Enbrel®): Consistency of product quality through major process revisions,” *MAbs*, vol. 10, no. 1, pp. 159–165, 2018.

[7] P. W. Tebbey, A. Varga, M. Naill, J. Clewell, and J. Venema, “Consistency of quality attributes for the glycosylated monoclonal antibody Humira® (adalimumab),” *MAbs*, vol. 7, no. 5, pp. 805–811, 2015.

[8] U.S. Department of Health and Human Service and Food and Drug Administration, “Guidance for Industry PAT - A Framework for Innovative Pharmaceutical Development, Manufacturing and Quality Assurance,” *Pharm. CGMPs*, no. September, 2004.

[9] J. M. Juran, “How to Think about Quality,” in *Juran’s Quality Handbook*, 5th Editio., J. M. Juran, A. B. Godfrey, R. E. Hoogstoel, and E. G. Schilling, Eds. New York: McGraw-Hill, 1999, p. 2.1-2.18.

[10] N. McGillicuddy, P. Floris, S. Albrecht, and J. Bones, “Examining the sources of variability in cell culture media used for biopharmaceutical production,” *Biotechnol. Lett.*, vol. 40, no. 1, pp. 5–21, 2018.

[11] H. Peng, K. M. Hall, B. Clayton, K. Wiltberger, W. Hu, E. Hughes, J. Kane, R. Ney, and T. Ryll, “Development of small scale cell culture models for screening poloxamer 188 lot-to-lot variation,”

*Biotechnol. Prog.*, vol. 30, no. 6, pp. 1411–1418, 2014.

[12] Y. Luo and G. Chen, “Combined approach of NMR and chemometrics for screening peptones used in the cell culture medium for the production of a recombinant therapeutic protein,” *Biotechnol. Bioeng.*, vol. 97, no. 6, pp. 1654–1659, 2007.

[13] W. Sommeregger, B. Sissolak, K. Kandra, M. von Stosch, M. Mayer, and G. Striedner, “Quality by control: Towards model predictive control of mammalian cell culture bioprocesses,” *Biotechnol. J.*, p. 1600546, 2017.

[14] Q. Su, S. Ganesh, M. Moreno, Y. Bommireddy, M. Gonzalez, G. V. Reklaitis, and Z. K. Nagy, “A perspective on Quality-by-Control (QbC) in pharmaceutical continuous manufacturing,” *Comput. Chem. Eng.*, vol. 125, pp. 216–231, 2019.

[15] M. Von Stosch, J. Hamelink, and R. Oliveira, “Hybrid modeling as a QbD / PAT tool in process development : an industrial E . coli case study,” *Bioprocess Biosyst. Eng.*, vol. 39, no. 5, pp. 773–784, 2016.

[16] A. Mesbah, J. A. Paulson, R. Lakerveld, and R. D. Braatz, “Model Predictive Control of an Integrated Continuous Pharmaceutical Manufacturing Pilot Plant,” *Org. Process Res. Dev.*, vol. 21, no. 6, pp. 844–854, 2017.

[17] L. X. Yu, G. Amidon, M. A. Khan, S. W. Hoag, J. Polli, G. K. Raju, and J. Woodcock, “Understanding pharmaceutical quality by design,” *AAPS J.*, vol. 16, no. 4, pp. 771–783, 2014.

[18] J. N. Sangshetti, M. Deshpande, Z. Zaheer, D. B. Shinde, and R. Arote, “Quality by design approach: Regulatory need,” *Arab. J. Chem.*, vol. 10, pp. S3412–S3425, 2017.

[19] M. Looby, N. Ibarra, J. J. Pierce, K. Buckley, E. O’Donovan, M. Heenan, E. Moran, S. S. Farid, and F. Baganz, “Application of quality by design principles to the development and technology transfer of a major process improvement for the manufacture of a recombinant protein,” *Biotechnol. Prog.*, vol. 27, no. 6, pp. 1718–1729, 2011.

[20] M. von Stosch and M. J. Willis, “Intensified design of experiments for upstream bioreactors,” *Eng. Life Sci.*, vol. 17, no. 11, pp. 1173–1184, 2017.

[21] V. Kumar, A. Bhalla, and A. S. Rathore, “Design of experiments applications in bioprocessing: Concepts and approach,” *Biotechnol. Prog.*, vol. 30, no. 1, pp. 86–99, 2014.

[22] S. Pereira, H. F. Kildegaard, and M. R. Andersen, “Impact of CHO Metabolism on Cell Growth and Protein Production: An Overview of Toxic and Inhibiting Metabolites and Nutrients,”

*Biotechnol. J.*, vol. 13, no. 3, pp. 1–13, 2018.

[23] H. Hefzi, K. S. Ang, M. Hanscho, A. Bordbar, M. Lakshmanan, C. A. Orellana, D. Baycin-hizal, Y. Huang, D. Ley, V. S. Martinez, S. Kyriakopoulos, D. C. Zielinski, L. Quek, T. Wulff, J. Arnsdorf, S. Li, J. S. Lee, G. Paglia, N. Loira, N. Philipp, L. E. Pedersen, J. M. Gutierrez, Z. A. King, A. Mathilde, H. Nagarajan, A. Thomas, A. M. Abdel-haleem, H. F. Kildegaard, Z. P. Gerdtzen, M. J. Betenbaugh, B. O. Palsson, M. R. Andersen, K. Lars, N. Borth, D. Lee, N. E. Lewis, S. Diego, S. Diego, N. Resources, and J. Hopkins, "A Consensus Genome-scale Reconstruction of Chinese Hamster Ovary (CHO) Cell Metabolism," *Cell Syst.*, vol. 3, no. 5, pp. 434–443, 2016.

[24] S. N. Galleguillos, D. Ruckerbauer, M. P. Gerstl, N. Borth, M. Hanscho, and J. Zanghellini, "What can mathematical modelling say about CHO metabolism and protein glycosylation ?," *Comput. Struct. Biotechnol. J.*, vol. 15, pp. 212–221, 2017.

[25] Z. Huang, D. Y. Lee, and S. Yoon, "Quantitative intracellular flux modeling and applications in biotherapeutic development and production using CHO cell cultures," *Biotechnol. Bioeng.*, vol. 114, no. 12, pp. 2717–2728, 2017.

[26] P. Gagnon, R. Nian, Y. Yang, Q. Yang, and C. L. Lim, "Non-immunospecific association of immunoglobulin g withchromatin during elution from protein a inflates host contamination, aggregate content, and antibody loss," *J. Chromatogr. A*, vol. 1408, pp. 151–160, 2015.

[27] G. Gaza-Bulseco, S. Faldu, K. Hurkmans, C. Chumsae, and H. Liu, "Effect of methionine oxidation of a recombinant monoclonal antibody on the binding affinity to protein A and protein G," *J. Chromatogr. B Anal. Technol. Biomed. Life Sci.*, vol. 870, no. 1, pp. 55–62, 2008.

[28] C. Herwig, I. Marison, and U. Von Stockar, "On-line Stoichiometry and Identification of Metabolic State Under Dynamic Process Conditions," *Biotechnol. Bioeng.*, vol. 75, no. 3, pp. 345–354, 2001.

[29] C. Franz, J. Kern, and B. Karl, "Sensor combination and chemometric modelling for improved process monitoring in recombinant E . coli fed-batch cultivations," *J. Biotechnol.*, vol. 120, pp. 183–196, 2005.

[30] J. Mairhofer, T. Scharl, K. Marisch, M. Cserjan-puschmann, and G. Striedner, "Comparative Transcription Profiling and In-Depth Characterization of Plasmid-Based and Plasmid-Free Escherichia coli Expression Systems under Production Conditions," *Appl. Environ. Microbiol.*, vol. 79, no. 12, pp. 3802–3812, 2013.

[31] P. Wechselberger and P. Sagmeister, “Real-time estimation of biomass and specific growth rate in physiologically variable recombinant fed-batch processes,” *Bioprocess Biosyst. Eng.*, vol. 36, pp. 1205–1218, 2013.

[32] P. S. Swain, K. Stevenson, A. Leary, L. F. Montano-gutierrez, I. B. N. Clark, J. Vogel, and T. Pilizota, “Inferring time derivatives including cell growth rates using Gaussian processes,” *Nat. Commun.*, vol. 7, no. May, pp. 1–8, 2016.

[33] P. Craven and G. Wahba, “Smoothing noisy data with spline functions - Estimating the correct degree of smoothing by the method of generalized cross-validation,” *Numer. Math.*, vol. 31, no. 4, pp. 377–403, 1978.

[34] M. D. Oner, L. E. Erickson, and S. S. Yang, “Utilization of spline functions for smoothing fermentation data and for estimation of specific rates,” *Biotechnol. Bioeng.*, vol. 28, no. 6, pp. 902–918, 1986.

[35] B. Bayer, B. Sissolak, M. Duerkop, M. Von Stosch, and G. Striedner, “The shortcomings of accurate rate estimations in cultivation processes and a solution for precise and robust process modeling,” *Bioprocess Biosyst. Eng.*, 2019.

[36] B. Krampe and M. Al-Rubeai, “Cell death in mammalian cell culture: Molecular mechanisms and cell line engineering strategies,” *Cytotechnology*, vol. 62, no. 3, pp. 175–188, 2010.

[37] P. Kroll, K. Eilers, J. Fricke, and C. Herwig, “Impact of cell lysis on the description of cell growth and death in cell culture,” *Eng. Life Sci.*, vol. 17, no. 4, pp. 440–447, 2017.

[38] K. M. Carroll, D. M. Simpson, C. E. Eyers, C. G. Knight, P. Brownridge, W. B. Dunn, C. L. Winder, K. Lanthaler, P. Pir, N. Malys, D. B. Kell, S. G. Oliver, S. J. Gaskell, and R. J. Beynon, “Absolute Quantification of the Glycolytic Pathway in Yeast:,” *Mol. Cell. Proteomics*, vol. 10, no. 12, p. M111.007633, 2011.

[39] M. R. de Moreno, J. F. Smith, and R. V. Smith, “Mechanism studies of coomassie blue and silver staining of proteins,” *J. Pharm. Sci.*, vol. 75, no. 9, pp. 907–911, 1986.

[40] X. Pan, C. Dalm, R. H. Wijffels, and D. E. Martens, “Metabolic characterization of a CHO cell size increase phase in fed-batch cultures,” *Appl. Microbiol. Biotechnol.*, vol. 101, no. 22, pp. 8101–8113, 2017.

[41] G. M.J., “Product Quality Considerations for Mammalian Cell Culture Process Development and Manufacturing,” in *Mammalian Cell Cultures for Biologics Manufacturing. Advances in*

*Biochemical Engineering/Biotechnology*, 1st ed., vol. 139, Z. Weichang and A. Kantardjieff, Eds. Berlin, Heidelberg: Springer, 2013, pp. 123–166.

[42] M. Kornecki, F. Mestmäcker, S. Zobel-Roos, L. Heikaus de Figueiredo, H. Schlüter, and J. Strube, “Host Cell Proteins in Biologics Manufacturing: The Good, the Bad, and the Ugly,” *Antibodies*, vol. 6, no. 3, p. 13, 2017.

[43] T. Klein, N. Heinzel, P. Kroll, M. Brunner, C. Herwig, and L. Neutsch, “Quantification of cell lysis during CHO bioprocesses: Impact on cell count, growth kinetics and productivity,” *J. Biotechnol.*, vol. 207, pp. 67–76, 2015.

[44] P. Kroll, I. V Stelzer, and C. Herwig, “Soft sensor for monitoring biomass subpopulations in mammalian cell culture processes,” *Biotechnol. Lett.*, vol. 39, no. 11, pp. 1667–1673, 2017.

[45] J. M. Newton, D. Schofield, J. Vlahopoulou, N. Incubator, T. W. Way, and C. D. Ts, “Detecting Cell Lysis Using Viscosity Monitoring in E . coli Fermentation to Prevent Product Loss,” *AIChE J.*, vol. 32, pp. 1069–1076, 2016.

[46] B. Sissolak, C. Zabik, N. Saric, W. Sommeregger, K. Vorauer-Uhl, and G. Striedner, “Application of the Bradford Assay for Cell Lysis Quantification: Residual Protein Content in Cell Culture Supernatants,” *Biotechnol. J.*, vol. 14, no. 7, 2019.

[47] S. Wang, S. Godfrey, J. Ravikrishnan, H. Lin, J. Vogel, and J. Coffman, “Shear contributions to cell culture performance and product recovery in ATF and TFF perfusion systems,” *J. Biotechnol.*, vol. 246, pp. 52–60, 2017.

[48] I. Martínez-Monge, R. Roman, P. Comas, A. Fontova, M. Lecina, A. Casablancas, and J. J. Cairó, “New developments in online OUR monitoring and its application to animal cell cultures,” *Appl. Microbiol. Biotechnol.*, pp. 6903–6917, 2019.

[49] I. Martínez-Monge, P. Comas, J. Triquell, M. Lecina, A. Casablancas, and J. J. Cairó, “A new strategy for fed-batch process control of HEK293 cell cultures based on alkali buffer addition monitoring: comparison with O.U.R. dynamic method,” *Appl. Microbiol. Biotechnol.*, vol. 102, no. 24, pp. 10469–10483, 2018.

[50] C. T. Goudar, J. M. Piret, and K. B. Konstantinov, “Estimating cell specific oxygen uptake and carbon dioxide production rates for mammalian cells in perfusion culture,” *Biotechnol. Prog.*, vol. 27, no. 5, pp. 1347–1357, 2011.

[51] S. Goldrick, K. Lee, C. Spencer, W. Holmes, M. Kuiper, R. Turner, and S. S. Farid, “On-Line

Control of Glucose Concentration in High-Yielding Mammalian Cell Cultures Enabled Through Oxygen Transfer Rate Measurements," *Biotechnol. J.*, vol. 13, no. 4, 2018.

[52] M. Pappenreiter, B. Sissolak, and W. Sommeregger, "Oxygen Uptake Rate Soft-Sensing via Dynamic k L a Computation : Cell Volume and Metabolic Transition Prediction in Mammalian Bioprocesses," *Front. Bioeng. Biotechnol.*, vol. 7, pp. 1–16, 2019.

[53] M. W. Handlogten, M. Zhu, and S. Ahuja, "Intracellular response of CHO cells to oxidative stress and its influence on metabolism and antibody production," *Biochem. Eng. J.*, vol. 133, pp. 12–20, 2018.

[54] J. Villadsen, J. Nielsen, and G. Liden, "Gas-Lquid Mass Transfer," in *Bioreaction Engineering Principles*, Third Edit., J. Villadsen, J. Nielsen, and G. Liden, Eds. 2011, pp. 459–496.

[55] X. Wang, Z. An, W. Luo, N. Xia, and Q. Zhao, "Molecular and functional analysis of monoclonal antibodies in support of biologics development," *Protein Cell*, vol. 9, no. 1, pp. 74–85, 2018.

[56] H. Liu, G. Gaza-Bulseco, D. Faldu, C. Chumsae, and J. Sun, "Heterogeneity of Monoclonal Antibodies," *J. Pharm. Sci.*, vol. 97, no. 7, pp. 2426–2447, 2008.

[57] M. J. Feige, L. M. Hendershot, and J. Buchner, "How antibodies fold," *Trends Biochem Sci.*, vol. 35, no. 4, pp. 189–198, 2010.

[58] G. Walsh and R. Jefferis, "Post-translational modifications in the context of therapeutic proteins," *Nat. Biotechnol.*, vol. 24, no. 10, pp. 1241–1252, 2006.

[59] Y. Du, A. Walsh, R. Ehrick, W. Xu, K. May, and H. Liu, "Chromatographic analysis of the acidic and basic species of recombinant monoclonal antibodies," *MAbs*, vol. 4, no. 5, pp. 578–585, 2012.

[60] G. Ponniah, C. Nowak, A. Neill, and H. Liu, "Characterization of charge variants of a monoclonal antibody using weak anion exchange chromatography at subunit levels," *Anal. Biochem.*, vol. 520, pp. 49–57, 2017.

[61] B. Beyer, M. Schuster, A. Jungbauer, and N. Lingg, "Microheterogeneity of Recombinant Antibodies: Analytics and Functional Impact," *Biotechnol. J.*, vol. 13, no. 1, pp. 1–26, 2018.

[62] S. Fekete, A. L. Gassner, S. Rudaz, J. Schappler, and D. Guillarme, "Analytical strategies for the characterization of therapeutic monoclonal antibodies," *TrAC - Trends Anal. Chem.*, vol. 42, pp. 74–83, 2013.

[63] V. Joshi, V. Kumar, and A. S. Rathore, "Rapid analysis of charge variants of monoclonal

antibodies using non-linear salt gradient in cation-exchange high performance liquid chromatography," *J. Chromatogr. A*, vol. 1406, pp. 175–185, 2015.

[64] N. Lingg, E. Tan, B. Hintersteiner, M. Bardor, and A. Jungbauer, "Highly linear pH gradients for analyzing monoclonal antibody charge heterogeneity in the alkaline range," *J. Chromatogr. A*, vol. 1319, pp. 65–71, 2013.

[65] S. Fekete, A. Beck, J. L. Veuthey, and D. Guillarme, "Ion-exchange chromatography for the characterization of biopharmaceuticals," *J. Pharm. Biomed. Anal.*, vol. 113, pp. 43–55, 2015.

[66] B. Sissolak, N. Lingg, W. Sommeregger, G. Striedner, and K. Vorauer-Uhl, "Impact of mammalian cell culture conditions on monoclonal antibody charge heterogeneity: an accessory monitoring tool for process development," *J. Ind. Microbiol. Biotechnol.*, vol. 46, no. 8, pp. 1167–1178, 2019.

[67] S. K. Singh, G. Narula, and A. S. Rathore, "Should charge variants of monoclonal antibody therapeutics be considered critical quality attributes?," *Electrophoresis*, vol. 37, no. 17–18, pp. 2338–2346, 2016.

[68] L. A. Khawli, S. Goswami, R. Hutchinson, Z. W. Kwong, J. Yang, X. Wang, Z. Yao, A. Sreedhara, T. Cano, D. Tesar, I. Nijem, D. E. Allison, P. Y. Wong, Y. H. Kao, C. Quan, A. Joshi, R. J. Harris, and P. Motchnik, "Charge variants in IgG1: Isolation, characterization, in vitro binding properties and pharmacokinetics in rats," *MAbs*, vol. 2, no. 6, pp. 613–624, 2010.

[69] B. Hintersteiner, N. Lingg, P. Zhang, S. Woen, K. M. Hoi, S. Stranner, S. Wiederkum, O. Mutschlechner, M. Schuster, H. Loibner, and A. Jungbauer, "Charge heterogeneity: Basic antibody charge variants with increased binding to Fc receptors," *MAbs*, vol. 8, no. 8, pp. 1548–1560, 2016.

[70] C. Quan, E. Alcala, I. Petkovska, D. Matthews, E. Canova-Davis, R. Taticek, and S. Ma, "A study in glycation of a therapeutic recombinant humanized monoclonal antibody: Where it is, how it got there, and how it affects charge-based behavior," *Anal. Biochem.*, vol. 373, no. 2, pp. 179–191, 2008.

[71] B. Wei, K. Berning, C. Quan, and Y. T. Zhang, "Glycation of antibodies: Modification, methods and potential effects on biological functions," *MAbs*, vol. 9, no. 4, pp. 586–594, 2017.

[72] B. Beyer, N. Walch, A. Jungbauer, and N. Lingg, "How Similar Is Biosimilar? A Comparison of Infliximab Therapeutics in Regard to Charge Variant Profile and Antigen Binding Affinity,"

*Biotechnol. J.*, vol. 14, no. 4, pp. 1–9, 2019.

[73] E. T. J. van den Bremer, F. J. Beurskens, M. Voorhorst, P. J. Engelberts, R. N. de Jong, B. G. van der Boom, E. M. Cook, M. A. Lindorfer, R. P. Taylor, P. H. C. van Berkel, and P. W. H. I. Parren, "Human IgG is produced in a pro-form that requires clipping of C-terminal lysines for maximal complement activation," *MAbs*, vol. 7, no. 4, pp. 672–680, 2015.

[74] L. Liu, "Antibody glycosylation and its impact on the pharmacokinetics and pharmacodynamics of monoclonal antibodies and Fc-fusion proteins," *J. Pharm. Sci.*, vol. 104, no. 6, pp. 1866–1884, 2015.

[75] F. Higel, A. Seidl, F. Sörgel, and W. Friess, "N-glycosylation heterogeneity and the influence on structure, function and pharmacokinetics of monoclonal antibodies and Fc fusion proteins," *Eur. J. Pharm. Biopharm.*, vol. 100, pp. 94–100, 2016.

[76] J. M. Hayes, M. R. Wormald, P. M. Rudd, and G. P. Davey, "Fc gamma receptors: Glycobiology and therapeutic prospects," *J. Inflamm. Res.*, vol. 9, pp. 209–219, 2016.

[77] T. S. Raju and R. E. Jordan, "Galactosylation variations in marketed therapeutic antibodies," *MAbs*, vol. 4, no. 3, pp. 385–391, 2012.

[78] B. Peschke, C. W. Keller, P. Weber, I. Quast, and J. D. Lünemann, "Fc-Galactosylation of Human Immunoglobulin Gamma Isotypes Improves C1q Binding and Enhances Complement-Dependent Cytotoxicity.," *Front. Immunol.*, vol. 8, p. 646, 2017.

[79] J. N. Arnold, M. R. Wormald, R. B. Sim, P. M. Rudd, and R. A. Dwek, "The Impact of Glycosylation on the Biological Function and Structure of Human Immunoglobulins," *Annu. Rev. Immunol.*, vol. 25, no. 1, pp. 21–50, 2007.

[80] R. Kapur, H. K. Einarsdottir, and G. Vidarsson, "IgG-effector functions: 'The Good, The Bad and The Ugly,'" *Immunol. Lett.*, vol. 160, no. 2, pp. 139–144, 2014.

[81] A. Ercan, J. Cui, D. E. W. Chatterton, K. D. Deane, M. M. Hazen, W. Brintnell, C. I. O. Donnell, L. A. Derber, M. E. Weinblatt, A. Nancy, D. A. Bell, E. Cairns, D. H. Solomon, V. M. Holers, M. Pauline, and D. M. Lee, "IgG galactosylation aberrancy precedes disease onset, correlates with disease activity and is prevalent in autoantibodies in rheumatoid arthritis," *Arthritis Rheum.*, vol. 62, no. 8, pp. 2239–2248, 2014.

[82] J. Ehret, M. Zimmermann, T. Eichhorn, and A. Zimmer, "Impact of cell culture media additives on IgG glycosylation produced in Chinese hamster ovary cells," *Biotechnol. Bioeng.*, vol. 116,

no. 4, pp. 816–830, 2019.

[83] M. Ivarsson, T. K. Villiger, M. Morbidelli, and M. Soos, “Evaluating the impact of cell culture process parameters on monoclonal antibody N -glycosylation,” *J. Biotechnol.*, vol. 188, pp. 88–96, 2014.

[84] N. A. Pereira, K. F. Chan, P. C. Lin, and Z. Song, “The ‘less-is-more’ in therapeutic antibodies: Afucosylated anti-cancer antibodies with enhanced antibody-dependent cellular cytotoxicity,” *MAbs*, vol. 10, no. 5, pp. 693–711, 2018.

[85] Y. Konno, Y. Kobayashi, K. Takahashi, E. Takahashi, S. Sakae, M. Wakitani, K. Yamano, T. Suzawa, K. Yano, T. Ohta, M. Koike, K. Wakamatsu, and S. Hosoi, “Fucose content of monoclonal antibodies can be controlled by culture medium osmolality for high antibody-dependent cellular cytotoxicity,” *Cytotechnology*, vol. 64, no. 3, pp. 249–265, May 2012.

[86] A. Nguyen Dang, M. Mun, C. M. Rose, P. Ahyow, A. Meier, W. Sandoval, and I. H. Yuk, “Interaction of cell culture process parameters for modulating mAb afucosylation,” *Biotechnol. Bioeng.*, vol. 116, no. 4, pp. 831–845, 2019.

[87] P. Zhang, S. Woen, T. Wang, B. Liau, S. Zhao, C. Chen, Y. Yang, Z. Song, M. R. Wormald, C. Yu, and P. M. Rudd, “Challenges of glycosylation analysis and control: An integrated approach to producing optimal and consistent therapeutic drugs,” *Drug Discov. Today*, vol. 21, no. 5, pp. 740–765, 2016.

[88] B. L. Duivelshof, W. Jiskoot, A. Beck, J.-L. Veuthey, D. Guillarme, and V. D’Atri, “Glycosylation of biosimilars: Recent advances in analytical characterization and clinical implications,” *Anal. Chim. Acta*, vol. 1089, pp. 1–18, 2019.

[89] L. Zhang, S. Luo, and B. Zhang, “The use of lectin microarray for assessing glycosylation of therapeutic proteins,” *MAbs*, vol. 8, no. 3, pp. 524–535, Apr. 2016.

[90] K. N. Jonnalagadda, L. R. A. Markely, B. Guan, C. Alves, and S. Prajapati, “Analytical Methods High-throughput sialylation measurement using lectins on an Octet platform for clone screening,” *Anal. Methods*, vol. 8, no. 18, pp. 7193–7198, 2016.

[91] J. Wallner, B. Sissolak, W. Sommeregger, N. Lingg, G. Striedner, and K. Vorauer-Uhl, “Lectin bio-layer interferometry for assessing product quality of Fc- glycosylated immunoglobulin G,” *Biotechnol. Prog.*, vol. 35, no. 5, pp. 1–9, 2019.

[92] N. Alt, T. Y. Zhang, P. Motchnik, R. Taticek, V. Quarmby, T. Schlothauer, H. Beck, T. Emrich,

and R. J. Harris, “Determination of critical quality attributes for monoclonal antibodies using quality by design principles,” *Biologicals*, vol. 44, no. 5, pp. 291–305, 2016.

[93] B. Kelly, “Industrialization of mAb production technology,” *MAbs*, vol. 1, no. 5, pp. 443–452, 2009.

[94] P. Basu, G. Joglekar, S. Rai, P. Suresh, and J. Vernon, “Analysis of manufacturing costs in pharmaceutical companies,” *J. Pharm. Innov.*, vol. 3, no. 1, pp. 30–40, 2008.

[95] F. Li, N. Vijayasankaran, A. (Yijuan) Shen, R. Kiss, and A. Amanullah, “Cell culture processes for monoclonal antibody production,” *MAbs*, vol. 2, no. 5, pp. 466–477, 2010.

[96] H. F. Liu, J. Ma, C. Winter, and R. Bayer, “Recovery and purification process development for monoclonal antibody production,” *MAbs*, vol. 2, no. 5, pp. 480–499, 2010.

[97] S. S. Farid, “Process Economic Drivers in Industrial Monoclonal Antibody Manufacture,” in *Process Scale Purification of Antibodies*, Second Edi., U. Gottschalk, Ed. Hoboken,NJ: John Wiley & Sons, Ltd, 2017, pp. 445–466.

[98] P. M. O’Callaghan and D. C. James, “Systems biotechnology of mammalian cell factories,” *Briefings Funct. Genomics Proteomics*, vol. 7, no. 2, pp. 95–110, 2008.

[99] F. Wurm, “CHO Quasispecies—Implications for Manufacturing Processes,” *Processes*, vol. 1, no. 3, pp. 296–311, 2013.

[100] D. Reinhart, L. Damjanovic, C. Kaisermayer, and R. Kunert, “Benchmarking of commercially available CHO cell culture media for antibody production,” *Appl. Microbiol. Biotechnol.*, vol. 99, no. 11, pp. 4645–4657, 2015.

Biotechnology Journal
www.biotechnology-journal.com

Biotechnol. J. 2017, 12, 1600546

DOI 10.1002/biot.201600546

Mini-Review

# Quality by control: Towards model predictive control of mammalian cell culture bioprocesses

*Wolfgang Sommeregger[1], Bernhard Sissolak[2], Kulwant Kandra[2], Moritz von Stosch[3], Martin Mayer[4] and Gerald Striedner[2]*

[1] Bilfinger Industrietechnik Salzburg GmbH, Salzburg, Austria
[2] DBT – University of Natural Resources and Life Sciences (BOKU), Vienna, Austria
[3] CEAM – Newcastle University, Newcastle, UK
[4] Evon GmbH – Gleisdorf, Austria

The industrial production of complex biopharmaceuticals using recombinant mammalian cell lines is still mainly built on a quality by testing approach, which is represented by fixed process conditions and extensive testing of the end-product. In 2004 the FDA launched the process analytical technology initiative, aiming to guide the industry towards advanced process monitoring and better understanding of how critical process parameters affect the critical quality attributes. Implementation of process analytical technology into the bio-production process enables moving from the quality by testing to a more flexible quality by design approach. The application of advanced sensor systems in combination with mathematical modelling techniques offers enhanced process understanding, allows on-line prediction of critical quality attributes and subsequently real-time product quality control. In this review opportunities and unsolved issues on the road to a successful quality by design and dynamic control implementation are discussed. A major focus is directed on the preconditions for the application of model predictive control for mammalian cell culture bioprocesses. Design of experiments providing information about the process dynamics upon parameter change, dynamic process models, on-line process state predictions and powerful software environments seem to be a prerequisite for quality by control realization.

| | |
|---|---|
| Received | 13 DEC 2016 |
| Revised | 17 FEB 2017 |
| Accepted | 09 MAR 2017 |

**Keywords:** Biopharmaceutical production · Design of experiments · Mathematical modelling · Process analytical technology · Soft-sensing

## 1 Introduction

Mammalian cells are the most frequently used hosts for the production of complex biopharmaceuticals [1]. Large scale production of up to 20 000 L is mainly performed in fed-batch mode using stirred tank reactors, although the interest in continuous production modes is steadily growing [2]. The cultivation step is one of the key units of recombinant protein production, since it impacts on both product yield and product quality (e.g. glycosylation profile of the product) [3]. Due to the lack of techniques for real-time measurement of product attributes, quality in biopharmaceutical processes is still mainly assured by repetition of identical process settings and extensive end-product testing [4]. However, the variability of inputs (e.g. raw materials, living cells) in a bioprocess with identical

**Correspondence:** Dr. Gerald Striedner, Department of Biotechnology (DBT), University of Natural Resources and Life Sciences (BOKU), Muthgasse 18, 1190 Vienna, Austria
**E-mail:** gerald.striedner@boku.ac.at

**Abbreviations: CHO,** Chinese hamster ovary; **CPP,** critical process parameter; **CQA,** critical quality attribute; **DCS,** distributed control system; **DoE,** design of experiments; **FDA,** Food and Drug Administration; **iDoE,** intensified design of experiments; **MBDoE,** model based design of experiments; **MPC,** model predictive control; **MVDA,** multivariate data analysis; **PAT,** process analytical technology; **QbD,** quality by design; **SCADA,** supervisory control and data acquisition; **TPP,** target product profile

process settings will likely lead to a variable quality output. Already in 2004 the US Food and Drug Administration published the Process Analytical Technology (PAT) guidance for industry [Guidance for Industry: PAT – a framework for innovative pharmaceutical development, manufacturing, and quality assurance, FDA, 2004], which aims to guide the industry to move from the rigid quality by testing to a flexible quality by design (QbD) approach. There are many possibilities for QbD implementation to biopharmaceutical production processes [5, 6]. Usually, the QbD strategy starts with the definition of the relevant target product profile and the critical quality attributes (CQAs) [ICH Harmonised Tripartite Guideline: Pharmaceutical Development Q8 (R2), ICH, 2009], which vary with regard to the product and area of application [7]. In a next step, during process development the likely impact of process parameters on the process response is considered based on a priori knowledge using risk assessment, for instance failure mode and effects analysis [8]. Then relations between the critical process parameters (CPPs) and product quality attributes are sought applying statistical design of experiments (DoE), multivariate data analysis [9] and mathematical modelling techniques. Subsequently, the process operation space can be defined and sensor-technologies are applied in order to monitor critical process variables in real-time. In a final step (advanced) control strategies are developed to minimize process variability. Ultimately QbD aims at closed-loop CQA control and for this purpose model predictive control (MPC), a methodology successfully applied in so many other process industries for multivariate control [10], seems to be most suitable. MPC aims at meeting various CQA specifications (set-points) by manipulation of the process inputs, while also considering process constraints.

Astonishingly enough, or maybe rather intentional, the PAT guidance reads much like a guide to realize advanced process control, just that the ultimate goal – closed loop CQA control – and the intermeshing of the different QbD steps for realization of closed-loop control is not explicitly addressed. Advanced process control requires the measurement of the key attributes (monitoring) and a process model that describes the relation between the CPPs and CQAs. Knowledge about the sensitivity of the CQAs with respect to changes in the CPPs is key to achieve excellent control performance. The systematic assessment of these relations via DoE approaches and the systematic selection of the critical parameters and attributes via risk-assessment, both proposed in the QbD strategy, is an excellent approach, but the process dynamics should additionally be considered. Thus, each part of the QbD strategy builds towards advanced process control, only that the implications of each outcome regarding process control are not clear in many cases. This review revisits the QbD strategy with the closed loop CQA control objective (via MPC) in mind, focusing on mammalian bioprocesses. The preconditions for the application of advanced process control are assessed along the following questions:

(i) Which DoE is most suitable to characterize the design space, capture the relation between CQAs and CPPs and the respective process dynamics?
(ii) Is it possible to measure relevant process variables and mathematically model the CQA dependencies in order to predict process performance and control product quality?
(iii) Is a software framework available that allows for real-time data-preprocessing, prediction and control of the CQAs?

## 2 Design of experiments

DoE describes a statistical methodology that is used to systematically screen and assess the impact of CPPs on the process response. Process response estimation is typically done by using optimization tools such as simplex algorithms (sequential design) or response surface methodologies (simultaneous design), respectively [11]. Numerous different DoE approaches have been established. Selecting the design for an application can have vast impact on the amount of gained information [12]. Due to the ease of handling, full factorial, fractional factorial-, central composite- or Doehlert designs are still in common use [13, 14]. When dealing with a large number of factors, which exhibit strong non-linear effects and orthogonal main effects, definitive screening designs are a noteworthy alternative [15].

However, depending on the desired resolution and the accuracy of the design, a solely, statistically driven approach can be extremely laborious. Either to increase the amount of information of a given (set of) experiment(s) or to decrease the variances of model parameters, a model based DoE (MBDoE), also called optimal experimental design can be applied [16, 19]. Since several decades this approach is known though it is still not commonly used as compared to classical DoE concepts [16, 17]. The approach is based on a semi-mechanistic model, built up on given process knowledge, which is employed to predict the information content of the next set of experiments. The sets can consist of sequential or parallel experiments, or can be a combination of both [17]. Recent advantages in this field, for instance include a lowered computational effort [18] or the development of an on-line information-driven redesign optimization approach [19, 20]. Nevertheless, MBDoE requires a process model, which might not be available at the beginning of the process development stage. Probably a model from a previous process could be adopted if the mammalian host and media are the same and also the product (CQAs) is similar to the previous process.

Recently, von Stosch et al. proposed an intensified DoE (iDoE) method, where several points of a classical

DoE are evaluated in one experiment, performing intra-experiment process condition shifts. It was shown that such iDoEs can lead to the same information with less experimental effort compared to a classical DoE strategy for an *E. coli* process. However, the analysis of the process response, which is dynamic, requires the adoption of a dynamic modeling approach, such as a semi-parametric hybrid modeling approach [21, 22]. The adoption of this methodology for mammalian cell culture processes must be considered carefully, since metabolic shifts and cell memory effects could come into play. However, variations of certain variables during operation, e.g. applying pulses [23], can help to elucidate the process dynamics better, which is important for model development and inevitable for the creation of dynamic process control strategies, such as MPC.

The MBDoE and the novel iDoE approach are promising complementary concepts for mammalian bioprocess development, due to the ability to significantly reduce the workload and also providing information about the dynamic nature of the process.

## 3 Mathematical modelling

Advanced process control methods, such as MPC, require a dynamic process model, which should be sufficiently detailed to provide a significant description of the process but at the same time considerably simple allowing for fast optimization of the control trajectory. The model quality in case of mammalian cultures seems to be critical, since inappropriate control action could provoke irreversible changes in the culture. The models that are reported for advanced control of mammalian cell cultures to date incorporate a relative small number of compounds [24–27], typically viable biomass, total biomass, glucose, glutamine, lactate and ammonia concentrations. Also the control degrees of freedom are limited to glucose, glutamine or both. Considering that there are several media compounds that could be used for control, more complex models that take the underlying metabolic network into account seem to be warranted. This idea is not new and has been used for the modeling of other bioprocesses [28–32]. Metabolic flux networks of mammalian cells have been investigated by a number of researchers [33, 34]. For hybridoma cells a genome scale metabolic network model has been described [35], but no Chinese hamster ovary (CHO) cell specific genome scale metabolic network was reported until recently [36, 37]. Modeling the metabolic fluxes provides a better insight into the cellular requirements for growth as well as into the metabolism of the cells [38], though probably cell line and product dependent. While metabolic modeling might provide direct targets for metabolic engineering [36], it does not elucidate the regulation of the fluxes as a consequence of extracellular stimuli, which would be the most interesting from a process control perspective. The development of dynamic metabolic network models, such as for CHO [39, 40], addresses this shortcoming, but these models are unsuitably complex for process control purposes and they also do not take temperature, osmolality or pH dependences into account. It seems that the combination of elementary flux modes (which are computed from the metabolic network) with the dynamic bioreactor model provides a suitable alternative, which has been applied with success to describe the dynamics of CHO cultivations [41, 42] and for advanced process control of a baby hamster kidney cell cultivation [26]. The latter uses a hybrid modeling approach to model the activity of the elementary modes (i.e. the regulation) as functions of the extracellular environment with an artificial neural network. Since the regulation is not well understood, the modeling of the unknown part via data-driven techniques seems particularly promising. Also the dependence of the regulation on the osmolality, temperature and pH can easily be integrated. The combination of fundamental knowledge (white-box) with data-driven techniques (black-box), which is referred to as hybrid (semi-parametric) modeling, also conforms to industrial preferences, as the model development is systematic and exhibits many of the advantages of fundamental models [43, 44]. The pitfalls of this approach are the lack of commercial software packages and the current shortage on experienced model developers.

Given the ultimate QbD objective of controlling the CQAs, such as the glycan profile or the charge variants of monoclonal antibodies, it is evident that the models must describe the formation of these attributes. In case of the glycan profile, progress has been made in the modeling of the Golgi apparatus and the underlying reaction network [36, 45–49]. However, in case of the charge variants only data-driven models have been applied to date [50, 51]. The sensitivity of e.g. the glycan formation to the changes in the extracellular environment, such as temperature, ammonia, manganese and nucleotide sugars [48, 49], but also that of the charge variants clearly highlight the potential for advanced process control to maintain the CQAs within the limits by suitable adaptation of the media, feeding and other process parameters. To this end, hybrid modeling seems to be a suitable modeling methodology as fundamentally known relationships can be combined with data-driven techniques that represent the unknown parts.

## 4 Soft-sensing

For closed-loop product quality control the model predictions of the compounds' concentrations must be corrected with measured values. Only if measurements of the compounds' concentrations are available, an adaptation of the control action with respect to the deviation becomes possible, i.e. the control loop is closed. The information

from off- and at-line analytical methods becomes available too late to be used for process control, as in many cases these techniques require laborious manual working steps. Furthermore, they are afflicted with different sources of error [52, 53]. Therefore, there is a high demand in real-time measurements that are capable of providing information about the state of the process and the quality of the product. Since these characteristics are usually not directly measurable, there is the need of so-called soft-sensing techniques. Soft-sensing is a very promising approach, where mostly unspecific measurements (e.g. spectra) from sensors are used to estimate/calculate bioprocess variables that can otherwise not be directly measured in real-time [54]. Even straightforward soft-sensors like the real-time calculation of oxygen uptake rate or carbon dioxide production rate can be beneficial to monitor the process [55]. Soft-sensors can be knowledge-driven and/or data-driven. Knowledge-driven approaches are developed from fundamental knowledge (e.g. first-principles), describing the relations between the process variables and the quality attributes. The accuracy of these models however depends on the presence of process knowledge [56, 57]. Multivariate data analysis tools, such as principal component analysis or partial least squares are often applied for data-driven sensors, as e.g. discussed by Kadlec et al. [57], though these methods cannot process non-linearity [58].

To date, over 1000 soft-sensor applications have been published in the area of engineering [59], but in the biotech sector only a few can be found [60]. An explanation may be the complexity of the cell's biology and the reproducibility of the monitored process. Successful examples of soft-sensing implementations in the bio-therapeutics manufacturing are given elsewhere [59]. In the last years, non-selective spectroscopically performing sensors became more important compared to other sensing methods. They are highly advantageous due to being non-invasive, robust, sensitive [61] and allow multi-usage concerning bioreactor designs and biological systems [62]. Recently, few applications have been reported in the field of mammalian bioprocessing. Ohadi et al. showed that multi-wavelength fluorescence spectroscopy could be used to predict viable and dead cell concentration, product titer as well as substrate (glucose) and waste product concentrations (ammonia) [63, 64]. Another very attractive method that gained high interest in the last years is Raman spectroscopy, which allows indirectly measuring various key bioprocess metabolic variables [27, 65–67].

In contrary to specific measurement principles, established soft-sensors might only be valid within a certain range, for a given process, cell line, product or type of culture media. Therefore careful validation of established soft-sensors before their transfer to new processes is vital. Summarizing, the application of soft-sensors in mammalian bioprocesses should lower the need of off-line analysis [59] for monitoring purposes. Additionally, the hope is for soft-sensing to provide real-time state estimations that allow for correcting the model predictions, ultimately enabling model predictive control.

## 5 Model predictive control

MPC is probably the most widely adopted advanced process control methodology [68]. The methodology optimizes the process inputs, which can be manipulated, such that contradicting objectives i.e. minimal deviation of selected process states from the set-points and minimal control effort, are met in a suitable compromise [69, 70]. This optimization, a minimization, is performed by using the process model for repeated simulation of a finite prediction horizon. As a result, the optimal process inputs fully respect the dynamic behavior of the process and, if defined, time-varying constraints. These constraints could for instance ensure that the process does not leave the predefined design space. For mammalian bioprocesses, which have long characteristic times, re-calculation of the optimal control strategy will be sufficient within several minutes to once an hour. Depending on the complexity of the underlying mathematical model and the applied constraints, dedicated mathematical solvers will have to be applied for the minimization problem. Mathematical frameworks, for instance MATLAB and linkable libraries such as CPLEX or GUROBI, cover the mentioned functionalities. Since bioprocesses are highly non-linear systems, likely the application of non-linear MPC methods using non-linear/dynamic models becomes necessary. Non-linear MPC strategies have already been successfully applied to bioprocesses [24, 69, 71]. The strategies reported for mammalian cultivations to date only use one or two manipulated variables, Craven et al [27] and Teixeira et al [26], respectively, but since MPC allows for multivariate control, potentially all media compounds could be used independently for control of the CQAs e.g. the glycan profile or charge variants. It should be stressed, that the success of MPC depends on (i) the process model; and (ii) on-line measurements of the modeled compounds, sought to be obtained through soft-sensing. If the latter is missing (or if a probe fails), MPC will still provide the process inputs computed from the process model. However, the inputs will not be optimal in the sense that a deviation between the model and the plant might occur and since the controller does not recognize it, the computed control action will not minimize this deviation (referred to as model-plant mismatch).

## 6 Software environment

Distributed control systems (DCS) used in industrial automation environments, do not provide a proper range of mathematical toolsets for applying non-linear MPC. One

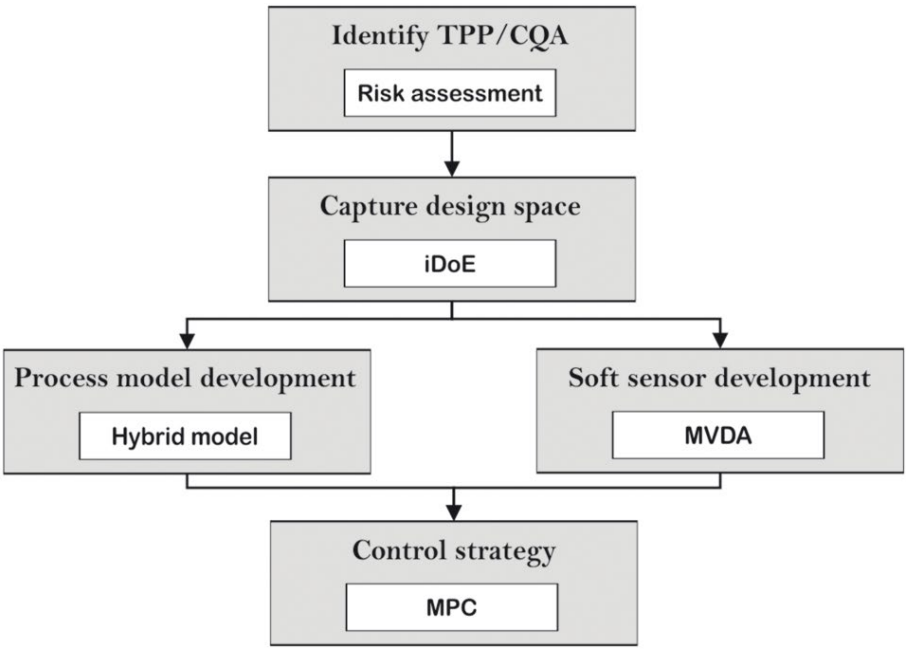


**Figure 1.** Illustration of the roadmap for quality by design and control implementation to mammalian bioprocesses. The proposed methodologies necessary for dynamic process control are indicated in each step.

reason is the limited calculation power of the usually applied microcontrollers/programmable logic controllers. Therefore more complex optimizations need to be performed on the supervisory control and data acquisition (SCADA) level. The number of solution providers offering a mathematical platform for complex optimization routines is still limited (f.i. IPCOS, PerceptiveAPC, Wolfram MathCore). Besides, these software frameworks are not integrated into commercial SCADA systems but linked via industrial interfaces.

Using soft-sensors as an input for the model, on-line data preprocessing (filtering, smoothing, outlier detection) also turns out to be relevant. The software environment (DCS, SCADA system) has to provide the possibilities of connecting advanced sensors and to perform complex statistical signal preprocessing steps [72]. Therefore, the integration of mathematical platforms directly into the SCADA becomes increasingly important or even inevitable.

## 7 Conclusions

Beneficial impacts of QbD finally reached the biopharmaceutical industry and in 2013 Roche received the first full QbD approval for the monoclonal antibody Gazyva® (Obinutuzumab) [6, 73]. However, there is yet no golden standard for the routes and methodologies to QbD implementation. In addition the enhanced process knowledge gained by QbD is still rarely used for dynamic control purposes. Three challenges have been identified that are critical for the realization and success of MPC within the QbD framework:

(i) Dynamic models are required that allow predicting changes in the CQAs resulting from changes in CPPs. New DoE approaches will lead to a reduced workload and/or better understanding of the bioprocess and its dynamics enabling the development of more meaningful and predictive dynamic models.
(ii) Soft-sensors are required that provide estimations of the states to enable correcting the dynamic model predictions and closing the control loop.
(iii) Flexible and powerful software frameworks will be essential, offering to incorporate different types of data sets, at- and in-line, respectively and using the built up model in real time [74].

We propose to follow the route depicted in Fig. 1 to realize non-linear MPC for mammalian cell culture bioprocesses.

*WS is partly and BS and KK are fully funded by Bilfinger Industrietechnik Salzburg and the Austrian Research Promotion Agency (FFG) (Competence Headquarters, grant number 849725). All authors wrote parts of the review and read the final manuscript.*

*The authors declare no commercial or financial conflict of interest.*

## 8 References

[1] Walsh, G., Biopharmaceutical benchmarks 2014. *Nat. Biotechnol.* 2014, *32*, 992–1000.
[2] Warikoo, V., Godawat, R., Brower, K., Jain, S. et al., Integrated continuous production of recombinant therapeutic proteins. *Biotechnol. Bioeng.* 2012, *109*, 3018–3029.
[3] Green, A., Glassey, J., Multivariate analysis of the effect of operating conditions on hybridoma cell metabolism and glycosylation of produced antibody. *J. Chem. Technol. Biotechnol.* 2015, *90*, 303–313.
[4] Pais, D. A., Carrondo, M. J., Alves, P. M., Teixeira, A. P., Towards real-time monitoring of therapeutic protein quality in mammalian cell processes. *Curr. Opin. Biotechnol.* 2014, *30*, 161–167.
[5] Rathore, A. S., Winkle, H., Quality by design for biopharmaceuticals. *Nat. Biotechnol.* 2009, *27*, 26–34.
[6] CMC Biotech Working Group, A-Mab: A Case Study in Bioprocess Development. CASSS, Emeryville, *CA* 2009.
[7] Eon-Duval, A., Broly, H., Gleixner, R., Quality attributes of recombinant therapeutic proteins: An assessment of impact on safety and efficacy as part of a quality by design development approach. *Biotechnol. Progr.* 2012, *28*, 608–622.
[8] Looby, M., Ibarra, N., Pierce, J. J., Buckley, K. et al., Application of quality by design principles to the development and technology transfer of a major process improvement for the manufacture of a recombinant protein. *Biotechnol. Progr.* 2011, *27*, 1718–1729.
[9] Rathore, A. S., Mittal, S., Pathak, M., Arora, A., Guidance for performing multivariate data analysis of bioprocessing data: Pitfalls and recommendations. *Biotechnol. Progr.* 2014, *30*, 967–973.
[10] Lee, J. H., Model predictive control: Review of the three decades of development. *Int. J. Control Autom. Syst.* 2011, *9*, 415.
[11] Lundstedt, T., Seifert, E., Abramo, L., Thelin, B. et al., Experimental design and optimization. *Chemom. Intell. Lab. Syst.* 1998, *42*, 3–40.
[12] Kumar, V., Bhalla, A., Rathore, A. S., Design of experiments applications in bioprocessing: Concepts and approach. *Biotechnol. Progr.* 2014, *30*, 86–99.
[13] Experimental design methods for bioengineering applications. *Crit. Rev. Biotechnol.* 2014, *8551*, 1–21.
[14] Hibbert, D. B., Experimental design in chromatography: A tutorial review. *J. Chromatogr. B* 2012, *910*, 2–13.
[15] Jones, B., Nachtsheim, C. J., A class of three-level designs for definitive screening in the presence of second-order effects. *J. Qual. Technol.* 2011, *43*, 1.
[16] Chakrabarty, A., Buzzard, G. T., Rundell, A. E., Model-based design of experiments for cellular processes. *Wiley Interdiscip. Rev. Syst. Biol. Med.* 2013, *5*, 181–203.
[17] Franceschini, G. Macchietto, S., Model-based design of experiments for parameter precision: State of the art. *Chem. Eng. Sci.* 2008, *63*, 4846–4872.
[18] Hoang, M. D., Barz, T., Merchan, V. A., Simultaneous solution approach to model-based experimental design. *AIChE J.* 2013, *59*, 4169–4183.
[19] De-Luca, R., Galvanin, F., Bezzo, F., A methodology for direct exploitation of available information in the online model-based redesign of experiments. *Comput. Chem. Eng.* 2016, *91*, 195–205.
[20] Bournazou, C., Barz, T., Nickel, D., Lopez Cárdenas, D. et al., Online optimal experimental re-design in robotic parallel fed-batch cultivation facilities for validation of macro-kinetic growth models using *E. coli* as an example. *Biotechnol. Bioeng.* 2016.
[21] von Stosch, M., Willis, M. J., Intensified design of experiments for upstream bioreactors. *Eng. Life Sci.* 2016, *2016*, 1–9.
[22] von Stosch, M.Hamelink, J.-M., Oliveira, R., Toward intensifying design of experiments in upstream bioprocess development: An industrial *Escherichia coli* feasibility study. *Biotechnol. Progr.* 2016, doi: 10.1002/btpr.2295.

**Gerald Striedner** is Associate Professor in the field of bioprocess engineering at the Department of Biotechnology (University of Natural Resources and Life Sciences, Vienna) (since 2015) and Co-founder of enGenes Biotech GmbH (2014). He is head of the working group Fermentation Technology and his research focus is laid on integrated host- and fermentation process design, process characterization, advanced process control and PAT/QbD implementation. *E. coli*, CHO, insect and vero cells producing recombinant proteins, viruses or virus like particles are used as representative model systems for biopharmaceutical production porcesses.

**Wolfgang Sommeregger** is currently leading a R&D project aiming to facilitate quality by design implementation to mammalian bioprocesses at the company Bilfinger Industrietechnik Salzburg. He graduated in Biotechnology at the University of Natural Resources and Life Sciences, Vienna (BOKU) in 2012. During his PhD studies, within the framework of the international PhD program in protein biotechnology (BioToP) at BOKU, he focused on the optimization of recombinant protein production using mammalian expression systems. He was awarded with the degree in 2015. His research interests are cell biology, bioprocessing and protein engineering.

[23] Spadiut, O., Rittmann, S. Dietzsch, C., Herwig, C., Dynamic process conditions in bioprocess development. *Eng. Life Sci.* 2013, *13*, 88–101.
[24] Aehle, M., Bork, K., Schaepe, S., Kuprijanov, A. et al., Increasing batch-to-batch reproducibility of CHO-cell cultures using a model predictive control approach. *Cytotechnology* 2012, *64*, 623–634.
[25] Frahm, B., Lane, P., Märkl, H., Pörtner, R., Improvement of a mammalian cell culture process by adaptive, model-based dialysis fed-batch cultivation and suppression of apoptosis. *Bioprocess Biosyst. Eng.* 2003, *26*, 1–10.
[26] Teixeira, A. P., Alves, C., Alves, P. M., Carrondo, M. J. T., Oliveira, R., Hybrid elementary flux analysis/nonparametric modeling: Application for bioprocess control. *BMC Bioinf.* 2007, *8*, 30.
[27] Craven, S., Whelan, J., Glennon, B., Glucose concentration control of a fed-batch mammalian cell bioprocess using a nonlinear model predictive controller. *J. Process Control* 2014, *24*, 344–357.
[28] Wiechert, W., Noack, S., Mechanistic pathway modeling for industrial biotechnology: Challenging but worthwhile. *Curr. Opin. Biotechnol.* 2011, *22*, 604–610.
[29] Sainz, J., Pizarro, F., Pérez-Correa, J. R., Agosin, E., Modeling of yeast metabolism and process dynamics in batch fermentation. *Biotechnol. Bioeng.* 2003, *81*, 818–828.
[30] Klipp, E., Modelling dynamic processes in yeast. *Yeast* 2007, *24*, 943–959.

[31] Niu, H., Daukandt, M., Rodriguez, C., Fickers, P., Bogaerts, P., Dynamic modeling of methylotrophic *Pichia pastoris* culture with exhaust gas analysis: From cellular metabolism to process simulation. *Chem. Eng. Sci.* 2013, *87*, 381–392.
[32] Koutinas, M., Kiparissides, A., Pistikopoulos, E. N., Mantalaris, A., Bioprocess systems engineering: Transferring traditional process engineering principles to industrial biotechnology. *Comput. Struct. Biotechnol. J.* 2012, *3*, 1–9.
[33] Orman, M. A., Berthiaume, F., Androulakis, I. P., Ierapetritou, M. G., Advanced stoichiometric analysis of metabolic networks of mammalian systems. *Crit. Rev. Biomed. Eng.* 2011, *39*, 511–534.
[34] Gerdtzen, Z. P., Modeling metabolic networks for mammalian cell systems: General considerations, modeling strategies, and available tools, in: Hu, W. S., Zeng, A.-P. (Eds.), *Genomics and Systems Biology of Mammalian Cell Culture*, Springer Berlin Heidelberg, Berlin, Heidelberg 2012, pp. 71–108.
[35] Selvarasu, S., Karimi, I. A., Ghim, G.-H., Lee, D.-Y., Genome-scale modeling and in silico analysis of mouse cell metabolic network. *Mol. Biosyst.* 2009, *6*, 152–161.
[36] Kaas, C. S., Fan, Y., Weilguny, D., Kristensen, C. et al., Toward genome-scale models of the Chinese hamster ovary cells: Incentives, status and perspectives. *Pharm. Bioprocess.* 2014, *2*, 437–448.
[37] Hefzi, H., Ang, K. S., Hanscho, M., Bordbar, A. et al., A Consensus genome-scale reconstruction of Chinese hamster ovary cell metabolism. *Cell Syst.* 2016, *3*, 434–443. e438.
[38] Locasale, Jason W., Cantley, Lewis C., Metabolic flux and the regulation of mammalian cell growth. *Cell Metab.* 2011, *14*, 443–451.
[39] Nolan, R. P., Lee, K., Dynamic model of CHO cell metabolism. *Metab. Eng.* 2011, *13*, 108–124.
[40] Robitaille, J., Chen, J., Jolicoeur, M., A single dynamic metabolic model can describe mAb producing CHO cell batch and fed-batch cultures on different culture media. *PLoS One* 2015, *10*, e0136815.
[41] Zamorano, F., Vande Wouwer, A., Jungers, R. M., Bastin, G., Dynamic metabolic models of CHO cell cultures through minimal sets of elementary flux modes. *J. Biotechnol.* 2013, *164*, 409–422.
[42] Provost, A., Bastin, G., Dynamic metabolic modelling under the balanced growth condition. *J. Process Control* 2004, *14*, 717–728.
[43] von Stosch, M., Oliveira, R., Peres, J., Feyo de Azevedo, S., Hybrid semi-parametric modeling in process systems engineering: Past, present and future. *Comput. Chem. Eng.* 2014, *60*, 86–101.
[44] von Stosch, M., Davy, S., Francois, K., Galvanauskas, V. et al., Hybrid modeling for quality by design and PAT-benefits and challenges of applications in biopharmaceutical industry. *Biotechnol. J.* 2014, *9*, 719–726.
[45] Krambeck, F. J., Betenbaugh, M. J., A mathematical model of *N*-linked glycosylation. *Biotechnol. Bioeng.* 2005, *92*, 711–728.
[46] Umaña, P., Bailey, J. E., A mathematical model of *N*-linked glycoform biosynthesis. *Biotechnol. Bioeng.* 1997, *55*, 890–908.
[47] Jimenez del Val, I., Nagy, J. M., Kontoravdi, C., A dynamic mathematical model for monoclonal antibody *N*-linked glycosylation and nucleotide sugar donor transport within a maturing Golgi apparatus. *Biotechnol. Progr.* 2011, *27*, 1730–1743.
[48] Villiger, T. K., Scibona, E., Stettler, M., Broly, H. et al., Controlling the time evolution of mAb *N*-linked glycosylation – Part II: Model-based predictions. *Biotechnol. Progr.* 2016, *32*, 1135–1148.
[49] O'Callaghan, P. M., James, D. C., Systems biotechnology of mammalian cell factories. *Briefings Funct. Genomics* 2008, *7*, 95–110.
[50] Bechmann, J., Rudolph, F., Gebert, L., Schaub, J. et al., Process parameters impacting product quality. *BMC Proc.* 2015, *9*, O7-O7.
[51] Björkman, T., Kärf, L., Ljunglöf, A., Falkman, T., Vitina, A., 2016.
[52] Teixeira, A. P., Duarte, T. M., Carrondo, M. J., Alves, P. M., Synchronous fluorescence spectroscopy as a novel tool to enable PAT applications in bioprocesses. *Biotechnol. Bioeng.* 2011, *108*, 1852–1861.
[53] Vojinović, V., Cabral, J., Fonseca, L., Real-time bioprocess monitoring: Part I: In situ sensors. *Sens. Actuators B* 2006, *114*, 1083–1091.
[54] Luttmann, R., Bracewell, D. G., Cornelissen, G., Gernaey, K. V. et al., Soft sensors in bioprocessing: A status report and recommendations. *Biotechnol. J.* 2012, *7*, 1040–1048.
[55] Aehle, M., Kuprijanov, A., Schaepe, S., Simutis, R., Lübbert, A., Simplified off-gas analyses in animal cell cultures for process monitoring and control purposes. *Biotechnol. Lett.* 2011, *33*, 2103–2110.
[56] Yu, J., A Bayesian inference based two-stage support vector regression framework for soft sensor development in batch bioprocesses. *Comput. Chem. Eng.* 2012, *41*, 134–144.
[57] Kadlec, P., Gabrys, B., Strandt, S., Data-driven soft sensors in the process industry. *Comput. Chem. Eng.* 2009, *33*, 795–814.
[58] Zhang, X., Yan, W., Shao, H., Nonlinear multivariate quality estimation and prediction based on kernel partial least squares. *Ind. Eng. Chem. Res.* 2008, *47*, 1120–1131.
[59] Mandenius, C. F., Gustavsson, R., Mini-review: Soft sensors as means for PAT in the manufacture of bio-therapeutics. *J. Chem. Technol. Biotechnol.* 2015, *90*, 215–227.
[60] Paulsson, D., Gustavsson, R., Mandenius, C.-F., A soft sensor for bioprocess control based on sequential filtering of metabolic heat signals. *Sensors* 2014, *14*, 17864–17882.
[61] Paul, A., Carl, P., Westad, F., Voss, J. P., Maiwald, M., Towards process spectroscopy in complex fermentation samples and mixtures. *Chem. Ing. Tech.* 2016, *88*, 756–763.
[62] Biechele, P., Busse, C., Solle, D., Scheper, T., Reardon, K., Sensor systems for bioprocess monitoring. *Eng. Life Sci.* 2015, *15*, 469–488.
[63] Ohadi, K., Aghamohseni, H., Legge, R. L., Budman, H. M., Fluorescence-based soft sensor for at situ monitoring of chinese hamster ovary cell cultures. *Biotechnol. Bioeng.* 2014, *111*, 1577–1586.
[64] Ohadi, K., Legge, R. L., Budman, H. M., Development of a soft-sensor based on multi-wavelength fluorescence spectroscopy and a dynamic metabolic model for monitoring mammalian cell cultures. *Biotechnol. Bioeng.* 2015, *112*, 197–208.
[65] Abu-Absi, N. R., Kenty, B. M., Cuellar, M. E., Borys, M. C. et al., Real time monitoring of multiple parameters in mammalian cell culture bioreactors using an in-line Raman spectroscopy probe. *Biotechnol. Bioeng.* 2011, *108*, 1215–1221.
[66] Esmonde-White, K. A., Cuellar, M., Uerpmann, C., Lenain, B., Lewis, I. R., Raman spectroscopy as a process nalytical technology for pharmaceutical manufacturing and bioprocessing. *Anal. Bioanal. Chem.* 2017, *409*, 637–649.
[67] Mehdizadeh, H., Lauri, D., Karry, K. M., Moshgbar, M. et al., Generic Raman-based calibration models enabling real-time monitoring of cell culture bioreactors. *Biotechnol. Progr.* 2015, *31*, 1004–1013.
[68] Love, J., *Process Automation Handbook: A Guide To Theory and Practice*, Springer Science & Business Media 2007.
[69] Novak, M., Koller, M., Braunegg, M., Horvat, P., Mathematical modelling as a tool for optimized PHA production. *Chem. Biochem. Eng. Q.* 2015, *29*, 183–220.
[70] Camacho, E. F., Alba, C. B., *Model Predictive Control*, Springer Science & Business Media 2013.
[71] Mears, L., Stocks, S. M., Sin, G., Gernaey, K. V., A review of control strategies for manipulating the feed rate in fed-batch fermentation processes. *J. Biotechnol.* 2017*, 245,* 34–46.
[72] Chopda, V. R., Gomes, J., Rathore, A. S., Bridging the gap between PAT concepts and implementation: An integrated software platform for fermentation. *Biotechnol. J.* 2016, *11*, 164–171.
[73] Martin-Moe, S., Nast, C., An overview of quality by design for drug product, in: Jameel, F., Hershenson, S., Khan, M. A., Martin-Moe, S. (Eds.), *Quality by Design for Biopharmaceutical Drug Product Development*, Springer 2015, pp. 47–59.
[74] Simon, L. L., Pataki, H., Marosi, G. r., Meemken, F. et al., Assessment of recent process analytical technology (PAT) trends: A multiauthor review. *Org. Process Res. Dev.* 2015, *19*, 3–62.

Bioprocess and Biosystems Engineering (2020) 43:169–178
https://doi.org/10.1007/s00449-019-02214-6

RESEARCH PAPER

# The shortcomings of accurate rate estimations in cultivation processes and a solution for precise and robust process modeling

**B. Bayer[1] · B. Sissolak[2] · M. Duerkop[1] · M. von Stosch[3] · G. Striedner[1]**

Received: 29 March 2019 / Revised: 21 June 2019 / Accepted: 10 September 2019 / Published online: 20 September 2019


## Abstract

The accurate estimation of cell growth or the substrate consumption rate is crucial for the understanding of the current state of a bioprocess. Rates unveil the actual cell status, making them valuable for quality-by-design concepts. However, in bioprocesses, the real rates are commonly not accessible due to analytical errors. We simulated *Escherichia coli* fed-batch fermentations, sampled at four different intervals and added five levels of noise to mimic analytical inaccuracy. We computed stepwise integral estimations with and without using moving average estimations, and smoothing spline interpolations to compare the accuracy and precision of each method to calculate the rates. We demonstrate that stepwise integration results in low accuracy and precision, especially at higher sampling frequencies. Contrary, a simple smoothing spline function displayed both the highest accuracy and precision regardless of the chosen sampling interval. Based on this, we tested three different options for substrate uptake rate estimations.

**Keywords** Bioprocess development · Cubic smoothing spline · Fed-batch fermentation · Growth rate · Substrate uptake rate

## Introduction

State variables, such as biomass, substrates, and product, are quantified via off-line measurements during cultivation processes of microbial, mammalian and yeast cells to understand how the process states evolve. To shed light into the biological subsystem, i.e., the cell state, as well as the metabolism [4, 6, 8, 12] or to compare different cultivations on the biological level, e.g., for media selection or cell line development [13, 16, 19], specific production/consumption rates are a necessity.

### Principle approaches to rate estimation

There are several approaches for estimating rates of a bioprocess [7, 15, 21]. A very simple method is to calculate the first derivative of a cubic smoothing spline function [15, 21]. The result is a continuous rate over the whole course of a bioprocess such as a fed-batch process, where for every time point, a rate value can be derived.

Although the applicability of this non-parametric method on bioprocess data is known for a longer time [3, 15], it still does not seem to be the method of choice for researchers in upstream bioprocess engineering, or related fields of biology. In most cases, the integral approach, a simple stepwise integral estimation is used [5, 10, 11, 25]. Hereby two measurements, one derived from sampling time point $t_i$ and the other from sampling time point $t_{i+1}$, are considered to estimate a rate for this interval $(t_i, t_{i+1})$. The same methodology is then applied to the next interval $(t_{i+1}, t_{i+2})$ and so on, estimating one rate value for each time interval, resulting in a trend over the course of the cultivation process. This, in turn, means that the rate is assumed to be constant for each

B. Bayer and B. Sissolak contributed equally.

**Electronic supplementary material** The online version of this article (https://doi.org/10.1007/s00449-019-02214-6) contains supplementary material, which is available to authorized users.

✉ B. Bayer
benjamin.bayer@boku.ac.at

✉ B. Sissolak
bernhard.sissolak@boku.ac.at

[1] Department of Biotechnology, University of Natural Resources and Life Sciences, Vienna, Austria

[2] Bilfinger Industrietechnik Salzburg GmbH, Salzburg, Austria

[3] School of Chemical Engineering and Advanced Materials, Newcastle University, Newcastle upon Tyne, UK

sampling interval, for which it was calculated, independent on its length.

### Parameters impacting rate estimation quality

Some parameters do have a high impact on the outcome of these rate estimations and if treated in the wrong way result in false estimations. For instance, dynamic process trends can remain unnoticed, e.g., if the sampling frequency is too low. In addition, if larger measurement errors are present, the rate is not feasible to describe the process anymore due to this inaccuracy. This can lead to a reduction of the accuracy of the rates and to a reasonably weakened hypothesis on the influences of certain variables or parameters. To make the calculations more applicable, different smoothing approaches for rates can be used. An often described and simple method is the moving average [9, 26]. Here, the rates from several sampling points are smoothed by taking the average value from a sampling window. In addition, more advanced moving average filters such as low-pass and Savitzky–Golay were already retrospectively used for rate modeling of bioprocesses [14, 17]. Such advanced filters require settings and appropriate knowledge for the ideal window size and smoothness, which are dependent on the process they are applied on. Using these methods, the true covariance matrix is often underestimated and the lack of automatic constraints for state variables may lead to suboptimal performances [23].

### Accurate estimation of a rate

Key figures existing in every cultivation process are the growth rate μ, which is defined as the time derivative of the logarithm of the change in population size and specific substrate uptake rates, which are feed dependent. Although stepwise integral estimation gives a simple estimation of the growth rates, this calculation possesses several drawbacks. One discrete estimation from one sampling time point to the next one is suboptimal for non-linear trends. Due to inaccurate biomass measurements, which is, in particular, true for cell culture cultivations, cell growth rates vary strongly between the samplings, indicating a false process status. On the other hand, variations in the amount of fed substrate can have substantial impacts on the specific uptake rate estimation due to error propagation. A switch in the cell's behavior is more likely to happen continuously and not spontaneously. It can be expected that calculations and model building attempts with these obtained biased values can lead to unreliable results containing much noise. To yield better descriptions of cultivation processes continuous rates should be preferred over sudden changes to yield.

Since the "true" rate is not accessible in a real fermentation process, because of the existence of analytical measurement errors [20] and biological differences from cultivation to cultivation, we present a simulated case study, at which linear and inhibited cell growth were simulated in-silico. Noise was added to the dataset to mimic a range of typical analytical measurement errors. 100 single fed-batch processes were simulated to obtain a statistical meaningful dataset. We compared the performance of the stepwise integral estimation including post-smoothing with a simple moving average with the cubic smoothing spline function. Hereby, different sampling intervals and analytical measurement errors have been simulated and both approaches were elucidated with respect to their precision and accuracy to obtain the real rates. Additionally, we also highlight an optimal solution to describe the substrate uptake rates, since for estimating substrate uptake rates, the feeding rate and feeding substrate concentration need to be taken into account. Any analytical error in this part can have a huge impact on the level of noise in the data.

The unique combination of different rate calculations applied on data with varying sampling frequencies and analytical deviations is very valuable for process understanding and modeling.

## Materials and methods

The detailed cultivation settings for the different simulated in-silico fed-batch fermentations (table 1) and all the necessary equations (Eqs. 1–4) are given in the *Bioprocess Simulation* section of the Online Resource 1.

### Noise generation

To account for process and analytic related variance, randomly generated multivariate normal distributed numbers were added, accounting for different precision levels in each process variable. Such noise was added to volume (1%), substrate (1%), and biomass, for every sampling point. For the biomass, five different levels of coefficient of variation (CV) were utilized (2.5, 5, 7.5, 10 and 12.5%). The CV (Eq. 1) is the standardized standard deviation, independent of the extent of the value and, therefore, a good estimation for accuracy:

$$\mathrm{CV} = \frac{\sigma}{\bar{X}} \times 100. \tag{1}$$

The CV describes the magnitude of variation for 68.2% of the data with the standard deviation σ and the average value $\bar{X}$.

## Stepwise integral estimation

The most commonly used method, the stepwise integral estimation, of calculating specific growth rates using the measured cell dry mass is described in the following equation:

$$\mu = \frac{\ln\left(\frac{X(t)}{X(t-1)}\right)}{\mathrm{d}t}. \tag{2}$$

As in Takuma et al. [22], $\mu$ is estimated for each time interval between two measurements by dividing the current total biomass $X(t)$ with the value of the previous measurement $X(t-1)$. This equation assumes that $\mu$ is constant for the described time interval.

### Moving average

A moving average filter was applied to smooth the stepwise integral estimation by calculating the mean of the observations using a fixed window size as stated in the following equation:

$$\mu_{\mathrm{MA}} = \frac{\mu_{(t)} + \cdots + \mu_{(t+n-1)}}{n}, \tag{3}$$

with $\mu_{\mathrm{MA}}$ as the smoothed value, $\mu$ the growth rate, and the chosen window size $n$.

## Cubic smoothing spline

For the specific growth rate estimation via cubic smoothing spline, the MATLAB function *csaps(x,y,p)* was applied with $x$ the total time of the process, the total cell mass $y$, and the chosen value for the fitting parameter $p$. This function is an implementation of the Fortran function SMOOTH [18]. The fitting parameter $p$ determines the relative weight to either smooth or perfectly match the data. Here, the least-squares solution ($p=0$) is a straight line fit, while $p=1$ is the natural cubic spline interpolation matching each data point. To find the optimal fit, the $p$ value was screened with a resolution of 0.1 and applied to the data. By choosing an appropriate value for $p$, the current growth rate can be determined by computing the functions respective time derivative (Eq. 4):

$$\frac{\mathrm{d}(xV)}{\mathrm{d}t} = \mu x V, \tag{4}$$

with $x$ representing the biomass concentration and $V$ the volume. The MATLAB script to apply the described cubic smoothing spline function to real data can be found in the Online Resource 2.

## Specific substrate uptake rate

For the calculation of the specific substrate uptake rate in g/g/h ($qS$), different approaches were considered and compared with regard to the respective accuracy. For the following equations, $uf$ represents the feed flowrate, $Sf$ the substrate feed concentration, $S$ the substrate concentration, $V$ the volume, and $x$ the biomass concentration. The change in substrate over time is determined by the amount of consumed and added substrate in the reactor (Eq. 5), accordingly:

$$\frac{\mathrm{d}(SV)}{\mathrm{d}t} = qSxV + ufSf. \tag{5}$$

### Option 1

For the first approach, the total substrate consumption (i.e., accumulation minus input) was calculated and set into a relationship to the $qS$ (Eq. 6). Accordingly, rearranging and integrating Eq. (5) resulted in:

$$\frac{\mathrm{d}(SV - S_0V_0 - \int ufSf\,\mathrm{d}t)}{\mathrm{d}t}\frac{1}{xV} = qS. \tag{6}$$

A cubic smoothing spline fit was performed on the total consumption ($SV - S_0V_0 - \int ufSf\ \mathrm{d}t$) and on the biomass term ($xV$).

### Option 2

For the second approach, the total amount of substrate in the supernatant was taken into consideration for the spline function and set into relation with the $qS$ (Eq. 7). The cubic smoothing spline fit was performed on the substrate term ($SV$) and on the biomass term ($xV$):

$$\left(\frac{\mathrm{d}(SV)}{\mathrm{d}t} - ufSf\right)\frac{1}{xV} = qS. \tag{7}$$

### Option 3

The last approach is similar to the second one, but only takes the substrate concentration in the supernatant into account. Accordingly, it follows from Eq. (5):

$$\frac{\mathrm{d}(SV)}{\mathrm{d}t} = V\frac{\mathrm{d}S}{\mathrm{d}t} + S\frac{\mathrm{d}V}{\mathrm{d}t} = qSxV + ufS, \quad \text{with}\ \frac{\mathrm{d}V}{\mathrm{d}t} = uf, \tag{8}$$

$$V\frac{\mathrm{d}S}{\mathrm{d}t} - ufSf + ufS = qSxV, \quad \text{with}\ D = \frac{uf}{V}, \tag{9}$$

$$\left(\frac{\mathrm{d}S}{\mathrm{d}t} - D(Sf - S)\right)\frac{1}{xV} = qS. \tag{10}$$

For this, an additional variable must be introduced, the dilution rate $D$, which is defined as the ratio of $uf$ to $V$ (Eq. 10). The cubic smoothing spline fit was performed on the substrate concentration term ($S$) and on the biomass term ($xV$).

### RMSE and MAPE calculation

The root-mean-square error (RMSE) was calculated according to Eq. (11) and the mean absolute percentage error (MAPE) according to Eq. (12), where $\hat{y}$ describes the actual value, $y$ the desired target value and $n$ the number of samples:

$$\mathrm{RMSE} = \sqrt{\frac{\sum_{t0}^{i}(\hat{y}(t) - y(t))^2}{n}}, \tag{11}$$

$$\mathrm{MAPE} = \frac{\sum \frac{\left|y(t) - \widehat{y(t)}\right|}{y(t)}}{n} \times 100. \tag{12}$$

## Results

### Bioprocess simulation

The two different bioprocess setups are displayed in Fig. 1. Simulation 1 describes a bioprocess were the cells are not induced or do not exhibit any growth inhibition (Fig. 1a). The second simulation describes a typical biomass trend of an induced microbial process (Fig. 1b). Due to this setup, we obtained completely different trends for the biomass as well as for the substrate concentrations. This allows to test if the distinct curvature of those trends leads to any unwanted effects when the different methods calculating the growth rate are applied.

When a process is performed with exactly the same process parameters for an infinite number of runs and with the exact same time interval at which samples are drawn, still random errors are likely to occur. Due to the analytical method precision, which depends on the utilized device different amounts of CV can be expected. The CV of biomass determination, for instance, is obviously depending on the used method. Gravimetric dried biomass determination for *E. coli* is expected to be quite accurate, whereas the measurement of the viable cell count via a microscope using a

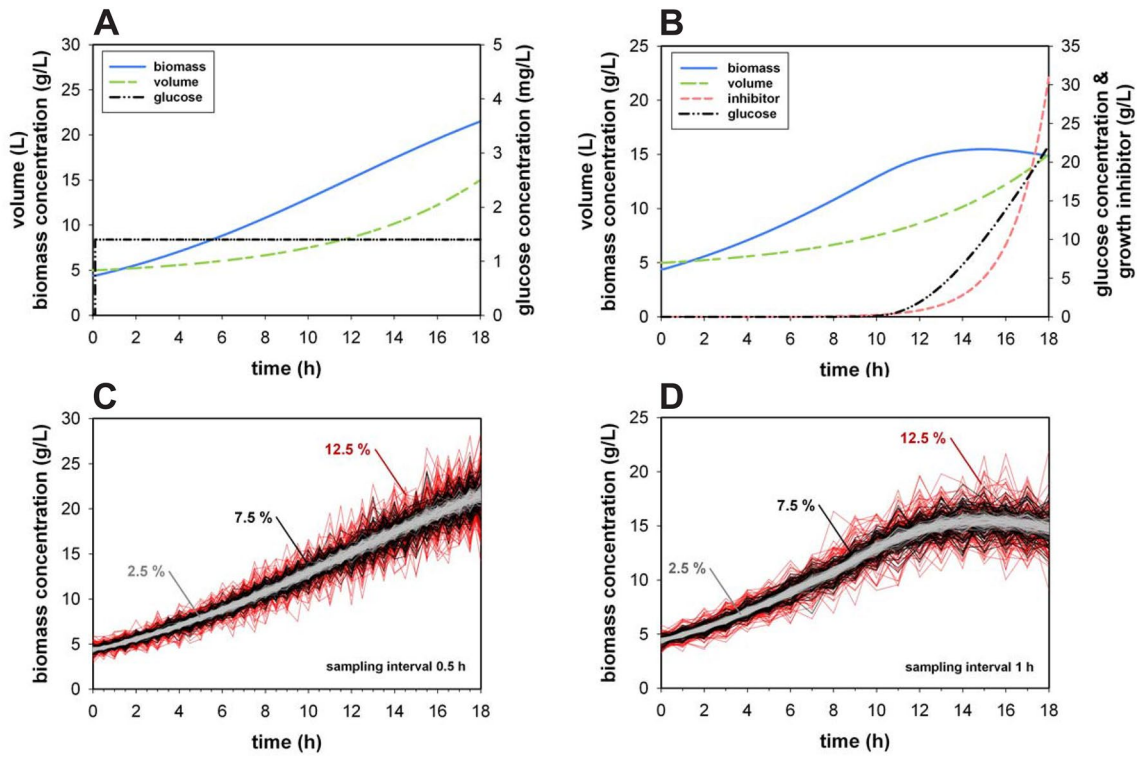


**Fig. 1** Simulated **a** Monod and **b** non-competitive model process parameters and biomass concentration variation due to random sampling error at 12.5%, 7.5% and 2.5% CV for the Monod model (**c**) with a sampling interval of 0.5 h and the non-competitive model (**d**) with a sampling interval of 1 h are presented. For **c**, **d** the number of simulated fed-batch processes $n = 100$

hemocytometer can be rather imprecise [1, 2]. The generated variations between 2.5 and 12.5% already represent very precise cell measurements. For instance, at 7.5% CV, the biomass at 20 g/L varies with ± 1.5 g/L, which is an absolutely realistic value (see Fig. 1c, d).

## Rate estimations via stepwise integral estimation and elucidation of sampling interval impact

In the first step, the growth rates for the 100 simulated fed-batch experiments were calculated and the accuracy and precision of the growth rate estimations were determined. For each rate $\mu(i)$ at time point $t(i)$, the average and the standard deviation were calculated (n = 100). On average, the stepwise integral estimation is able to determine the rate quite precisely, independently if the growth rate is constant (Fig. 2a) or not (Fig. 2b). However, it is attended by low accuracy and further depends on the sampling interval and biomass accuracy. At an interval of 0.5 h, for instance, the minimal CV is already around 50% (Fig. 2c, d). Additionally, at a low biomass determination accuracy, the CV even increases fivefold. If the growth rate is following a dynamic trend, the maximum CV at the highest sampling frequency is almost 400%. For both bioprocesses, the CV for almost half of the dataset was higher than 50%.

This behavior of the stepwise integration has huge implications on the evaluation of the current growth rates. For instance, if the growth rate would be rapidly changed back and forth due to a modification in the experimental condition, the stepwise integration approach would not be able to recognize this and the information would remain hidden because of the weak performance.

## Rate estimation via cubic smoothing spline

The cubic smoothing spline function was applied to the whole data for each run. The performance of the smoothing spline curve is displayed in Fig. 3. Additionally for the smoothing spline, also the perfect value for a general purpose of $p$ was screened. A fitting parameter $p$ of 1 led to a very low error but also to a generalization of the data and a $p$ of 0 to an increasingly high error due to the simple straight line fit (Fig. 3a). Therefore, both were not displayed in Fig. 3b. To obtain the optimal $p$, the RMSE (Eq. 11) of

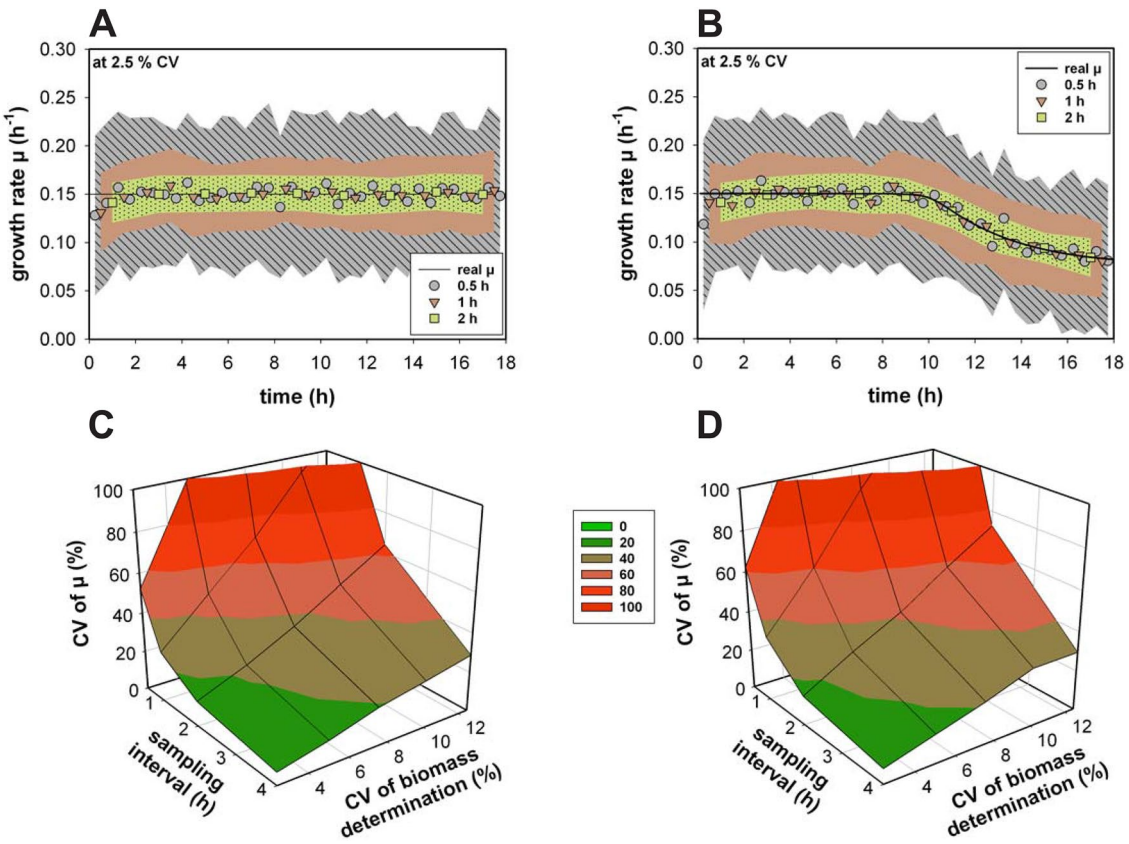


**Fig. 2** **a**, **b** The estimated growth rates at different sampling intervals and their respective standard deviations (depicted by the area) at a biomass determination precision of 2.5% coefficient of variation (CV). **c**, **d** The resulting CV of the growth rate $\mu$ as a function of the sampling interval and at different biomass determination precisions for Monod model (**a**, **c**) and the non-competitive model (**b**, **d**) The number of simulated processes $n = 100$. Data above 100% are not depicted

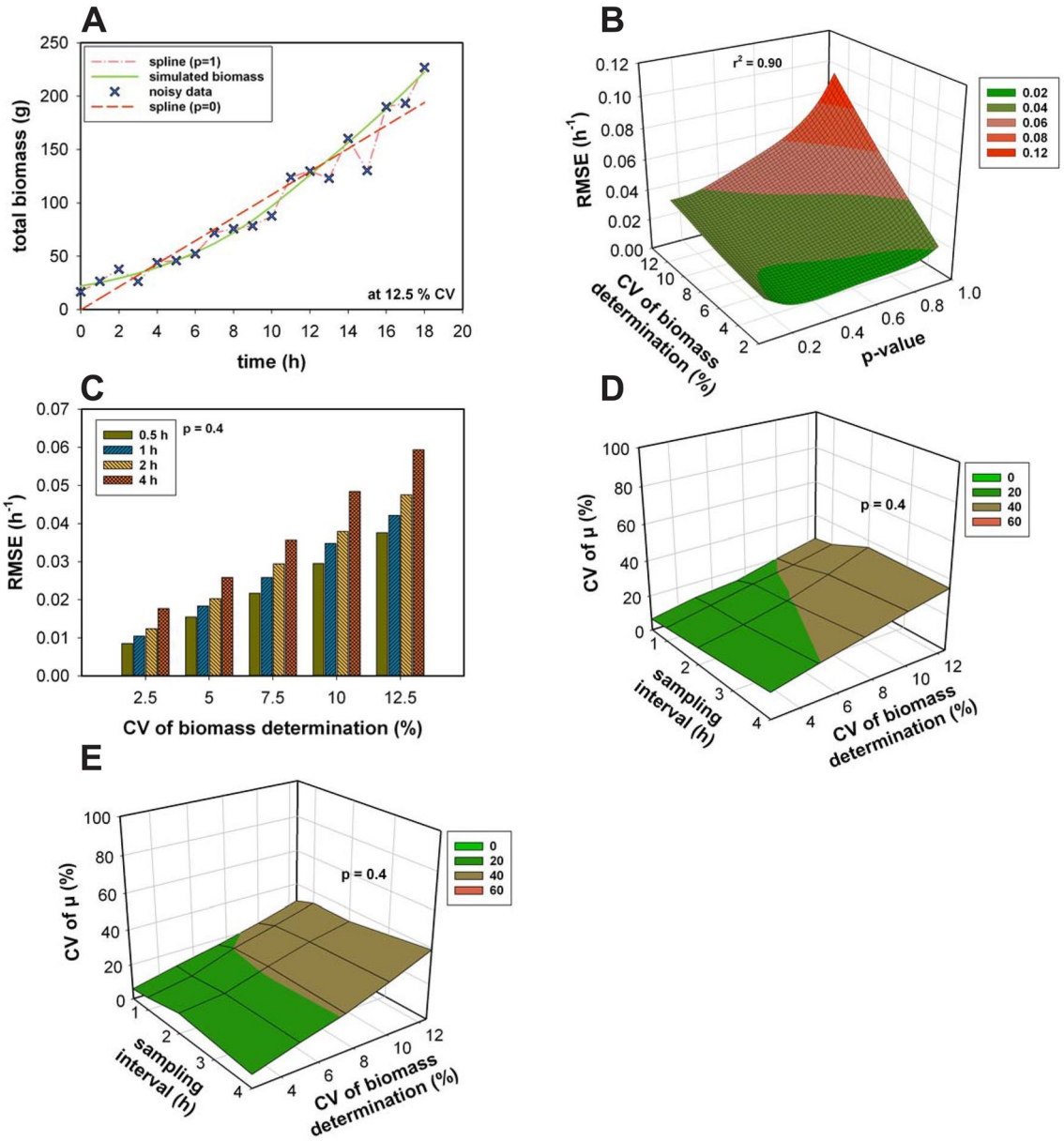


**Fig. 3** **a** Spline fittings with $p$ 0 and 1 of noisy biomass data (12.5% CV of biomass determination). **b** RMSE as a function of the sampling interval, the CV of biomass determination and the fitting parameter $p$ of the spline function. **c** RMSE at a $p$ of 0.4 at different sampling intervals. The coefficient of variation (CV) of the growth rate for the Monod model (**d**) and the non-competitive model (**e**) as a function of the sampling interval and CV of biomass determination for a fitting parameter $p$ of 0.4. For **b**–**e** the number of simulated processes $n = 100$

the rates for 100 simulated fed-batch experiments at different sampling frequencies and CV for biomass determination was calculated (Fig. 3b) and described as a function of $p$, added noise, and sampling frequencies. The RMSEs of all the sampling intervals resulted in a similar shape. The surface exhibited a minimum at a $p$ around 0.4 for all noise and sampling frequency combinations except for noise levels > 10% and the lowest sampling frequency of 4 h where a slightly lower $p$ of 0.2 would be more preferable (see also Fig. 3c). Consequently, a fitting parameter of 0.4 was chosen for all further processes. At this magnitude, also the overall error at high sampling intervals and large measurement errors is reasonable low. Once the fit is applied sufficiently, the time derivative of this function represents the current growth rate. A very precise and accurate fit can be generated, which is sampling interval independent using the applied smoothing spline function. Even if the rate estimations became slightly inaccurate at the beginning and at the end of the processes,

still the precision for the rate estimations via spline is high. No differences between the estimation of a constant and a decreasing growth rate were evident. Also, if large noise was present, the spline was still able to estimate the rates correct and precise (Fig. 3d, e). With a biomass measurement error of 12.5%, the calculated CV ranged around 50% ($n = 100$).

## Methodical comparison: stepwise integral estimation and cubic smoothing spline

The combination of stepwise integration and a moving average is a widely used approach for gathering smoothed rates. In the following, we elucidate the differences of using this combined method with the cubic smoothing spline.

The rate estimations described via the cubic smoothing spline outperformed the stepwise integral estimation. While the spline is considering the whole data, the stepwise integral estimation only takes two consecutive time points into account. Hence, smoothing splines can better deal with the error in the data compared to stepwise integral estimations. Regarding stepwise integral estimation, the error in the data is further propagated into the rate calculation. The spline fit already smooths the data before it gets even further processed. Considering this fact, it is obvious that spline functions are more accurate and precise.

A very common approach to further process the rates derived from stepwise integral estimations is to apply a moving average filter to smooth the data. For this study, we have chosen an averaging window size of 3 and 4. As expected the larger is the window size, the smaller the variations. Even with a window size of 3, the RMSE was reduced to an acceptable level. At a window size of 4, the error in the rate estimations in some cases was even better than the ones calculated with the cubic smoothing spline (Fig. 4).

However, due to the moving average, the rate change will seem to occur at different time points than it is the case. This is, in particular, a problem for non-constant rates (Fig. 4b). This effect will get even stronger at lower sampling frequencies. Further, averaging rates over several time points reduces the ability to describe the dynamics in the system, whereas exactly this should be described by the rates. The more likely process changes occur and the larger the averaging window is, the more likely they are overseen. Hence, the increased precision is traded for a reduced rates description.

The user also has to face the so-called endpoint problem. Due to the application of the moving average, the end of the process is not determined. Depending on the window size, the timeline of the rates will be inevitable shorter. Consequently, the utilization of moving average will reduce variation in the prediction, but will also lead to a reduced descriptiveness of the process and to misleading assumptions.

## Specific substrate uptake rate estimations via the cubic smoothing spline

Other important process characteristics are substrate uptake rates. In this specific case, the amount of fed substrate must be incorporated into the calculation and with it any possible variations and errors, which might come along. Since we already verified the superiority of a cubic smoothing spline we only focused on the performance of this approach. A simulation of 100 fed-batch processes using the non-competitive model was performed in which a feed variation of 1% occurs. The sampling interval was chosen to be 1 h and the worst case of 12.5% CV for the biomass determination was used

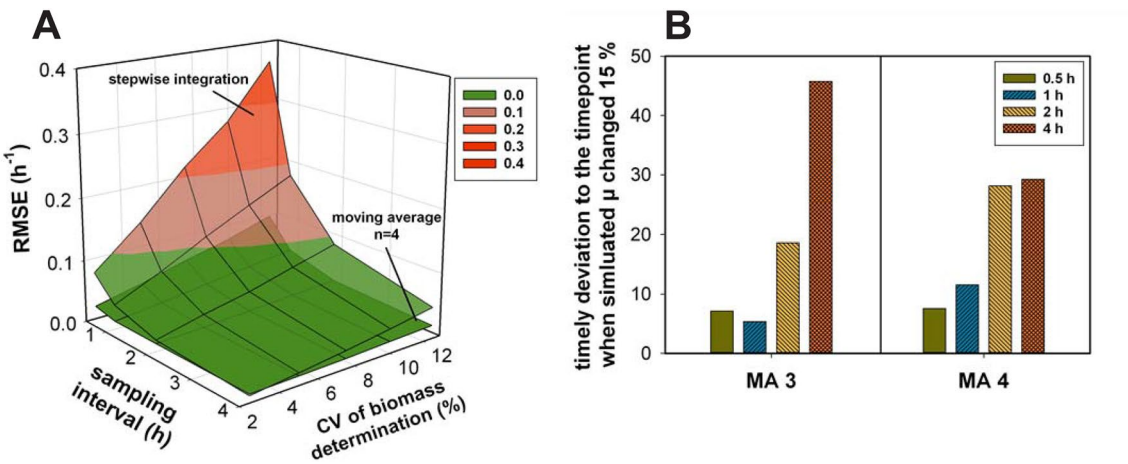


**Fig. 4** Comparing the RMSE values of the stepwise integral estimations (**a**) and stepwise integral estimations using a moving average ($n = 4$) as a function of the sampling interval and CV of biomass determination. **b** The timely deviation (%) from the time point when the simulated $\mu$ changed 15% (non-competitive model) derived from utilizing moving average with a window size of 3 and 4. The number of simulated processes $n = 100$

and the fitting parameter $p$ was set to 0.4. There are three possible options for the estimation of a feed-dependent rate. Either the total amount of consumed substrate (Option 1), the total amount of substrate in the supernatant (Option 2) or the substrate concentration in the supernatant (Option 3) can be taken into consideration for the cubic smoothing spline fitting (Fig. 5a–c).

All three options can in average accurately describe the specific substrate uptake rate (Fig. 5d). However, the incorporation of the feed into the calculation beforehand increased the precision to a great extent (Option 1) and also the feeding noise can be almost completely erased. Interestingly, between option 2 and 3, respectively, using the total amount of substrate or the substrate concentration, no significant difference was observed (see Fig. 5e). Only at the end of the fed-batch process, option 2 underestimates the specific substrate uptake rate. However, already 1% variation in the feeding system can have a substantial impact. As a consequence of using the wrong approach, the error will increase almost fourfold (Fig. 5f) from around 5% up to 20% MAPE (Eq. 12). If the feed is not incorporated into the calculation beforehand, such as it

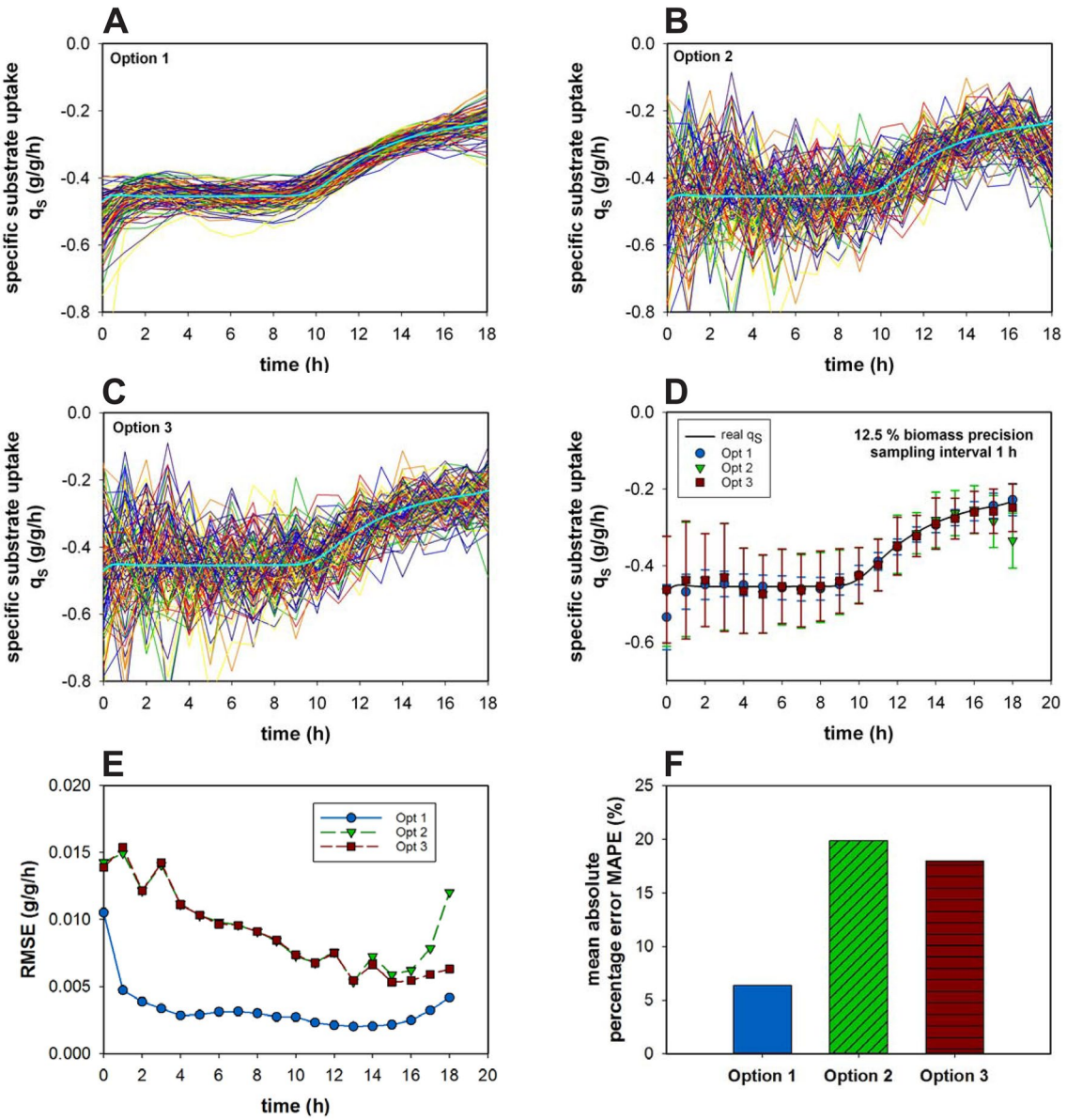


**Fig. 5** Specific substrate uptake rate estimation via option 1 (**a**) 2 (**b**) and 3 (**c**) over the time course of a fed-batch ($n = 100$) for a sampling interval of 1 h and precision of 12.5% CV for the biomass determination are presented. The averaged values and their respective standard deviations of the three different options over the time course of the process (**d**), the resulting RMSE values for each option and sampling point (**e**), and MAPE for all three options (**f**) are displayed. The number of simulated processes $n = 100$

is the case in Option 2 and 3, the feeding error propagates further into the rate estimation.

## Discussion

### Stepwise integral estimation issues

The key to process development and process modeling is to estimate rates accurately and precisely. In average ($n = 100$), the stepwise integral approach calculated an accurate rate value. This was expected considering that a large number of repetitive experiments should always meet in average the desired target value. But, we demonstrated that the stepwise integral estimation will end up in large variations. It is not surprising that the inaccuracy rises with an increased sampling frequency [24], but such an increasing variation at higher sampling frequencies was on first sight rather unexpected. Due to the magnitude of the sampling errors, the slope of the linear function will either be more positive or negative, in comparison to the real value. Every new sampling point will add its failure to it and, consequently, the deviation will increase over the time course of the cultivation. Therefore, with an increased sampling frequency, the rate estimation error increases although the measurement error remains constant. Since this behavior is counterintuitive, it is most likely overseen. This is a major disadvantage since for accurate process characterization and to gather process know-how a large dataset, thus a high sampling frequency, is a necessity. The application of the moving average would be a simple tool to reduce such variances but the user will eventually end up in less accurate values. Therefore, rates calculated by stepwise integral estimation should be handled carefully for modeling purposes.

### Application of cubic spline and specific substrate rate estimation

In this study, we focused on the cubic smoothing spline function as an alternative to rate estimations via stepwise integral estimation. With a reduced precision of the analytical determination, also the variation in the estimation increased but not to the same extent as when the stepwise integral estimation was applied. In the best case, at a high sampling frequency and biomass determination inaccuracy, the CV was around a factor of 4 lower. Moreover, the cubic smoothing spline was not affected by the sampling frequency. In real bioprocesses, a good trade-off between sampling frequency, process dynamics and the analytical error should be considered. For high analytical errors and slow process dynamic changes, a high sampling interval does not increase precision and accuracy.

Additionally, we elucidated three different approaches for estimating substrate uptake rates via the established spline fit. If the substrate feed is not incorporated beforehand a cubic spline is performed, feed variations can have a substantial impact on the propagated error. Hence, it is important to first calculate the total amount of consumed substrate before the rates are estimated.

The only "drawback" using the cubic smoothing spline function is that one degree of freedom is present, the fitting parameter $p$. Therefore, before processing the optimal $p$ must be reconsidered with respect to the given magnitude of the $x$ ordinate. Another powerful alternative to spline functions can be found in Gaussian distributions. It was shown that for processes with high sampling numbers (100–1000), the Gaussian distribution outperforms the spline function while for samplings below 100, it is vice-versa [21]. Typically, mammalian cell culture processes lead to only 10–20 observations. Likewise, also microbial fermentations do not comprise such a high sampling frequency, also resulting in only 15–25 observations per process. These considerations and the remarkably easy use of this method due to no data pre- or post-processing are clearly stating the advantage of the smoothing spline compared with other methods.

## Conclusion

In this study, the specific growth rate and the specific substrate uptake rate were chosen as representative examples. It was shown that cubic spline estimations are a simple but powerful tool to determine rates, compared to the most commonly used standard procedure the stepwise integral estimation. The presented method:

- is easy to apply and to implement for off-line analytical purposes,
- is to a major extent sample interval independent,
- can cope with large analytical variances,
- allows the user to assess a rate value at every time point.

In addition, we showed that a small error in the feeding system can lead to huge impacts in the estimation of specific substrate uptake rates. Hereby, it is important to take the feeding into account before the actual spline fit takes part.

For this level of complexity, the spline is sufficiently enough and more complex algorithms such as the Gaussian distribution or functions with more degrees of freedom (e.g., Kalman filters) are not necessary. It is easy to implement into existing codes and can add a reasonable value to process development and process comparability.

**Acknowledgements** Open access funding provided by University of Natural Resources and Life Sciences Vienna (BOKU). We would like

to thank Bilfinger Industrietechnik Salzburg and the Austrian Research Promotion Agency (FFG) for their support. (Research Studio Austria, 859219 and Competence Headquarters, 849725).

## Compliance with ethical standards

**Conflict of interest** The authors have declared no conflicts of interest.



## References

1. Bratbak G, Dundas IAN (1984) Bacterial dry matter content and biomass estimations. Appl Environ Microbiol 48(4):755–757
2. Cadena-Herrera D, Lara JEE, Ramírez-Ibañez ND, López-Morales CA, Pérez NO, Flores-Ortiz LF, Medina-Rivero E (2015) Validation of three viable-cell counting methods: manual, semi-automated, and automated. Biotechnol Rep 7:9–16. https://doi.org/10.1016/j.btre.2015.04.004
3. Craven P, Wahba G (1978) Smoothing noisy data with spline functions - Estimating the correct degree of smoothing by the method of generalized cross-validation. Numer Math 31(4):377–403. https://doi.org/10.1007/BF01404567
4. Ferreira AR, Dias JML, Teixeira AP, Carinhas N, Portela RMC, Isidro IA (2011) Projection to latent pathways (PLP): a constrained projection to latent variables (PLS) method for elementary flux modes discrimination. BMC Syst Biol 5(1):181. https://doi.org/10.1186/1752-0509-5-181
5. Franz C, Kern J, Karl B (2005) Sensor combination and chemometric modelling for improved process monitoring in recombinant *E. coli* fed-batch cultivations. J Biotechnol 120:183–196. https://doi.org/10.1016/j.jbiotec.2005.05.030
6. Galleguillos SN, Ruckerbauer D, Gerstl MP, Borth N, Hanscho M, Zanghellini J (2017) What can mathematical modelling say about CHO metabolism and protein glycosylation? Comput Struct Biotechnol J 15:212–221. https://doi.org/10.1016/j.csbj.2017.01.005
7. Glassey J, Gernaey KV, Clemens C, Schulz TW, Oliveira R, Striedner G, Mandenius C-F (2011) Process analytical technology (PAT) for biopharmaceuticals. Biotechnol J 6:369–377. https://doi.org/10.1002/biot.201000356
8. Hefzi H, Ang KS, Hanscho M, Borth N, Lee D, Lewis NE (2016) Consensus genome-scale reconstruction of Chinese hamster ovary cell metabolism. Cell Syst 3:434–443. https://doi.org/10.1016/j.cels.2016.10.020
9. Herwig C, Marison I, Stockar U Von (2001) On-line stoichiometry and identification of metabolic state under dynamic process conditions. Biotechnol Bioeng 75(3):345–354
10. Li J, Jaitzig J, Lu P, Süssmuth RD, Neubauer P (2015) Scale-up bioprocess development for production of the antibiotic valinomycin in *Escherichia coli* based on consistent fed—batch cultivations. Microb Cell Fact. https://doi.org/10.1186/s12934-015-0272-y
11. Mairhofer J, Scharl T, Marisch K, Cserjan-Puschmann M, Striedner G (2013) Comparative transcription profiling and in-depth characterization of plasmid-based and plasmid-free *Escherichia coli* expression systems under production conditions. Appl Environ Microbiol 79(12):3802–3812. https://doi.org/10.1128/AEM.00365-13
12. Niklas J, Schräder E, Sandig V, Noll T, Heinzele E (2011) Quantitative characterization of metabolism and metabolic shifts during growth of the new human cell line AGE1. HN using time resolved metabolic flux analysis. Bioproc Biosyt Eng 34:533–545. https://doi.org/10.1007/s00449-010-0502-y
13. Noh SM, Shin S, Lee GM (2018) Comprehensive characterization of glutamine synthetase-mediated selection for the establishment of recombinant CHO cells producing monoclonal antibodies. Sci Rep 1–11. https://doi.org/10.1038/s41598-018-23720-9
14. Ohadi K, Legge RL, Budman HM (2014) Development of a soft-sensor based on multi-wavelength fluorescence spectroscopy and a dynamic metabolic model for monitoring mammalian cell cultures. Biotechnol Bioeng 112(1):197–208. https://doi.org/10.1002/bit.25339
15. Oner MD, Erickson LE, Yang SS (1986) Utilization of spline functions for smoothing fermentation data and for estimation of specific rates. Biotechnol Bioeng 28(6):902–918. https://doi.org/10.1002/bit.260280618
16. Pan X, Streefland M, Dalm C (2017) Selection of chemically defined media for CHO cell fed-batch culture processes. Cytotechnology 69:39–56. https://doi.org/10.1007/s10616-016-0036-5
17. Paulsson D, Gustavsson R, Mandenius C (2014) Filtering of metabolic heat signals. Sensors 14:17864–17882. https://doi.org/10.3390/s141017864
18. R. J, de Boor C (2006) A practical guide to splines. Math Comput 34(149):325. https://doi.org/10.2307/2006241
19. Sieck JB, Cordes T, Budach WE, Rhiel MH, Suemeghy Z, Leist C, Soos M (2013) Development of a scale-down model of hydrodynamic stress to study the performance of an industrial CHO cell line under simulated production scale bioreactor conditions. J Biotechnol 164(1):41–49. https://doi.org/10.1016/j.jbiotec.2012.11.012
20. Sonnleitner, B. (2007). Bioanalysis and biosensors for bioprocess monitoring. Springer, Berlin, pp 1–64. https://doi.org/10.1007/3-540-48773-5_1
21. Swain PS, Stevenson K, Leary A, Montano-Gutierrez LF, Clark IBN, Vogel J, Pilizota T (2016) Inferring time derivatives including cell growth rates using Gaussian processes. Nat Commun 7(May):1–8. https://doi.org/10.1038/ncomms13766
22. Takuma S, Hirashima C, Piret JM (2007) Dependence on glucose limitation of the $pCO_2$ Influences on CHO cell growth. Metab IgG Prod 97(6):1479–1488. https://doi.org/10.1002/bit
23. Ungarala S, Dolence E, Li K (2007) Constrained extended Kalman filter. IFAC Proc 2:63–68
24. Wechselberger P, Herwig C (2012) Model-based analysis on the relationship of signal quality to real-time extraction of information in bioprocesses. AlChE J 28(1):265–275. https://doi.org/10.1002/btpr.700
25. Wechselberger P, Sagmeister P (2013) Real-time estimation of biomass and specific growth rate in physiologically variable recombinant fed-batch processes. Bioproc Biosyst Eng 36:1205–1218. https://doi.org/10.1007/s00449-012-0848-4
26. Zahel T, Sagmeister P, Suchocki S, Herwig C (2016) Accurate information from fermentation processes-optimal rate calculation by dynamic window adaptation. Chem-Ing-Tech 88(6):798–808. https://doi.org/10.1002/cite.201500085

frontiers in Bioengineering and Biotechnology

ORIGINAL RESEARCH
published: 21 August 2019
doi: 10.3389/fbioe.2019.00195

# Oxygen Uptake Rate Soft-Sensing via Dynamic $k_La$ Computation: Cell Volume and Metabolic Transition Prediction in Mammalian Bioprocesses

*Magdalena Pappenreiter[1†], Bernhard Sissolak[1†], Wolfgang Sommeregger[1*] and Gerald Striedner[2]*

[1] R&D - Bilfinger Industrietechnik Salzburg GmbH, Salzburg, Austria, [2] Department of Biotechnology (DBT), University of Natural Resources and Life Sciences (BOKU), Vienna, Austria

OPEN ACCESS

**Edited by:**
Roland Wohlgemuth,
Lodz University of Technology, Poland

**Reviewed by:**
Peter Neubauer,
Technische Universität Berlin, Germany
David Lynn Hacker,
École Polytechnique Fédérale de Lausanne, Switzerland

***Correspondence:**
Wolfgang Sommeregger
wolfgang.sommeregger@bilfinger.com

[†] These authors have contributed equally to this work

**Specialty section:**
This article was submitted to Bioprocess Engineering, a section of the journal Frontiers in Bioengineering and Biotechnology

**Received:** 16 April 2019
**Accepted:** 29 July 2019
**Published:** 21 August 2019

**Citation:**
Pappenreiter M, Sissolak B, Sommeregger W and Striedner G (2019) Oxygen Uptake Rate Soft-Sensing via Dynamic $k_La$ Computation: Cell Volume and Metabolic Transition Prediction in Mammalian Bioprocesses. Front. Bioeng. Biotechnol. 7:195. doi: 10.3389/fbioe.2019.00195

In aerobic cell cultivation processes, dissolved oxygen is a key process parameter, and an optimal oxygen supply has to be ensured for proper process performance. To achieve optimal growth and/or product formation, the rate of oxygen transfer has to be in right balance with the consumption by cells. In this study, a 15 L mammalian cell culture bioreactor was characterized with respect to $k_La$ under varying process conditions. The resulting dynamic $k_La$ description combined with functions for the calculation of oxygen concentrations under prevailing process conditions led to an easy-to-apply model, that allows real-time calculation of the oxygen uptake rate (OUR) throughout the bioprocess without off-gas analyzers. Subsequently, the established OUR soft-sensor was applied in a series of 13 CHO fed-batch cultivations. The OUR was found to be directly associated with the amount of viable biomass in the system, and deploying of cell volumes instead of cell counts led to higher correlations. A two-segment linear model predicted the viable biomass in the system sufficiently. The segmented model was necessary due to a metabolic transition in which the specific consumption of oxygen changed. The aspartate to glutamate ratio was identified as an indicator of this metabolic shift. The detection of such transitions is enabled by a combination of the presented dynamic OUR method with another state-of-the-art viable biomass soft-sensor. In conclusion, this hyphenated technique is a robust and powerful tool for advanced bioprocess monitoring and control based exclusively on bioreactor characteristics.

**Keywords: $k_La$, oxygen transfer rate, oxygen uptake rate, biomass prediction, metabolic states, quality by control, CHO**

## INTRODUCTION

The primary role of a bioreactor is to provide a suitable environment for cell growth and product formation. Stirred tank reactors (STRs) are currently the most widely used bioreactor type to cultivate aerobic organisms in suspension culture or on carriers. In aerobic upstream bioprocesses, the oxygen uptake rate (OUR) is crucial for cellular activity and a good indicator of changes in the metabolic state of the culture (Deshpande and Heinzle, 2004; Wahrheit et al., 2015), which

can be induced by changing substrate availabilities (Toye et al., 2010; Niklas et al., 2011; Young, 2013; Zhang et al., 2016). Thus, in the context of implementing Quality by Design and Process Analytical Technology (QbD/PAT) in bioprocesses, the OUR could be an informative process indicator (Sommeregger et al., 2017).

According to the QbD/PAT concept real-time measurements of meaningful process variables are a necessity. Soft(ware)-sensors can provide information about the actual state and quality of the process. Thereby on-line process variables are measured by associated sensors (hardware) using an estimation algorithm (software) to deliver estimated unmeasured bioprocess variables (Luttmann et al., 2012).

Before being consumed by cells, oxygen disperses through the culture medium in a series of transport resistances from gas bubbles to each individual cell. The highest resistance occurs during the transport through the liquid film surrounding the gas bubbles, which is described by the volumetric mass transfer coefficient ($k_La$). This coefficient and the concentration gradient ($c_L^*$-$c_{O2}$) in the liquid phase defines the gas-liquid transfer rate and the oxygen transfer rate (OTR), respectively (Villadsen et al., 2011).

Precise OTR calculations during a bioprocess are challenging, because different phenomena occur simultaneously. Process conditions (e.g., pressure, temperature, mixing, and gas-flow) in a previously chosen operational mode (e.g., batch or fed-batch cultivation) together with physicochemical properties (e.g., media composition or viscosity) may change over time and influence the overall OTR (Garcia-ochoa and Gomez, 2009). Temperature and pressure greatly impact the maximum oxygen solubility in aqueous solutions, and therefore mainly influence the concentration gradient. Regarding the physicochemical properties of the medium, the amount of electrolytes (salts, ions) in so-called non-coalescing fluids can have beneficial effects on $k_La$, due to suppressing bubble coalescence (Villadsen et al., 2011). Other additives, such as Pluronic F68, which is typically added for shear protection, have been shown to reduce bubble size at high concentrations (Sieblist et al., 2013). Moreover, certain antifoam agents, such as silicone oils, can act as oxygen vectors, resulting in a significant increase in oxygen transfer and the oxygen transfer capacity in STRs (Quijano et al., 2009). In contrast, in bubble column reactors, $k_La$ values decrease with the addition of hydrophilic or hydrophobic surface active compounds (Mcclure et al., 2015). In addition, increasing biomass particle size and by-product formation can reduce $k_La$ values due to enhanced bubble coalescence (Vandu and Krishna, 2004).

**Abbreviations:** Ala, Alanine; Asn, Asparagine; Asp, Aspartate; ATP, Adenosine tri phosphate; BAC, Bacterial artificial chromosome; CHO, Chinese hamster ovary; CFD, Computational fluid dynamics; DoE, Design of experiments; FMOC, Fluorenylmethoxycarbonyl; Gln, Glutamine; Glu, Glutamate; HPLC, High performance liquid chromatography; IgG, Immunoglobulin G; mAb, Monoclonal antibody; NADPH, Nicotinamide adenine dinucleotide phosphate; OPA, o-Phthalaldehyde; PA, Process Air; PAT, Process Analytical Technology; PCV, Packed Cell Volume; PID, Proportional Integral Derivative; QbD, Quality by Design; RO, Reverse Osmosis; STR, Stirred Tank Reactor; TCA, Tricarboxylic acid cycle.

In aerobic bioprocesses the dissolved oxygen concentration should not drop below a certain threshold. Therefore, a PID control circuit is usually used to counteract shortages. The output parameters of such a controller can be different among processes but usually includes stirrer speed, gas-flow or composition, pressure, or combinations thereof. By utilizing design of experiments (DoE), the influence of those parameters on $k_La$ and $c_L^*$ can be determined within the operational process space. Consequently, OTR can be estimated at each time point during the process.

Though the OTR and $k_La$ in particular are decisive parameters for the design of bioreactors, the OUR calculated in real-time provides information about the cells being cultured and the overall process performance. The OUR is a good indicator of cellular activity that closely correlates with the viable biomass. Within a bioprocess, the OUR is usually calculated via oxygen mass balancing. Therefore, the use of gas-analyzers is required to determine the oxygen and $CO_2$ concentration in the off-gas stream, and these compounds can be quantified using flow rates. Another approach is to use the combination of OTR and the time-progression of the actual dissolved oxygen (DO) concentration (Lovrecz and Gray, 1994; Eyer et al., 1995). However, the published methods usually do not correct for changes in either $k_La$ or $c_L^*$ due to process dynamics, or rely on empirical $k_La$ calculations based on water experiments.

In this study, a soft-sensor was established for real-time estimation of the OTR and respectively, OUR. For this purpose, a 15 L bioreactor was thoroughly characterized to develop a dynamic model for $k_La$ that can account for changing operational (temperature, PID controller output) and physicochemical properties of the medium (oxygen transfer and solubility). The model was applied, to a wide-spread dataset of 13 recombinant Chinese hamster ovary (CHO) cell culture fed-batch processes producing a monoclonal antibody (mAb) to elucidate the association of OUR with biomass and the metabolic states throughout the process. In summary, this study presents an estimation of the OUR based on standard measurements (PA and $CO_2$ inlet gas flow-rates, temperature, volume, pressure) and precise system characterization that takes into account the dynamic $k_La$ throughout progression of the process. This OUR soft-sensor was then used for biomass prediction. We also show an advanced technique for monitoring metabolic transitions of cells during cultivation simply by combining the dynamic OUR with a state of the art capacitance sensor.

# MATERIALS AND METHODS

## Operational Conditions

A 15 L (max. working volume) stainless steel stirred tank bioreactor with a tank diameter (D) of 0.242 m and total height (H) of 0.484 m (LabQube, Bilfinger Industrietechnik Salzburg GmbH, Austria) was equipped with two three-bladed elephant ear impellers ($d_i = 0.1$ m) connected to a bottom-driven magnetic impeller shaft. Aeration was maintained by a submerged I-shaped frit and calibrated mass flow controllers (8711, Burkert, Germany). The temperature was measured using the built in Pt100 resistance thermometer. The DO concentration

was monitored using an optical oxygen sensor (VisiFerm DO Arc120, Hamilton Switzerland) and pH by a pH probe (EasyFerm Plus PH Arc120, Hamilton, Switzerland). The oxygen and $CO_2$ content in the off-gas stream was measured using a gas analyzer (BlueInOneFERM, BlueSens, Germany). A capacitance probe (Incyte, Hamilton, Switzerland) was used to evaluate the biomass estimations and establish the metabolism sensor.

## $k_La$ Measurements

The experimental determination of $k_La$ was performed using the dynamic gassing in/gassing out method (Van't Riet, 1979). Dissolved oxygen was measured by step changes in the oxygen concentration of the inlet gas. $k_La$ was determined from the slope of the natural logarithmic DO concentration over time in an oxygen saturation range of 20–80%. Application of this method is restricted when the oxygen transfer is faster than the probe response. As proposed by (Van't Riet, 1979), the time constant of the measurement probe can be neglected if the following condition in Equation (1) is fulfilled:

$$\tau_p \leq \frac{1}{k_La} \tag{1}$$

As the mass transfer coefficients within the chosen process space for mammalian cell culture bio-production are relatively low, the response time determined for the used probe ($\tau_p = 49.6$ s, experimentally) was sufficient. All measurements were performed according to a pre-defined experimental set-up with varying parameters (working volume, impeller speed, aeration rates, and culture temperature).

Two liquids, RO-$H_2O$ and a chemically defined culture medium (Dynamis AGT, A26175-01, Thermo Fisher Scientific, USA) both supplemented with 0.1% (v/v) antifoam C (A8011, Sigma Aldrich, Germany), were used to determine $k_La$. All measurements were performed in triplicate. Data accuracy was within ±5% for all measurements; thus, only the average values are shown in the respective depictions.

## Oxygen Transfer

Methods to quantify OUR and OTR are based on a gas-liquid mass balance of oxygen as described in Equation (2),

$$\frac{dC}{dt} = k_La\ \left({c_L}^* - c_{O2}\right) - q_{O2}{*}X \tag{2}$$

where the timely changes in oxygen concentration are influenced by the oxygen mass transfer coefficient ($k_La$), maximum solubility of oxygen ($c_L^*$), actual oxygen concentration ($c_{O2}$), specific OUR ($q_{O2}$), and viable cell concentration ($X$). The OUR ($OUR = q_{O2}^* X$) and OTR are equal during steady-state conditions (controlled DO concentration), hence $dC/dt = 0$, leaving OTR as described in Equation (3):

$$OTR = k_La\ ({c_L}^* - c_{O2}) \tag{3}$$

The OUR model described in this work is based on a detailed bioreactor characterization, in which physiological and kinetic changes from a dynamic process, resulting in varying dynamic $k_La$ values are considered. The on-line bioprocess data including the $O_2$ and $CO_2$ aeration rates, temperature, filling level and DO concentrations measured by an oxygen probe, as well as pre-determined oxygen solubility in water and cell culture medium were used for the model derivation.

## OUR Calculation by Oxygen Mass Balancing

One possibility for acquiring the consumed mass of oxygen on-line involves balancing the oxygen mass between the gas entering and leaving the bioreactor, which applies to animal cell cultures (Eyer et al., 1995). An accurate gas analyzer is required for this technique to measure the $Vol.O_{2,out\%}$ in the off-gas stream. In addition, the gas flow rate ($G_{in} = G_{\text{out}}$) and composition of the aeration gas that enters the bioreactor together with the liquid volume ($V_L$) and molar gas volume [$V_{m,in}$ ($p$,$T$,$R$); assumed $T_{in} = 22°C$, $T_{out} =$ measured gas outlet temperature], needs to be taken into account to calculate the OUR as described in Equation (4):

$$OUR_{MB} = \frac{O_2\ in - O_2\ out}{V_L} = \frac{\left(\frac{Vol.O_{2in\%} * G_{in}}{V_{m,in}}\right) - \left(\frac{Vol.O_{2out\%} * G_{out}}{V_{m,out}}\right)}{V_L} \tag{4}$$

## Maximum Oxygen Solubility: The Thermodynamic Approach

The maximum solubility of oxygen in water ($c^*$) under ambient air was calculated using Equation (5), the temperature and pressure dependent thermodynamic equation described by Tromans (1998):

$$c^*(T) = pO_2 * \exp\left\{\frac{0.046\ T^2 + 203.357\ T \ln\left(\frac{T}{298}\right) - (299.378 + 0.092\ T)\ (T - 298) - 20.591{*}10^3}{R\ T}\right\} \tag{5}$$

$R$ represents the ideal gas constant and $T$ the temperature in K.

## Determination of Oxygen Solubility in Medium

To investigate the solubility of oxygen in the presence of (non)ionic compounds and sugars, the solubility in the cell culture medium was determined experimentally as described by (Storhas, 2018). Briefly, in two steps, either oxygen saturated or degassed RO-$H_2O$ with known Henry coefficient was mixed in equal amounts with the cell culture medium and the resulting dissolved oxygen concentration was measured ($DO_1$). The second value ($DO_2$) is determined using the same liquids with vice versa oxygen saturations. The obtained difference was used to correct the maximum absolute oxygen saturation in media.

## $CO_2$ Influence on Solubility in Medium

Changing $CO_2$ concentrations in the gas inlet due to pH control influence the oxygen solubility in the culture. To analyze the maximum saturation in the presence of $CO_2$, gassing experiments applying up to 20% (v/v) $CO_2$ in process air were performed and the maximum oxygen solubility in cell culture medium recorded.

**TABLE 1 |** Overview of all bioprocess runs at different parameter settings.

| Bioprocess run | Shift 1 (72 h) | Shift 2 (120 h) | Shift 3 (192 h) | Shift 4 (240 h) |
|---|---|---|---|---|
| 1 | 36.3°C/F3 | – | – | – |
| 2 | 36.3°C/F3 | – | – | – |
| 3 | 34°C/F1 | – | – | – |
| 4 | 37°C/F3 | - | 37°C/F1 | - |
| 5 | 34°C/F2 | 37°C/F2 | 34°C/F1 | 31°C/F1 |
| 6 | 31°C/F2 | 34°C/F2 | 37°C/F3 | 34°C/F3 |
| 7 | 34°C/F1 | 31°C/F1 | 31°C/F2 | 34°C/F2 |
| 8 | 37°C/F2 | 34°C/F3 | 31°C/F2 | 34°C/F1 |
| 9 | 34°C/F3 | 37°C/F2 | 31°C/F2 | 37°C/F3 |
| 10 | 34°C/F2 | – | – | – |
| 11 | 34°C/F2 | – | – | – |
| 12 | 34°C/F2 | – | – | – |
| 13 | 34°C/F2 | – | – | – |

*Intra-experimental variations were performed at four shifts in temperature (31, 34, or 37°C), additional D-glucose concentration in the feed medium (+10, +20, or +30 g $L^{-1}$; identified as F1, F2, F3), or both.*

## Fed-Batch Experiments

### Cell Line Propagation

We used a recombinant monoclonal Chinese Hamster Ovary (CHO) cell line (Antibody Lab GmbH, Austria) generated by the *Rosa26* Bacterial Artificial Chromosome (BAC) strategy (Zboray et al., 2015) using a serum-free derivate of CHO-K1 (ATCC CLL-61) as the host. The cells produce an IgG1 monoclonal antibody. The cell line was cultured in chemically defined cell culture medium (Dynamis AGT, A26175-01, Thermo Fisher Scientific, USA) supplemented with 8 mM L-glutamine. The cells were maintained in shake flask cultures at 37°C in a humidified incubator under 5% (v/v) $CO_2$ in air, shaken at constant rpm and passaged every 3–4 days for propagation and scale-up. After four passages, the bioreactor was seeded at a density of $2.5 \times 10^5$ cells $mL^{-1}$.

### Bioprocess

Thirteen CHO cultivations were performed in a chosen (DoE) setting with either static or dynamic changes (intra-experimental shifts) in two varying parameters. The changeable parameters were temperature and variable D-glucose concentration in the feed medium (see **Table 1**). For simplification, runs 1 and 2 were treated as processes performed at 37°C.

The feed medium (CHO CD EfficientFeed A, A1442001, Thermo Fisher Scientific, USA) was supplemented with 0.1% (v/v) antifoam C (A8011, Sigma Aldrich, Germany) and additional 10, 20, or 30 g $L^{-1}$ D-glucose and 7 g $L^{-1}$ L-asparagine monohydrate. Temperature was maintained at 37°C during the batch phase and changed after 72 h to 31 or 34°C or remained constant according to the pre-defined experimental set-up. The minimum DO level was set to 30% of saturation and maintained by gassing with process air (PA) flow and increasing stirrer speed. The agitation rate was variable, from 91 to 228 rpm and the gas-flow range was 0.3–1.5 L $min^{-1}$ (maximum values at maximum PID controller output). The culture pH was kept constant at 7.0 and controlled via the $CO_2$ gas flowrate. Base addition was not necessary.

## Off-line Analyses

The total cell concentration (TCC) was determined by counting the cell nuclei using the particle counter Z2 (Beckman Coulter, USA). Therefore, an appropriate amount of cell suspension was centrifuged at 200 *g* for 10 min. The cell pellet was resuspended in 0.1 M citric acid monohydrate and 2% (v/v) Triton X-100 buffer to lyse the cells, for a minimum of 1 h before measurement. Sample dilution was performed using a 0.9% (m/m) NaCl solution.

Culture viability was assessed using a hemocytometer and trypan blue exclusion. The viable cell concentration (VCC) was calculated by multiplying viability by TCC.

Packed cell volume (PCV) was measured using PCV tubes (#87007, TPP, Switzerland) after spinning the cell suspension for 1 min at 2,000 *g*. PCV is expressed as a percentage (%v/v) of the total culture volume. Determinations were performed in duplicates. Viable PCV was determined by multiplying the viability by the PCV.

Carbohydrates were determined via ion exclusion chromatography (HPX 87H, 300 × 7.8 mm, #1250140, BioRad, USA) on an Agilent 1200 series (Agilent, USA) at 25°C. The mobile phase consisted of 5 mM sulfuric and the flow rate was set to 0.45 mL $min^{-1}$. Measurement was performed using a Refractive Index detector (35°C). The calibration range for D(+)-glucose was 100–2,000 mg $L^{-1}$. The chromatograms were evaluated using Chemstation software (revision B.04.01, Agilent, USA).

The amino acid concentrations were determined by HPLC. After using an automated pre-column derivatization method, amino acids were separated on a chromatography column (Eclipse Plus C18 column) at 40°C using a flow rate of 0.64 mL $min^{-1}$. As solvent A 10 mM $K_2HPO_4$ and 10 mM $K_2B_4O_7$ and Solvent B an acetonitrile, methanol, water mix (45/45/10; %v/v/v) was used. Amino acids were excited at 230 nm and the fluorescence signal was detected at 450 nm for OPA derivatives and at 266/305 nm for FMOC derivatives. Samples were quantified using an internal standard calibration.

## Assessing Model Accuracy

To compare the model's quality, accuracy, and overall performance, the mean absolute percentage error (MAPE) was calculated. Errors were normalized by the inverse of the number of fitted points ($n$) regarding the sum of deviation from actual values ($x_i$) to forecast values ($x_{target}$) divided by the actual value again, calculated as a percentage error (%) as described in Equation (6):

$$MAPE = \frac{\sum_{i=1}^{n} \left| \frac{x_i - x_{target}}{x_i} \right|}{n} * 100 \quad (6)$$

# RESULTS

## Assessing Parameters for Dynamic $k_La$ Estimation

As oxygen transfer is determined by the system's operational and physicochemical characteristics, varying process conditions can affect the oxygen solubility and mass transfer properties and need to be taken into account for $k_La$ model development.

Viscosity behavior was investigated using the harvest samples of bioprocess run 2 and media supplemented with antifoam at two different temperatures (30 and 37°C; **Figure 1A**). The viscosity was close to that of water and significant changes between the media and harvest sample were not observed. Due to the insignificance of the divergence, viscosity changes were not implemented in the present model.

Osmolality within all presented fed-batch processes was 295 ± 26 mOsm $kg^{-1}$. Similar to the viscosity, the minor osmolality variations were assumed to only minimally influence the maximum oxygen solubility in culture medium or the $k_La$ and therefore, were neglected.

Volumetric mass transfer coefficients were measured in a chosen process design space (**Figure 1B**). Process air and stirrer speed variation were linked in the PID controller output; therefore, the influence on $k_La$ was quantified based on the percentage of the PID controller output. During all fermentations, the main operational space increased to a maximum PID controller output of 65%. At maximum operational stirrer speed (PID65 = 160 rpm), a specific agitation power of 12 W $m^{-3}$ was calculated.

The volume dependency of $k_La$ between 10 L (inoculum) and 15 L (max. working volume) was investigated experimentally. No significant volume influence on $k_La$ was determined in the bioreactor system.

As the pH in mammalian cell culture processes is typically controlled by varying the $CO_2$ concentration in the inlet gas, the maximum oxygen solubility in cell culture medium was determined under varying $CO_2$ molar fractions in the gas in-flow (**Figure 1C**). Gassing with ambient air led to a maximum relative solubility of ∼95 % in media compared to water under the same settings. This result is in accordance with the experimentally determined maximum oxygen solubility in medium compared to water using the method described by (Storhas, 2018), resulting in a decrease of 5.2% in culture medium compared to RO-$H_2O$. With increasing molar fractions of $CO_2$ the oxygen solubility dropped to 82% at a molar $CO_2$ fraction of 20%. The resulting linear fit was incorporated into the model to account for $O_2$ displacement by $CO_2$ (Equation 8).

The physicochemical properties of the culture medium had a strong positive impact on $k_La$ values in this bioreactor setup (**Figure 1D**). The $k_La$ values determined with medium were more than 3-times higher than those generated with water in the presence of 0.1% v/v antifoam solution. A linear increase was observed in $k_La$ in cell culture medium with increasing PID (PID = f($v_s$,*rpm*). The increase in superficial gas velocity together with increasing stirrer speed as a function of PID output had the greatest impact, whereas temperature had only a slight effect. A linear curve fit was created with averaged triplicate values. The $k_La$ determination in medium was performed up to a PID controller output of 60%, with linear extrapolation of higher values. This function was used to estimate $k_La$ in real-time throughout the process as the PID set-up was the same for all fed-batches. By determining factors that directly influence oxygen solubility, several correlations have been developed for the prediction of $k_La$ (Gill et al., 2008; Garcia-ochoa and Gomez, 2009). The most common and conventional approach is based on the energy input criterion. However, direct relation of $k_La$ dependence to volumetric power consumption ($P_g/V_L$) or superficial gas velocity ($v_s$) was not necessary due to coupling via the PID controller. The simplified model $k_La = f(T, PID)$ is only true within the chosen process space and needs to be adapted for prevalent use. As an alternative, computational fluid dynamics (CFD) simulations can provide a tool for predicting $k_La$ on larger scales in which the location of the oxygen probe in the bioreactor plays a significant role (Kerdouss et al., 2008; Wutz et al., 2016).

## OUR Model Set-Up

OUR at time point $t$ is a function of the dynamic $k_La$ and the oxygen solubility at given temperature $c^*(T)$ as described in Equation (7) (adapted from Equation 2).

$$OUR\,(t) = k_La_{dyn.}\,(t) * \left(c^*_M\,(t) - c_{DO}\,(t)\right) - \frac{dC}{dt} \tag{7}$$

Dissolved oxygen concentrations with the subscript DO were obtained from the DO values measured by the oxygen probe. The *dC/dt* term equals zero if DO is constant. At the beginning of the processes, when DO was not constant, *dC/dt* in the short interval of on-line recording (seconds) was much smaller than OUR. Therefore, *dC/dt* was neglected for the on-line OUR calculations described in this work.

Oxygen solubility in fermentation medium $c^*_M(t_1)$ was calculated using the thermodynamic equation in the presence of medium solutes (Equation 8) and accounts for the $O_2$ displacement by $CO_2$.

$$c^*_M\,(t_1) = c^*(T)\left(\frac{-0.638^* y_{CO_2}(t_1) + 95.63}{100}\right) \tag{8}$$

with

$$y_{CO_2} = \frac{Q_{CO_2}}{(Q_{PA} + Q_{CO_2})} * 100 \tag{9}$$

Q represents the inlet gas flowrate of $CO_2$ ($Q_{CO2}$) and process air ($Q_{PA}$) gathered from the mass flow controller. Therefore, $c^*_M(t_1)$ is dependent on the process temperature and amount of dissolved $CO_2$.

$DO(t_1)$ is the dissolved oxygen measured at the respective time point. In addition, as the used DO probe performs an internal temperature correction, a correction factor was introduced for the temperature dependence of the actual oxygen saturation. $c_{DO}(t1)$ is then defined as described in Equation (10):

$$c_{DO}\,(t_1) = c^*_M\,(t_1) * \left(DO\,(t_1) * \frac{c^*\,(T_1)}{c^*\,(T_2)}\right) \tag{10}$$

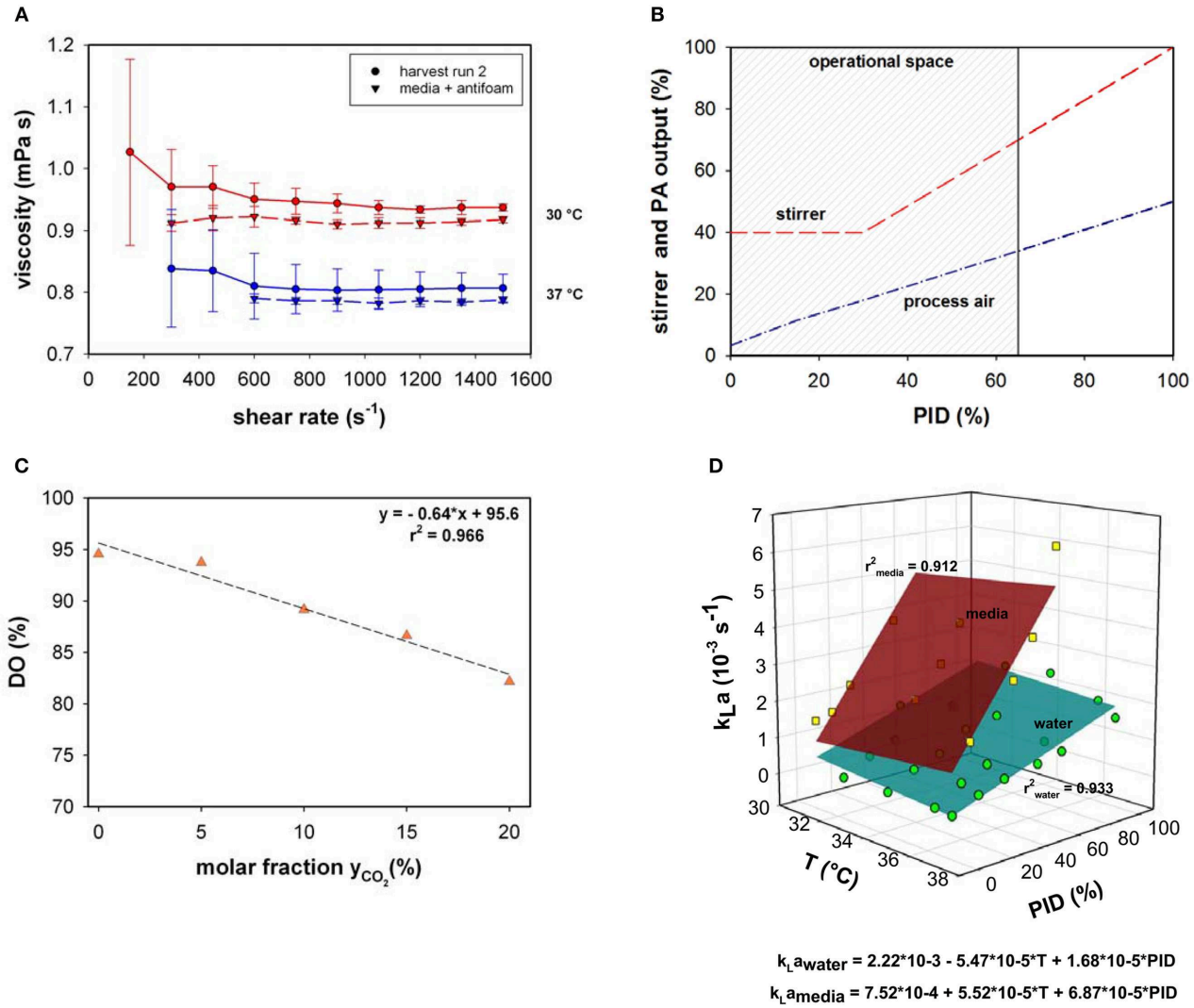


**FIGURE 1 | (A)** Viscosity as a function of shear rate measured in cell suspension and media supplemented with antifoam at 30 and 37°C. **(B)** Stirrer speed and process air (PA) output as a function of PID controller output (%). **(C)** Relative dissolved oxygen saturation (DO%) determined in medium upon variation of the molar $CO_2$ fractions in the inlet gas compared to RO-$H_2O$. **(D)** $k_La$ as a function of temperature ($T$) and PID controller output (%) for water and culture medium supplemented with 0.1% v/v antifoam solution.

## Assessing the Model Performance

During the dynamic fed-batch processes (see **Table 1**) up to four temperature shifts were applied to capture the process dynamics (**Figure 2A**). Process air-flow at the beginning of the process was usually set to 0.3 L $min^{-1}$ to constantly strip $CO_2$, and increased with cell density when the set point of 30% DO was reached (**Figures 2A,B**).

Temperature-shifts influenced the PID output, as a reason of the temperature dependency of the maximum oxygen solubility. It follows that the temperature shifts are also evident in the concentration gradient (**Figures 2A,C**). With changing PID output and temperature, $k_La$ changes over the progression of the fed-batch process. These dynamic profiles are very similar to those of the PID and PA-flow, as the main factor influencing $k_La$ within the chosen process space is the superficial gas velocity (**Figures 2B,C**). After temperature correction and incorporating oxygen solubility, the OUR profile is calculated in real-time (**Figure 2D**).

Total amounts of mol $O_2$ consumed during each process were determined for five bioprocesses (**Figure 3A**). The results obtained with the generated model and values calculated by the mass-balance method were in good agreement (Equation 4). The $O_2$ solubility approach in medium compared to the mass-balance method for all runs obtained slightly lower values. The mean relative deviation of the model compared to off-gas analysis was 8%. Due to humidity in the off-gas stream as well as handling errors, not all reactor runs could be evaluated by mass balance.

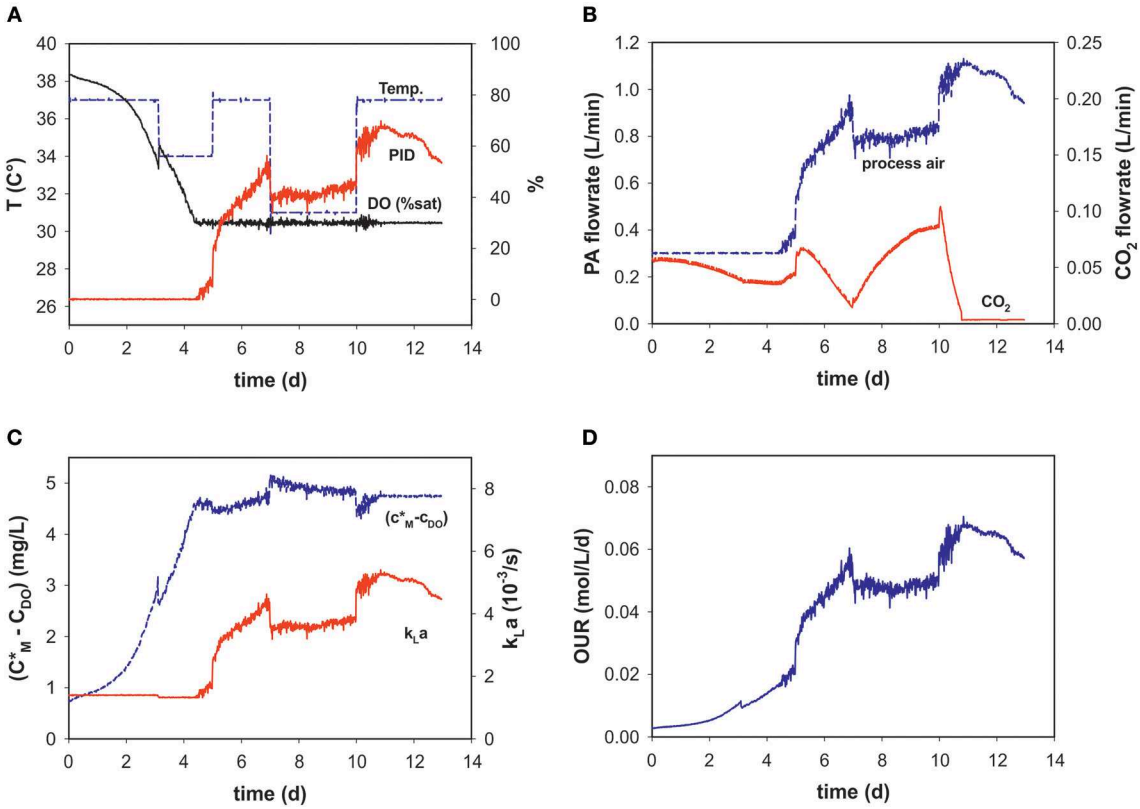


**FIGURE 2 |** Process variables **(A)** temperature (*T*), dissolved oxygen (DO% sat), and PID output (%), **(B)** process air (PA) and $CO_2$ flow rates, **(C)** calculated solubility difference ($c^*_M$-$c_{DO}$), $k_La$ and **(D)** OUR over the time course of an intensified fed-batch process (run 9).

For example, **Figure 3B** shows the calculated OUR trend of a static fed-batch (run 3) in the developed model and the mass-balance method over the duration of cultivation. The same trends were gathered from both methods. However, the generated model seems to be unaffected by process disturbances. In particular, the rate calculation at the beginning of the processes, was mostly negative for the gas balancing method, whereas the soft-sensor illustrates the initial process phase in an exponential increase. Step changes and fluctuations during the process (especially temperature shifts) also impacted other reactor runs for the mass-balance method.

## Linking OUR to Cell Numbers

In principle, estimation of the OUR provides broad information on cell performance during the process. The OUR is the direct product of specific consumed oxygen rates ($q_{O2}$) and the number of viable metabolically active cells. Thus, the OURs calculated by the model can be theoretically given as a function of VCCs measured off-line at each time point (**Figure 4A**). However, the OUR was linearly dependent only up to a cell concentration of $\sim 10^7$ cells $mL^{-1}$. At higher cell densities and later process stages, variations occur and the data are widely scattered: OURs no longer exhibit a clear relationship with the VCC. The data distribution indicates two process stages in the cells. Volumetric oxygen uptake is temperature-independent in a sigmoidal progression of cell numbers. The cell-specific oxygen consumption rate ($q_{O2}$) is independent on the growth rate ($\mu$) and the cell cycle, with constant, but temperature-dependent behavior (**Figure 4B**). Linear regression was carried out for each culture temperature.

## Linking OUR to Cell Volume

An alternative means for biomass quantification in cell culture processes is the determination of PCV, which represents the average cell volume and closely correlates with oxygen uptake (Wagner et al., 2012). A growth profile comparison of cell numbers and PCV showed different curve characteristics (see **Appendix Figure 1**). Due to intra-experimental shifts in two parameters (added D-glucose in the feed medium and culture temperature), the viable PCV data as a function of time in all fermentation runs spanned a broad range. Nevertheless, these variations are not visible when correlating the viable cell volumes measured off-line to the OURs of all runs (**Figure 5A**).

**Figure 5A** shows that the magnitude of the OUR was highly dependent on PCV. No significant temperature dependence or association to the cell viability (>80%) was evident. The data are less scattered and a more accurate correlation, in comparison to cell number is observed. However, the OUR as a function of PCV exhibited a sharp kink at ~1.4% (v/v) PCV. Thus, a linear regression was calculated for each section. For this purpose,

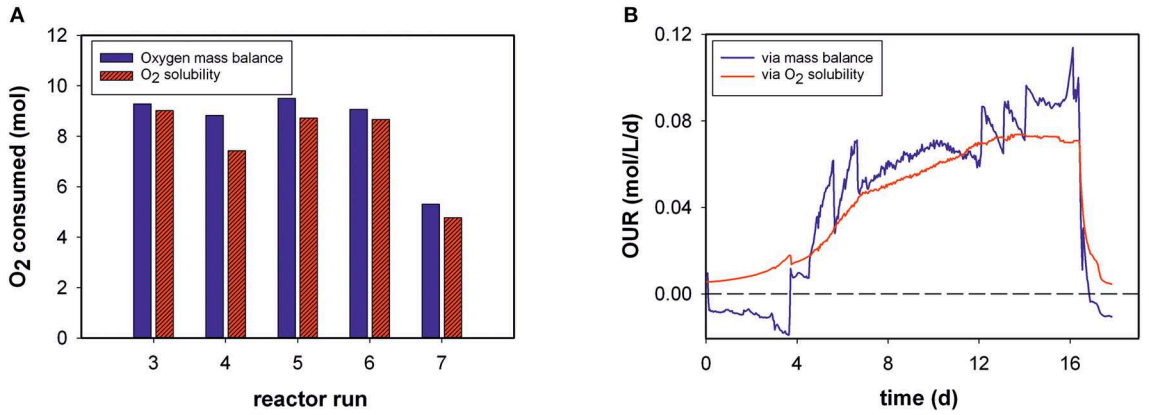


**FIGURE 3 | (A)** Total oxygen consumption determined by the two different methods for five bioprocesses **(B)** Volumetric oxygen uptake rates (OURs) over the time course of fed-batch run 3. For clarity, only every 20th data point is displayed.

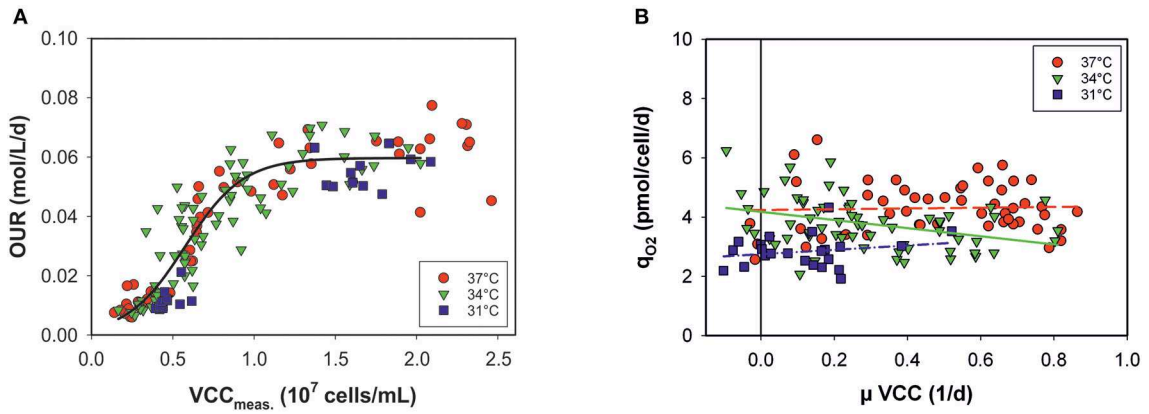


**FIGURE 4 | (A)** Volumetric oxygen uptake rates (OURs) as a function of viable cell concentrations (VCCs) measured off-line for all bioprocesses. Data <80% viability were excluded. **(B)** Specific consumed oxygen rates ($q_{O2}$) as a function of the growth rate (μ) for three culture temperatures (31, 34, and 37°C).

the data were divided into a training data set and a test data set. The test set consisted of three similar experiments with static conditions (runs 10, 11, and 12). All other experiments were used for development of the model. The optimal point of intersection between the two linear fits was calculated iteratively at 1.395% (v/v) PCV. For the first section, a linear function of $f_1 = 0.042^*x - 0.011$ and for the second one $f_2 = 0.001^*x + 0.032$ was calculated, where the slope $k$ represents the specific uptake rate per cell volume in the respective section. After the transition, the OUR decreased and $k_2$ was roughly one-fourth the value of $k_1$. The error for the biomass prediction was calculated as MAPE = 19% for the training data set and 14% for the test data set (**Figure 5B**). Good performance of the predicted PCV was also seen in comparisons with the real PCV data for the test data sets (**Figure 5C**) over the time course of the process. Interestingly, two growth curves (runs 12 and 13) were still during exponential growth phase when reaching a PCV of ∼1.4% (v/v). Therefore, partitioning the data into two stages could not be linked to the cell cycle (growth and maintenance).

## Capacitance Measurements for Soft-Sensing of Cell Volumes

Off-line PCV data correlated with the permittivity and conductivity signals of an on-line capacitance probe (**Figure 6A**). The permittivity exhibited linear behavior relative to the viable PCV, and conductivity output was used to correct the model for temperature changes. The cell factor determined by linear regression was used to predict the viable PCV. Again, data were split into a training data set and a test data set and the model's performance was evaluated using $MAPE_{training}$ = 15% and $MAPE_{test}$ = 18% for the on-line biomass soft-sensor (**Figure 6B**). The on-line soft sensor estimated the PCV trends for the test data sets over time in a meaningful manner (**Figure 6C**).

## Monitoring Metabolic Transitions

The transition step in the OUR profile indicated that a metabolic shift occurred (see **Figure 5A**) at a viable PCV of 1.4% (v/v) in the given process set-up.

The evolved OUR model combined with the viable PCV predictions via on-line permittivity and conductivity signals from

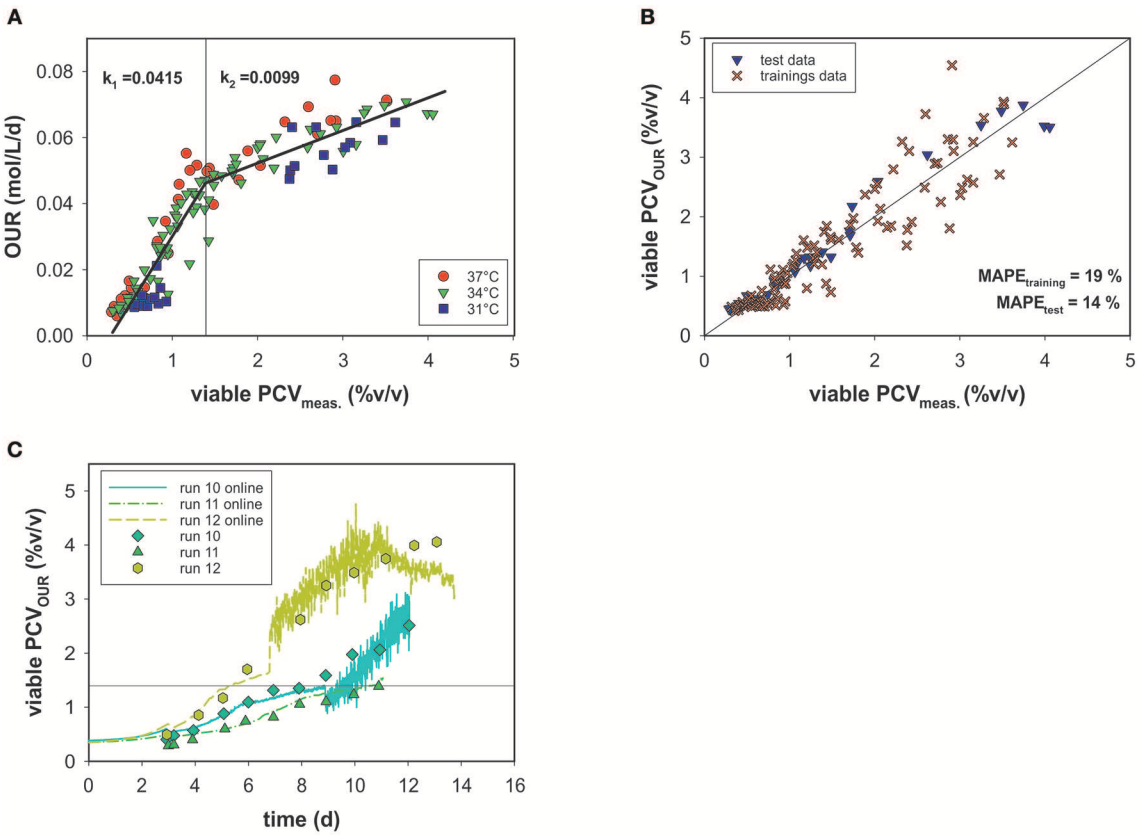


**FIGURE 5 | (A)** Linear correlation of OUR and viable PCV for three culture temperatures (31, 34, and 37°C). Data with <80% viability were excluded. **(B)** PCV estimated by the segmented linear model vs. viable off-line PCV data. **(C)** PCV model predictions over time for the test data compared to values measured off-line.

a capacitance sensor of all fed-batch runs is shown (**Figure 7A**). The combination of the two models led to the development of an on-line metabolic soft-sensor (see **Appendix Figure 3**). Hereby, the objective function is that the linear function $PCV_{OUR}$ (function 1) must intercept with $PCV_{OUR}$ (function 2) and the $PCV_{capacitance}$. The sensor specifies the first metabolic state with the value 0 and the second with the value 1. If both conditions are fulfilled, hence, a metabolic shift is evident, the sensor jumps from 0 to 1. For 12 runs the application of the metabolic sensor was successful. In average, the metabolic shift was detected at a viable PCV of ∼1.4% (v/v). As an example, the performance of run 12 is depicted in **Figure 7B**. During the process the metabolic shift can be traced by the output signal of the metabolic sensor.

The variations in the amino acid concentrations of glutamine (Gln), glutamate (Glu), asparagine (Asn), aspartate (Asp), and alanine (Ala) are of particular importance in mammalian cell culture (Zhang et al., 2016). Though Glu and Gln exhibited a similar trend over the course of the fed-batch for all experimental runs, Ala, Asn, and Asp progressed differently (see **Appendix Figure 2**).

In a recent study, the ratio of asparagine and glutamine was found to be important, to some extent, in terms of process performance (Zhang et al., 2016). However, glutamine was depleted and asparagine concentrations were sufficiently high throughout the process (**Figure 7C**) and did not exhibit significant dependence. In the metabolic fate of glutamine and asparagine, glutamate and aspartate, respectively follow as secondary key products (**Figure 7D**). The Asp concentration decreased, whereas the Glu concentration increased consistently. These amino acids exhibited a linear relationship with OUR (data not shown).

Glu and Gln as a function of PCV exhibited reciprocal behavior. At ∼1.4% (v/v) PCV, glutamine was almost completely consumed and glutamate plateaued at ∼6 mM (**Figures 7C,D**).

The Asp/Glu ratio as a function of PCV exhibited a significant pattern (**Figure 7E**). The Asp/Glu ratio decreased linearly. At a PCV value of ∼1.4% (v/v), the progression bent and resulted in a shallower slope. Accordingly, at an Asp/Glu ratio of 2, cell volumes and specific OURs changed after a metabolic alteration. The observed inflection point was at the same value as in the OUR vs. PCV regression (1.4% (v/v) PCV; see **Figure 5A**).

The Ala profile suggested the same metabolism switch (**Figure 7F**). The Ala concentration slightly increased at high Asp/Glu ratios until a certain point (around 2), when Ala production started to increase steeply (Asp/Glu = low). Ala accumulated in the cell culture supernatant to a great extent.

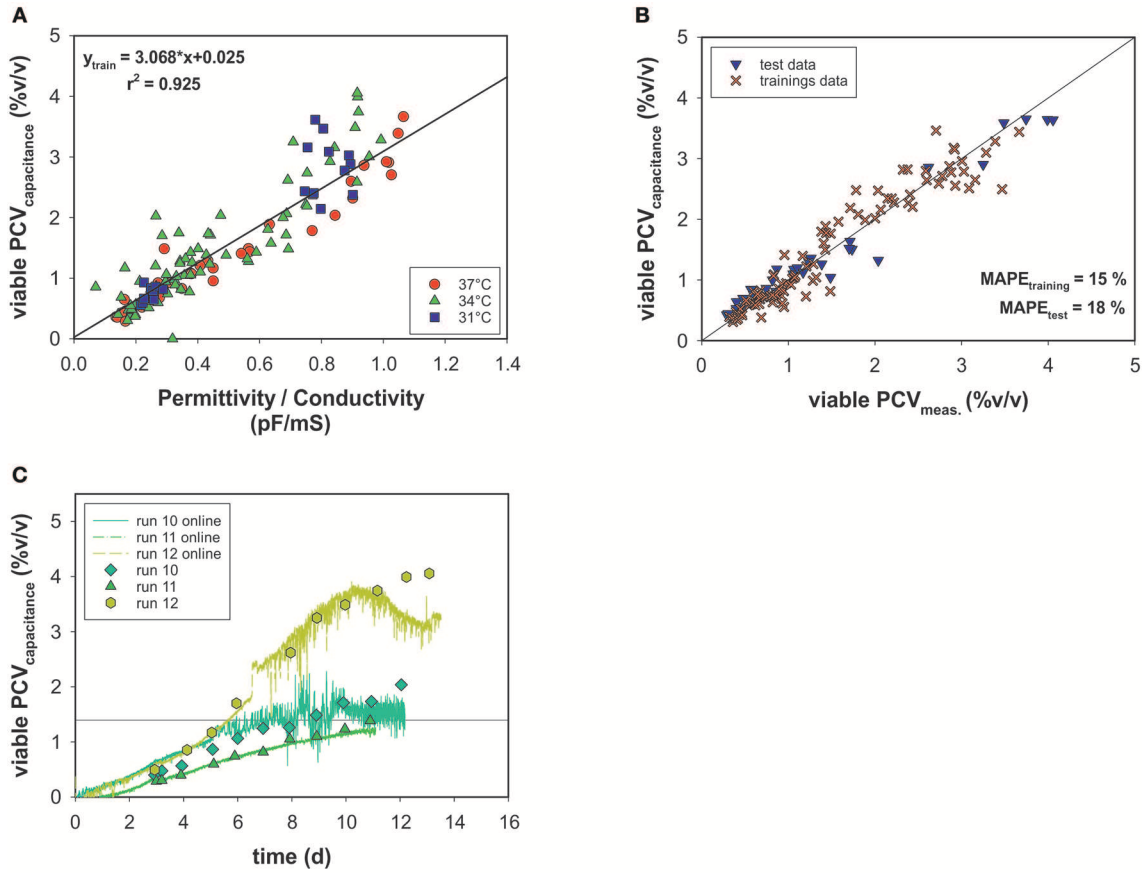


**FIGURE 6 | (A)** Linear model of on-line capacitance signals as a function of viable PCV off-line data. **(B)** Estimated vs. real off-line PCV. **(C)** PCV capacitance model predictions over time for the test data.

# DISCUSSION

## Benefit of Dynamic $k_La$ Determination and Real-Time OUR Calculation

The dynamic technique for $k_La$ determination provided reliable results. We showed that the assumption of a dynamic volumetric mass transfer coefficient is necessary to calculate the OTR and, subsequently, the OUR throughout a changing process. Temperature and PID controller output were the two main bioreactor operating variables affecting the OTR in this setting. The influence of physicochemical properties of certain substances in the cell culture medium led to a strong $k_La$ increase more than 3-times higher compared to water. This is probably due to the presence of Pluronic F68 within the medium, which has been reported to mainly change bubble size at higher concentrations. Smaller bubbles lead to an increase in gas holdup and available surface areas for overall mass transfer (Sieblist et al., 2013). Similar results were reported in the presence of ionic solutes, which generally exhibit coalescence-inhibiting characteristics, resulting in smaller bubbles and greater surface area and overall $k_La$ (Puthli et al., 2005). Moreover, the effects of so-called oxygen vectors (e.g., hydrocarbons, oil as antifoam agents) can enhance mass transfer rates to significantly higher levels than in water. The enhancement was mainly due to an increase in the air/water transfer rate, which is partially explained by the change in the water surface tension (Morao et al., 1999; Quijano et al., 2009).

According to these observations, the influence of culture medium composition on oxygen mass transfer has to be considered. Moreover, a maximum decrease was recorded in the relative oxygen saturation of ∼18% in fed-batch medium during $CO_2$ stripping. These results demand particular consideration of solubility changes with shifts in gas composition and temperature. Considering only the saturation $O_2$ concentration in water instead of determining the prevailing saturation concentrations would lead to inaccuracies during specific OUR calculations (Henzler and Kauling, 1993).

The application of the dynamic OTR as a soft-sensor for calculating the OUR is demonstrated by the highly linear relationship between OUR calculated by a global mass-balance and OUR calculated by the model for a wide range. The presented model enables real-time prediction of the OUR without sophisticated off-gas measurements. The advantage of this approach is that it is simply based on DO measurement, knowledge of oxygen solubility properties in the medium, and recording process temperatures, pressure and volumetric inlet flow- rates of PA and $CO_2$. The established model

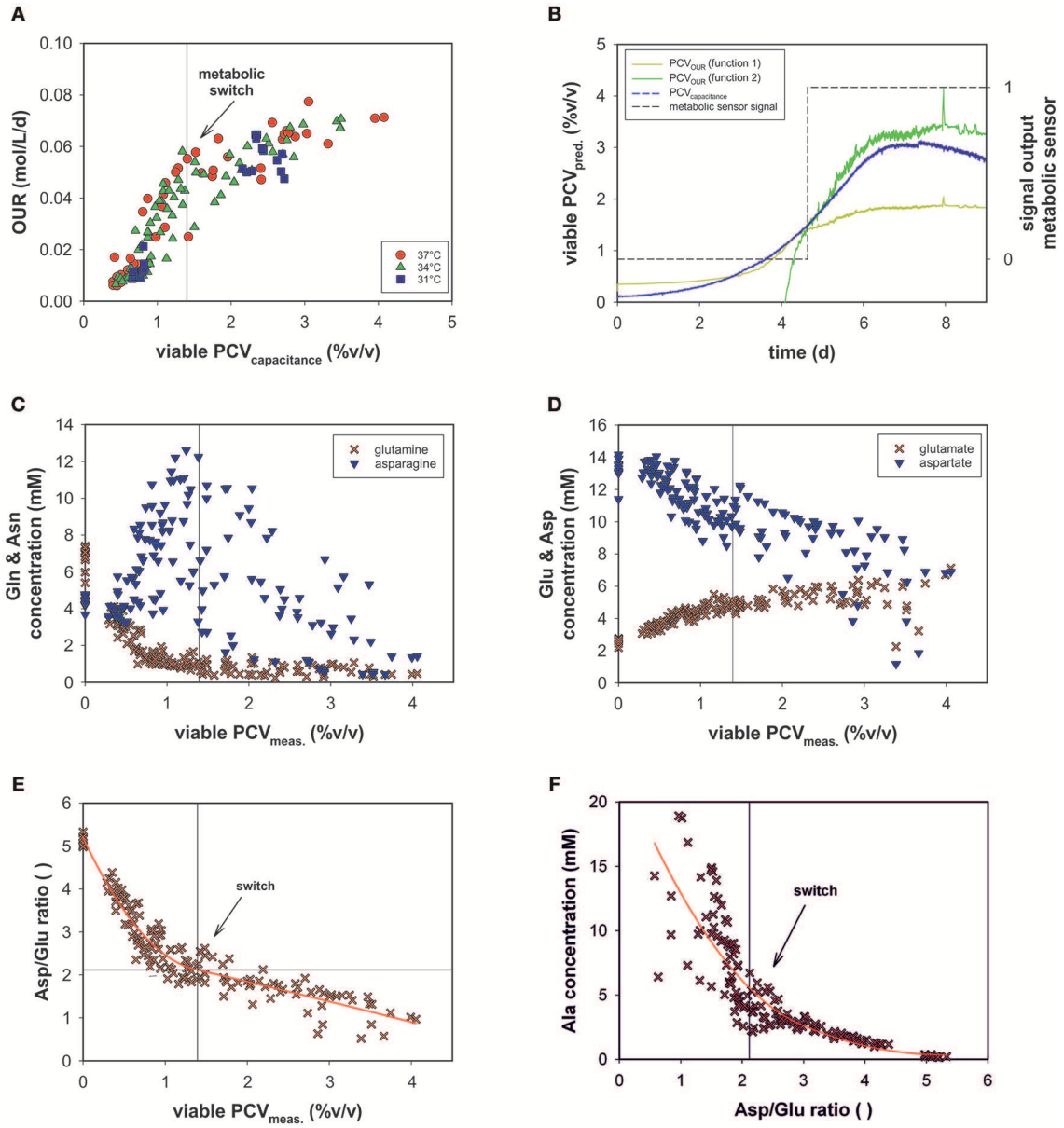


**FIGURE 7 | (A)** OUR combined with PCV prediction by on-line capacitance probe signal of all bioprocesses. **(B)** The performance of the metabolic sensor in run 12 predicts the metabolic shift occurring in the culture. **(C)** Metabolic profiles of all fed-batch runs of glutamine (Gln) and asparagine (Asn) **(D)** glutamate (Glu) and aspartate (Asp) as a function of viable PCV. **(E)** The ratio of aspartate/glutamate (Asp/Glu) vs. viable PCV. **(F)** Alanine concentration (Ala) vs. the Asp/Glu ratio.

is in good agreement with the conventional technique. The minor off-set due to the inlet gas flow temperature for the mass-balance method was not determined, as it was generally assumed to be 22°C. More importantly, the generated profiles were smooth and, even at temperature shifts, no great disturbances were observed. Due to fluctuations from the off-gas analyzer, the methods could not be compared for every process run.

Overall, the established model with incorporated dynamic $k_La$ determination demonstrated high potential for online monitoring of (specific) OURs during a cell culture bioprocess. This concept can be realized for all aerobic bioprocesses. However, in the field of microbial fermentation, where the $k_La$ values can be up to more than 10-times higher, the probe response time used for $k_La$ determination needs to be considered.

Moreover, the developed method has high potential in parallel bioreactor systems since it only relies on physical parameters. Therefore, once one bioreactor is characterized, the model may be transferred to all equivalent ones. However, in small-scale systems the experimental design may need to be adapted due to diverging influence factors arising from difference in scales or media.

## Application of Dynamic OUR for Cell Monitoring

In principle, an estimation of the OURs provides broad information on the overall process performance during the process but does not report detailed information about cell growth and physiology. The OUR is the direct product of the specific consumed oxygen rate $q_{O2}$ and the biomass (Wagner et al., 2012). Conclusively, the prediction of biomass via oxygen consumption should be possible if $q_{O2}$ was constant over the process progression.

Temperature changes impact cell growth and size, and this applies to respiration as well (Moore et al., 1997; Goudar et al., 2011). By presenting the OUR as a function of viable cell concentration, no clear temperature dependency was observed (see **Figure 4A**). Data from all bioprocesses were equally distributed in a sigmoidal progression. At later process stages no linear behavior was observed between the OUR and VCC. After a switch in the cellular metabolism, OURs seem to approach a plateau, independently of increasing cell concentrations. However, the cell physiology changed during the progression, affecting the OUR but this was not accounted for by the model. A minor temperature influence on $q_{O2}$ was observed when plotted against the growth rate, $\mu$, of the viable cells. Cells seem to require less oxygen at lower temperatures. Nevertheless, a dependency on cell cycle and growth was ruled out.

Applying the model for accurately predicting viable cell number has its limitations, especially during later process stages, most likely due to changes in the cell size. In this study, we showed that oxygen consumption is rather related to cell volume than to cell count. Another study has also pointed to this fact (Wagner et al., 2012). A segmented linear model was established, able to cope with the metabolic shift occuring during the process. Remarkably, the clear metabolic shift was evident for all process runs despite massive variations within the design space and the segmented linear model could cope with it. The prediction error was calculated using a $MAPE_{training}$ of 19% and $MAPE_{test}$ of 14%, but due to the shallower slope in the second segment, the PCV prediction was more prone to error at higher cell volumes. This can be explained by the fact that cell growth includes an increase in both cell volume and number. Thus, deviations occur, particularly in stationary and death phases, when cell lysis is followed by the presence of cell fragments and increased aggregates (Lovrecz and Gray, 1994). The shift in the metabolic state of the cells led to roughly a quarter less oxygen consumption in the second stage, which may be driven by a truncated TCA cycle (**Figure 8**). Glutamine and other amino acids can have alternative fates entering the citrate cycle to supply ATP and/or NADPH. In a truncated cycle, less energy is produced and less oxygen is consumed. The OUR soft-sensor allows the

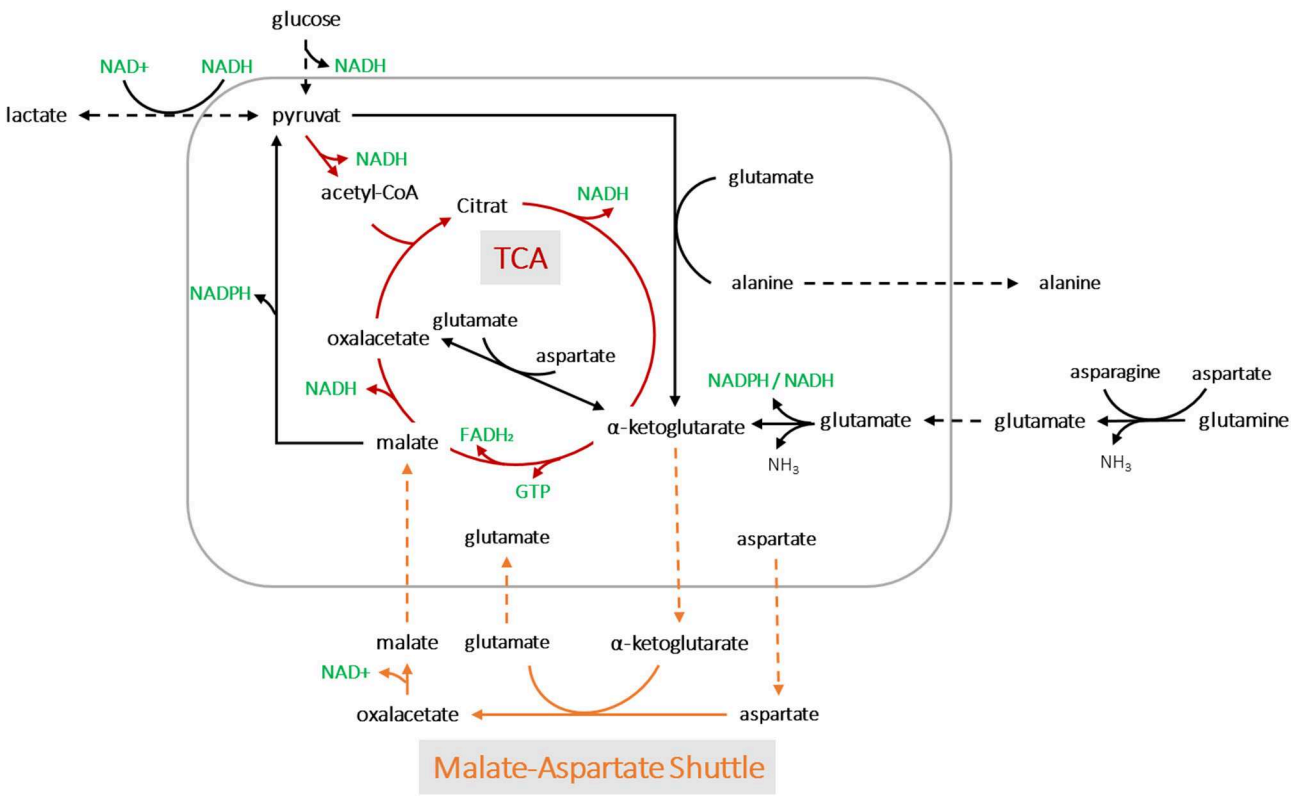


**FIGURE 8 |** A simplified metabolic network of CHO-K1 cells. The detection of two metabolic states led to possible pathway assumptions in the TCA cycle and amino acid metabolisms for product synthesis.

viable cell volume to be predicted with reasonable accuracy. The method represents a simple and economic solution for bioprocess monitoring as no additional (off-gas) sensor systems are required.

### On-line Soft-Sensing of Cell Volumes Using a Capacitance Probe

The on-line monitored permittivity signal during each bioprocess was converted directly into a more meaningful dimension, the viable PCV, using the correlation (cell) factor predetermined with a linear regression. As a result, a temperature-independent function was generated using the conductivity signal for temperature correction, but no metabolic transition was observed. The estimated vs. measured values exhibit a normal distribution and, with respect to accuracy, all states could be determined with an adequate MAPE which is comparable to deviations in the two-segment linear model predictions (**Figure 6B**). The trends for the test data set were calculated with acceptable estimated errors: a drift in the estimation was observed only in the stationary and death phases. The time-resolved information obtained by the soft-sensor could be linked to the OUR soft-sensor for real-time identification of metabolic behavior in mammalian cell culture processes.

### OUR as a Metabolic Sensor

We assumed that varying process conditions (e.g., altered temperature profiles and D-glucose concentrations) during all bioprocesses may trigger different cellular responses with respect to oxygen consumption. However, all cells tended to alter their metabolic activity to a different state at a certain point, regardless of whether they were cultured in a dynamic or static process. In all fed-batch cultivations, we observed a clear effect of Gln consumption on the excretion of ammonia, Ala and Glu, as expected due to their direct connection to Gln metabolism (Doverskog et al., 1997; Zhang et al., 2016). A clear link was also evident between Asp and Glu (see **Figure 7D**). Both amino acids could be linearly linked to viable PCV; Glu increased constantly, whereas Asp was fleetly consumed. Asn can be converted into Asp and then further into Glu, followed by the building of alpha ketoglutarate. However, after a certain threshold [1.4% (v/v) PCV] presumably caused by a high glutamate concentration, the cells were assumed to be pressured to break down Glu and build alpha ketoglutarate out of pyruvate. Accordingly, Ala was produced and transported out of the mitochondria (see **Figures 7F**, **8**). This behavior has been described in several publications (Altamirano et al., 2001; Sellick et al., 2011; Duarte et al., 2014; Pereira et al., 2018). Most interesting is the fact that this switch happened at an Asp/Glu ratio of ∼2 (**Figure 7E**). We propose that, at this threshold, the cells tend to by-pass the citrate cycle, resulting in less oxygen consumption (see **Figure 8**). The results indicate that Asp and Glu, in particular, need to be taken into consideration to maintain the respiratory activity and energy metabolism.

The combined technique presented here (capacitance and OUR) will add great value for process characterization and allow the development of control algorithms, especially to maintain respiratory activity. The technique exemplifies a simple tool for metabolic sensing. The metabolic status of the cultured cells can be tracked in real-time. To the best of our knowledge, real-time estimation of a metabolic transition in mammalian cell culture processes has not been reported previously. Future research in this field could include investigations of detailed amino acid fluxes, as well as the dependence of product titer on OURs.

## CONCLUSION

We have demonstrated that simple bioreactor characterization in terms of $k_La$ coefficients and measurement of standard parameters can provide broad information about the cells cultured in this system. Compared to conventional off-gas analyses, the dynamic $k_La$ strategy was equally or better suited to calculate OUR trends. Thus, the strategy is highly applicable and easy to implement on multiple scales and in a wide variety of processes, organisms, and cell lines. The generated model allows for real-time visualization of OURs, enabling enhanced understanding of growth characteristics and metabolic reactions with varying process conditions. The presented soft-sensors provide numerous insights: (i) a dynamic $k_La$ model needs to be considered in a varying process, (ii) OURs are related more to cell volume than viable cell counts, and (iii) the model cell line switches to another metabolic state when the proportion of Asp to Glu drops in the chosen process setting.

The OUR profile alone gives a first indication of the cellular activity in a process and will add great value to process development. Moreover, a combined soft-sensor with an on-line capacitance measurement presents opportunities for more advanced process optimization through real time monitoring and control of metabolic states.

## DATA AVAILABILITY

All datasets generated for this study are included in the manuscript and/or the **Supplementary Files**.

## AUTHOR CONTRIBUTIONS

WS and BS designed the experiments. MP performed the experiments. MP and BS derived the models and analyzed the data. MP and BS wrote the manuscript in consultation with WS and GS.

## FUNDING

The authors declare that this study received funding from Bilfinger Industrietechnik Salzburg GmbH and The Austrian Research Promotion Agency (FFG) (Competence Headquarters, Grant Number 849725). Bilfinger Industrietechnik Salzburg GmbH participated in the study design, data collection and analysis and decision to publish. The

Austrian Research Promotion Agency (FFG) had no role in study design, data collection and analysis, decision to publish.

## ACKNOWLEDGMENTS

We would like to thank Nataša Sarić and Markus Kneißl as well as the entire PATPlant research team for their practical contribution to this work. In addition, we would like to thank Prof. Winfried Storhas for advice and proofreading the article before submission.

## SUPPLEMENTARY MATERIAL

The Supplementary Material for this article can be found online at: https://www.frontiersin.org/articles/10.3389/fbioe.2019.00195/full#supplementary-material

**Appendix Figure 1 | (A)** Viable cell concentrations (VCC) and **(B)** Packed cell volume (PCV) viable over the time progression of all fed batch runs.

**Appendix Figure 2 | (A)** Alanine, **(B)** asparagine, **(C)** aspartate, **(D)** glutamine, and **(E)** glutamate over the time progression of all fed batch runs.

**Appendix Figure 3 |** Algorithm for on-line prediction of metabolic stages in the cells.

## REFERENCES

Altamirano, C., Illanes, A., Casablancas, A., Gámez, X., Cairó, J. J., and Gòdia, C. (2001). Analysis of CHO cells metabolic redistribution in a glutamate-based defined medium in continuous culture. *Biotechnol. Prog.* 17, 1032–1041. doi: 10.1021/bp0100981

Deshpande, R. R., and Heinzle, E. (2004). On-line oxygen uptake rate and culture viability measurement of animal cell culture using microplates with integrated oxygen sensors. *Biotechnol. Lett.* 26, 763–767. doi: 10.1023/B:BILE.0000024101.57683.6d

Doverskog, M., Ljunggren, J., Öhman, L., and Häggström, L. (1997). Physiology of cultured animal cells. *J. Biotechnol.* 59, 103–115. doi: 10.1016/S0168-1656(97)00172-7

Duarte, T. M., Carinhas, N., Barreiro, L. C., Carrondo, M. J. T., Alves, P. M., and Teixeira, A. P. (2014). Metabolic responses of CHO cells to limitation of key amino acids. *Biotechnol. Bioeng.* 111, 2095–2106. doi: 10.1002/bit.25266

Eyer, K., Oeggerli, A., and Heinzlet, E. (1995). On-line gas analysis in animal cell cultivation: II. Methods for oxygen uptake rate estimation and its application to controlled feeding of G lu tami ne. *Biotechnol. Bioeng.* 45, 54–62. doi: 10.1002/bit.260450108

Garcia-ochoa, F., and Gomez, E. (2009). Bioreactor scale-up and oxygen transfer rate in microbial processes: an overview. *Biotechnol. Adv.* 27, 153–176. doi: 10.1016/j.biotechadv.2008.10.006

Gill, N. K., Appleton, M., Baganz, F., and Lye, G. J. (2008). Quantification of power consumption and oxygen transfer characteristics of a stirred miniature bioreactor for predictive fermentation scale-up. *Biotechnol. Bioeng.* 100, 1144–1155. doi: 10.1002/bit.21852

Goudar, C. T., Piret, J. M., and Konstantinov, K. B. (2011). Estimating cell specific oxygen uptake and carbon dioxide production rates for mammalian cells in perfusion culture. *Biotechnol. Prog.* 27, 1347–1357. doi: 10.1002/btpr.646

Henzler, H.-J., and Kauling, D. J. (1993). Oxygenation of cell cultures. *Bioprocess Eng.* 9, 61–75. doi: 10.1007/BF00369033

Kerdouss, F., Bannari, A., Proulx, P., Bannari, R., Skrga, M., and Labrecque, Y. (2008). Two-phase mass transfer coefficient prediction in stirred vessel with a CFD model. *Comput. Chem. Eng.* 32, 1943–1955. doi: 10.1016/j.compchemeng.2007.10.010

Lovrecz, G., and Gray, P. (1994). Use of on-line gas analysis to monitor recombinant mammalian cell cultures. *Cytotechnology* 14, 167–175. doi: 10.1007/BF00749613

Luttmann, R., Bracewell, D. G., Cornelissen, G., Gernaey, K. V., Glassey, J., Hass, V. C., et al. (2012). Soft sensors in bioprocessing: a status report and recommendations. *Biotechnol. J.* 7, 1040–1048. doi: 10.1002/biot.201100506

Mcclure, D. D., Lee, A. C., Kavanagh, J. M., Fletcher, D. F., and Barton, G. W. (2015). Impact of surfactant addition on oxygen mass transfer in a bubble column. *Chem. Eng. Technol.* 38, 44–52. doi: 10.1002/ceat.201400403

Moore, A., Mercer, J., Dutina, G., Donahue, C. J., Bauer, K. D., Mather, J. P., et al. (1997). Effects of temperature shift on cell cycle, apoptosis and nucleotide pools in CHO cell batch cultues. *Cytotechnology* 23, 47–54. doi: 10.1023/A:1007919921991

Morao, A., Maia, C. I., Fonseca, M. M. R., Vasconcelos, J. M. T., and Alves, S. S. (1999). Effect of antifoam addition on gas-liquid mass transfer in stirred fermenters. *Bioprocess Eng.* 20, 165–172. doi: 10.1007/s004490050576

Niklas, J., Schräder, E., Sandig, V., Noll, T., and Heinzele, E. (2011). Quantitative characterization of metabolism and metabolic shifts during growth of the new human cell line AGE1. HN using time resolved metabolic flux analysis. *Boprocess. Biosyt. Eng.* 34, 533–545. doi: 10.1007/s00449-010-0502-y

Pereira, S., Kildegaard, H. F., and Andersen, M. R. (2018). Impact of CHO metabolism on cell growth and protein production: an overview of toxic and inhibiting metabolites and nutrients. *Biotechnol. J.* 13, 1–13. doi: 10.1002/biot.201700499

Puthli, M. S., Rathod, V. K., and Pandit, A. B. (2005). Gas-liquid mass transfer studies with triple impeller system on a laboratory scale bioreactor. *Biochem. Eng. J.* 23, 25–30. doi: 10.1016/j.bej.2004.10.006

Quijano, G., Revah, S., Gutiérrez-Rojas, M., Flores-Cotera, L. B., and Thalasso, F. (2009). Oxygen transfer in three-phase airlift and stirred tank reactors using silicone oil as transfer vector. *Process Biochem.* 44, 619–624. doi: 10.1016/j.procbio.2009.01.015

Sellick, C. A., Croxford, A. S., Maqsood, A. R., Stephens, G., Westerhoff, H. V., Goodacre, R., et al. (2011). Metabolite profiling of recombinant CHO cells: designing tailored feeding regimes that enhance recombinant antibody production. *Biotechnol. Bioeng.* 108, 3025–3031. doi: 10.1002/bit.23269

Sieblist, C., Jenzsch, M., and Pohlscheidt, M. (2013). Influence of pluronic F68 on oxygen mass transfer. *Am. Inst. Chem. Eng.* 29, 1278–1288. doi: 10.1002/btpr.1770

Sommeregger, W., Sissolak, B., Kandra, K., von Stosch, M., Mayer, M., and Striedner, G. (2017). Quality by control: towards model predictive control of mammalian cell culture bioprocesses. *Biotechnol. J.* 12, 1–7. doi: 10.1002/biot.201600546

Storhas, W. (Ed.) (2018). "Ergänzende theorien: methode zur bestimmung des henry-koeffizienten," in *Angewandte Bioverfahrensentwicklung* (Weinheim: Wiley-VCH), 30–35.

Toye, D., Galifi, A., Salmon, T., Marchot, P., Verdin, E., and Crine, M. (2010). Influence of medium composition on oxygen transfer rate in animal cell culture. *Can. J. Chem. Eng.* 88, 671–676. doi: 10.1002/cjce.20302

Tromans, D. (1998). Temperature and pressure dependent solubility of oxygen in water: a thermodynamic analysis. *Hydrometallurgy* 48, 327–342. doi: 10.1016/S0304-386X(98)00007-3

Vandu, C. O., and Krishna, R. (2004). Volumetric mass transfer coefficients in slurry bubble columns operating in the churn-turbulent flow regime. *Chem. Eng. Process. Process Intensif.* 43, 987–995. doi: 10.1016/j.cep.2003.09.007

Van't Riet, K. (1979). Review of measuring methods and results in nonviscous gas-liquid mass transfer in stirred vessel. *Ind. Eng. Chem. Process Des. Dev.* 18, 357–364. doi: 10.1021/i260071a001

Villadsen, J., Nielsen, J., and Liden, G. (2011). "Gas-liquid mass transfer," in *Bioreaction Engineering Principles,* eds J. Villadsen, J. Nielsen, and G. Liden (Boston, MA: Springer), 459–496. doi: 10.1007/978-1-4419-9688-6_10

Wagner, B. A., Venkataraman, S., and Buettner, G. R. (2012). The rate of oxygen utilization by cells. *Free Radic. Biol. Med.* 51, 700–712. doi: 10.1016/j.freeradbiomed.2011.05.024

Wahrheit, J., Nonnenmacher, Y., Sperber, S., and Heinzle, E. (2015). High-throughput respiration screening of single mitochondrial substrates using permeabilized CHO cells highlights control of mitochondria metabolism. *Eng. Life Sci.* 15, 184–194. doi: 10.1002/elsc.201400175

Wutz, J., Lapin, A., Siebler, F., Schäfer, J. E., Wucherpfennig, T., Berger, M., et al. (2016). Predictability of kLa in stirred tank reactors under multiple operating

conditions using an Euler–Lagrange approach. *Eng. Life Sci.* 16, 633–642. doi: 10.1002/elsc.201500135

Young, J. D. (2013). Metabolic flux rewiring in mammalian cell cultures. *Curr. Opin. Biotechnol.* 24, 1108–1115. doi: 10.1016/j.copbio.2013.04.016

Zboray, K., Sommeregger, W., Bogner, E., Gili, A., Sterovsky, T., Fauland, K., et al. (2015). Heterologous protein production using euchromatin-containing expression vectors in mammalian cells. *Nucleic Acids Res.* 43:e102. doi: 10.1093/nar/gkv475

Zhang, L., Zhang, W., Wang, C., Liu, J., Deng, X., Liu, X., et al. (2016). Responses of CHO—DHFR cells to ratio of asparagine to glutamine in feed media: cell growth, antibody production, metabolic waste, glutamate, and energy metabolism. *Bioresour. Bioprocess.* 3, 1–12. doi: 10.1186/s40643-015-0072-6

**Conflict of Interest Statement:** MP, BS, and WS are employed by the company Bilfinger Industrietechnik Salzburg GmbH.

The remaining author declares that the research was conducted in the absence of any commercial or financial relationships that could be construed as a potential conflict of interest.

## NOMENCLATURE

| | | |
|---|---|---|
| $a$ | Specific interfacial area | [$m^{-1}$] |
| $c*$ | Maximum solubility in water at equilibrium | [mol $L^{-1}$] |
| $c_{DO}$ | Temperature corrected actual oxygen concentration | [mol $L^{-1}$] |
| $c_L*$ | Maximum solubility of oxygen in the broth under prevailing gas-phase composition, temperature, and pressure | [mol $L^{-1}$] |
| $c_M*$ | Maximum oxygen solubility in media | [mol $L^{-1}$] |
| $c_{O2}$ | Actual oxygen concentration in the broth | [mol $L^{-1}$] |
| D | Tank diameter | m |
| $d_i$ | Impeller diameter | m |
| DO | Dissolved oxygen | [%] |
| $G_{in/out}$ | Gas flow rate at real conditions in/out of bioreactor | [mL $min^{-1}$] |
| H | Tank height | m |
| $k_L$ | Mass transfer coefficient | [m $s^{-1}$] |
| $k_La$ | Volumetric oxygen mass transfer coefficient | [$s^{-1}$] |
| MAPE | Mean absolute percentage error | [%] |
| N | stirrer speed | [$s^{-1}$ or rpm] |
| OTR | Oxygen transfer rate | [mol $L^{-1}$ $d^{-1}$] |
| OUR | Oxygen uptake rate | [mol $L^{-1}$ $d^{-1}$] |
| $p_{O2}$ | Partial pressure of oxygen | [Pa] |
| $Q$ | Gas flow rate | [$m^3$ $s^{-1}$] |
| $q_{O2}$ | Specific oxygen uptake rate | [mol $cell^{-1}$ $day^{-1}$] |
| $R$ | Gas constant | [J $mol^{-1}$ $K^{-1}$] |
| $T$ | Temperature | [°C];[K] |
| TCC | Total cell concentration | [cells $mL^{-1}$] |
| $\tau_P$ | Response time | [s] |
| $v_s$ | Superficial gas velocity | [m $s^{-1}$] |
| VCC | Viable cell concentration | [cells $mL^{-1}$] |
| $V_L$ | Volume of the liquid in vessel | [$m^3$] |
| $x_{target}$ | target value | |
| $x_i$ | value of sample | |
| n | number of samples | |
| X | Biomass concentration | [g $L^{-1}$] |
| $y_{CO2}$ | Molar fraction of $CO_2$ | [%] |

Biotechnology Journal
www.biotechnology-journal.com

# Application of the Bradford Assay for Cell Lysis Quantification: Residual Protein Content in Cell Culture Supernatants

*Bernhard Sissolak,* Christian Zabik, Natasa Saric, Wolfgang Sommeregger, Karola Vorauer-Uhl, and Gerald Striedner*

**Frequently measured mammalian cell culture process indicators include viability and total cell concentration (TCC). Cell lysis, an additional important process characteristic that substantially contributes to the overall product purity profiles, is often not addressed in detail. In the present study, an inexpensive and simple application of the Bradford assay is developed to determine the residual protein content (RPC) in cell culture supernatants. The reliability and reproducibility of the method are tested in a long-term study and compared with lysis quantification via the DNA measurement. The results show that its performance is more robust and accurate over time and the respective concentration range. Additionally, both methods are used for cell lysis process monitoring in a recombinant Chinese hamster ovary fed-batch process. In the presented process, by applying the established assay, the lysis rate $k_{DL}$ is determined to be constant over time at $4.6 \times 10^{-4}$ lysed cell concentration (LCC) per TCC and time (LCC/TCC/h). In contrast, DNA data did not confirm the constant lysis rate due to variations of the content per cell during cultivation. Thus, information on the RPC can facilitate the determination of the optimal harvest time point with respect to purity and in improving process characterization.**

## 1. Introduction

Total cell concentrations (TCCs) and viable cell concentrations (VCCs) are typical process performance indicators for mammalian bioprocesses. These, their time derivatives, and their respective rates are commonly used to describe the state of bioprocesses. Viability is a commonly derived key process indicator used to illustrate the vitality status of cell culture processes, but it is dependent on the magnitude of the lysis rate.[1] However, cell lysis and the amount of host cell proteins (HCPs) in the culture broth are often not determined during cultivation although these variables significantly affect further process steps.[2] Consequently, the amount of living, dead, and lysed cells must be considered to achieve a comprehensive picture of the process.

The lysis of a mammalian cell is defined as the loss of an intact membrane and the release of the intracellular content. Therefore, lysed cells cannot be directly detected via cell counting methods. Thus, they are usually indirectly measured through the detection of the released internal constituents, such as DNA,[3,4] lactate dehydrogenase,[3] or via the detection of cell debris.[10] The change in rheological characteristics represents an additional opportunity to account for cell lysis;[11,12] however, this is only applicable for microbial systems or high cell density cell culture systems.

An additional lysis research opportunity involves the detection of HCPs in the supernatant.[13] Although the HCP content is regarded as a critical quality attribute of the final product,[14] the implementation of HCP as a routine process variable in mammalian cell culture has not been reported to date. Nevertheless, for integrated or continuous processes, monitoring and control of HCP content could be of particular importance,[15] such as in avoidance of fouling or blocking in chromatography resins[16,17] during downstream operations.

Enzyme-linked immunosorbent assay (ELISA) is a common method used to quantitatively determine the HCP content of a given sample though it lacks coverage of the complete spectrum of HCPs and is likely to miss weak or nonimmunogenic species.[18,19] Moreover, this procedure is costly and can result

B. Sissolak, Prof. K. Vorauer-Uhl, Prof. G. Striedner
Department of Biotechnology
University of Natural Resources and Life Sciences (BOKU)
Muthgasse 18, A-1190
Vienna, Austria
E-mail: bernhard.sissolak@boku.ac.at

C. Zabik, N. Saric, W. Sommeregger
Research and Development
Bilfinger Industrietechnik Salzburg GmbH
Mooslackengasse 17, A-1190
Vienna, Austria

The ORCID identification number(s) for the author(s) of this article can be found under https://doi.org/10.1002/biot.201800714.



**DOI: 10.1002/biot.201800714**

in a huge work, particularly when many samples need to be analyzed. The application of ELISA for the routine tracking of HCP generation during a bioprocess to uncover cell lysis can be regarded as not economically feasible. This is also true for 1D- or 2D-polyacrylamide gel electrophoresis or any type of mass spectrometry-based methods.[14]

In the present work, we describe a simple and inexpensive Bradford assay method to determine the HCP content in culture supernatants, which is referred to as residual protein content (RPC). The present study provides critical considerations regarding the reliability and precision of the developed RPC method in comparison to the standard DNA technique to estimate cell lysis. Furthermore, we demonstrate that RPC data allows the identification of the process state and provides additional information for the understanding and modeling of the process.

## 2. Experimental Section

### 2.1. Fed-Batch Process

For the fed-batch model process, a recombinant monoclonal Chinese hamster ovary (CHO) cell line (The Antibody Lab GmbH, Austria) producing an anti-tumor necrosis factor-α (TNF-α) immunoglobulin G1 (IgG1) was used. The cell line was generated by applying the Rosa26 bacterial artificial chromosome expression strategy[20] to a serum-free adapted host cell line derived from CHO-K1 (American Type Culture Collection [ATCC] CCL-61). A working cell bank, where each vial contained $5 \times 10^6$ cells, served as the starting material for all experiments. Cells were thawed in chemically defined culture medium (Dynamis AGT, A26175; Thermo Fisher Scientific, USA) supplemented with 8 mM L-glutamine (25030081; Sigma-Aldrich, Germany), 3 mL $L^{-1}$ phenol red solution (RNBD642; Sigma-Aldrich, Germany), 1:1000 anti-clumping agent (0010057DG; Thermo Fisher Scientific), and 1 mg $mL^{-1}$ G418 (G8168; Sigma-Aldrich, Germany).

Subculturing was performed three times (every third or fourth day) using the aforementioned media without any anti-clumping agent and G418. Fed-batch experiments were performed in shake flasks (#431147; Corning, USA) with a starting volume of 300 mL and an initial cell density of $2.5 \times 10^5$ cells per mL. The medium for the batch was additionally supplemented with 0.1% v/v antifoam C (A8011; Sigma-Aldrich, Germany) to mimic the typical large-scale cultivation conditions. A 2D (glucose and process temperature), three-stage, factorial design of experiments was used to capture the design space. To the feed medium, 0.1% antifoam (CHO CD EfficientFeed A AGT Kit, A1442002; Thermo Fisher Scientific) was added alongwith 10 g $L^{-1}$, 20 g $L^{-1}$, or 30 g $L^{-1}$ glucose (G7021; Sigma-Aldrich, Germany). Pulse feeding started at day 3 and lasted until day 13, which involved a linear pulsed feed rate with a total added volume of 33% v/v with respect to the end volume. The process starting temperature of 37 °C was changed at day 4 to 31 °C or 34 °C, or kept constant at 37 °C. Sampling was performed once per day, and the experiments were terminated after cell viability dropped below 70%. All cultivations were conducted in a humidified $CO_2$ incubator (Heracell VIOs 160i; Thermo Fisher Scientific) with 5% v/v $CO_2$ in ambient air and at 200 rpm on an orbital shaker (MaxQ 2000 CO2 Plus; Thermo Fisher Scientific). For the mock control experiment, the serum-free host cell line was cultivated at a constant temperature of 37 °C using the feed containing an additional 30 g $L^{-1}$ glucose. Further fed-batch conditions were as previously described.

All cell culture experiments were performed in duplicate.

### 2.2. Cell Cycle Staining

Two samples of $1.5 \times 10^6$ cells from the cell broth were taken and centrifuged (10 min, $180 \times g$); and the pellets were washed two times with 1.0 mL of phosphate-buffered saline (PBS) (9150.1; Roth, Germany). The remaining cell pellet was dissolved in 1.0 mL of ice-cold 70% high-purity ethanol, added dropwise. The fixed cells were stored at 4 °C.

Prior to analysis, the samples were centrifuged and washed twice. Then 1.0 mL of Tris buffer (T3253; Sigma-Aldrich, Germany) was added dropwise. In the last step, cells were resuspended in 500 µL of Tris, including 1 µg $mL^{-1}$ 4′,6-diamidino-2-phenylindole (DAPI) (10236276001; Sigma-Aldrich, Germany), incubated for 30 min, and subsequently measured using the Gallios Flow Cytometer (B43620; Beckman Coulter, USA) (FL9, number of events is equal to 10 000). The percentages of cells in the G1/G0 and G2/M phases were determined by calculating the respective peak areas.

### 2.3. Cell Lysate Generation

For the cell lysate generation, a fed-batch process with the producing cell line was carried out as described in the previous section. The process temperature was set to 34 °C, and the feed with an additional 20 g $L^{-1}$ glucose was used. In the stationary phase (day 12), a sample was drawn for lysate generation. A total of $1.5 \times 10^6$ cells were washed with PBS and resuspended in 0.7 mL radioimmunoprecipitation assay (RIPA) lysis buffer (20-188; Merck, Germany) supplemented with an ethylenediaminetetraacetic acid (EDTA)-free protease inhibitor (COEDTAF-RO Roche; Sigma-Aldrich, Germany). The solution was then incubated for 1 h at 4 °C, centrifuged at $8000 \times g$ for 10 min; the supernatant was stored overnight at 4 °C.

### 2.4. Antibody Titer Quantification

The antibody titer was determined via bio-layer interferometry (BLI) using the Octet system (Octet QK; Pall ForteBio, USA) with protein A tips (18-5010; Pall ForteBio). For sample preparation, the culture broth was centrifuged at $180 \times g$ for 10 min at room temperature. The supernatant was stored at −20 °C until measurement. All dilutions were performed in PBS with 1% Tween 20 (P2287; Sigma-Aldrich, Germany). The binding to protein A was measured at 30 °C, and the resulting binding rate was calculated using Octet data analysis software 6.4 (Octet QK; Pall ForteBio). Sample readings were quantified using an IgG calibration curve in concentrations ranging from 10.0 µg $mL^{-1}$ to 50.0 µg $mL^{-1}$.

### 2.5. Residual Protein Content

The RPC in the bioprocess supernatants of CHO cells was determined using the Bradford assay (B6916; Bio-Rad Laboratories, USA) and the absorbance of Coomassie brilliant blue G

 

(CBB) was measured at 595 nm. Sample preparation was performed as previously described for the titer quantification. Measurement was performed using a plate reader (Infinite M1000; Tecan, Switzerland) in 96-well plates (P7366; Nunc, USA). Bovine serum albumin (BSA) (5000002; Bio-Rad Laboratories) and IgG (Lot-No. 046M4855V, 12511; Sigma-Aldrich, USA) were measured in a concentration range of 81.0–520.0 µg mL$^{-1}$ and 40.6–325.0 µg mL$^{-1}$, respectively, along with the analysis of each unknown samples.

### 2.6. DNA Assay

Double-stranded DNA (dsDNA) concentration in the fermentation supernatants of CHO cells was determined by fluorescence measurements using Picogreen dsDNA reagent (P7581; Thermo Fisher Scientific). The dye was excited at 480 nm, and emissions were measured at 520 nm. All dilutions were performed in Tris-EDTA buffer (10 mM Tris-HCl, 1 mM EDTA, pH 7.5). Two different DNA standards were used: Lambda DNA standard (P7589; Thermo Fisher Scientific) and Calf Thymus DNA standard (1702482; Bio-Rad Laboratories). A calibration curve was recorded for concentrations ranging from 13.13 ng mL$^{-1}$ to 1680 ng mL$^{-1}$. Measurements were performed using a plate reader (Infinite M1000; Tecan) in a 96-well black bottom plate (NNC#237108; Thermo Fisher Scientific).

### 2.7. Statistics

Statistical analyses were performed using SigmaPlot13.0 software (Systat Software Inc., USA). Residual distributions were tested on normality (Shapiro–Wilk test) and on constant variance (Levene's median test). The confidence bands, prediction bands, and variances were calculated using the delta method.[21]

The mean deviation of the parameters $k$ and $d$ was calculated according to Equation (1):

$$\text{mean deviation}(\%) = \frac{x_{\text{target}} - x_{\text{actual}}}{x_{\text{target}}} \times 100 \quad (1)$$

## 3. Results and Discussion

### 3.1. RPC: Method Development and Evaluation

A recombinant CHO-K1 cell line consists of roughly 70 wt% protein,[22] which is released when a cell undergoes lysis. For the measurement of the RPC in cell culture supernatants of recombinant cell lines cultivated in serum-free media, the secreted recombinant product must be considered. It is well known that the CBB dye interferes differently depending on the protein composition.[23] In the present study, we used a set of experiments to elucidate this interference.

The cell lysate from the producer cell line was obtained by incubating in the RIPA lysis buffer; the RPC was determined using the Bradford assay. The cell lysate contained 676 µg mL$^{-1}$ protein on average. This corresponds to 315 ± 16 pg protein per cell, which is fairly a reasonable value, in the view of the reported values for mammalian cells such as 180 pg per cell for HEK293T,[24] 246 pg per cell for a producing CHO-K1 cell line,[22] and 410 pg per cell for Madin–Darby canine kidney cells.[23] In a recent study even >500 pg of protein per cell was reported for a CHO cell line, which was cell size-dependent.[25] The first and the last study used the Lowry assay, the second measured the amino acid composition of a cell pellet, and the third used a CBB dye to determine the protein content.

However, the resulting absorbance of dilutions from the lysate resulted in a linear function matching the slope of the BSA standard curve (**Figure 1**A). As expected, the standard curve of the reference IgG and the polyclonal IgG standard were different from the BSA function.

Linear regression was obtained for both standards. Residuals were normally distributed and followed homoscedastic behavior. The BSA calibration range was from 81 µg mL$^{-1}$ to 520 µg mL$^{-1}$, whereas the calibration from IgG ranged from 40 µg mL$^{-1}$ to 325 µg mL$^{-1}$. The slope of the linear function represents the extinction coefficients ε of BSA and IgG. Accordingly, considering the resulting path length in the well (8.4 mm), a ε of 1.4 AU mg$^{-1}$ mL$^{-1}$ cm$^{-1}$ and 1.7 AU mg$^{-1}$ mL$^{-1}$ cm$^{-1}$ for IgG and BSA, respectively, was determined.

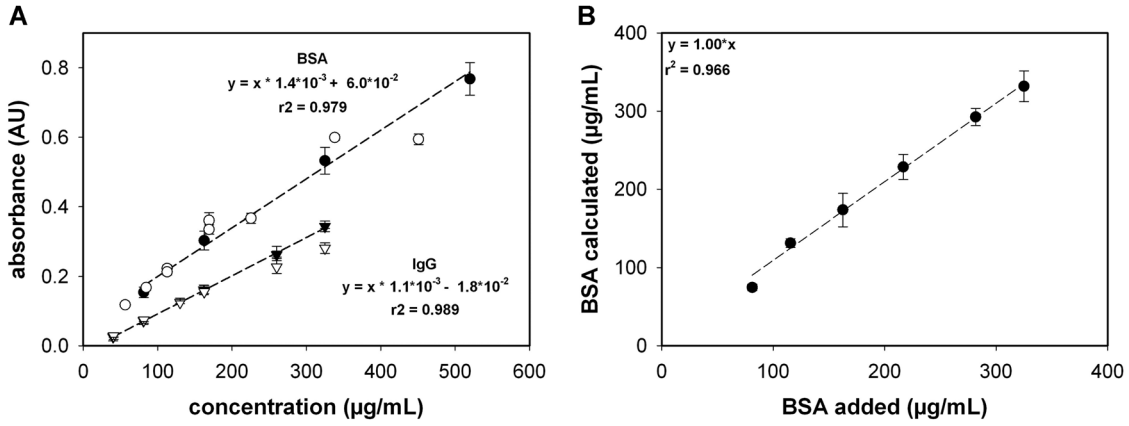


**Figure 1.** A) Absorbance of the BSA standard (●) and polyclonal IgG standard (▼) as a function of the respective concentration ($n = 10$). Measured triplicates of the total protein content of a cell lysate (○) and the anti-TNF-α reference standard (▽). Linear function is depicted. B) Linear regression of the calculated BSA value versus the theoretical values of different spike-in IgG/BSA mixtures ($n = 7$).

 

The binding of CBB to proteins obeys the Lambert–Beer law.[26] Accordingly, the absorbance $A$ of a sample is related to its concentration and the path length. As more species are present, the total absorbance $A$ can be described as a linear function of each individual absorbance $A_i$ (Equation (2)):

$$AU_{\text{total}} = AU_{\text{RPC}} + AU_{\text{IgG}} + AU_{\text{Blank}} \quad (2)$$

This implies that the absorbance of the residual protein ($AU_{\text{RPC}}$) content should be quantifiable by subtracting the medium ($AU_{\text{Blank}}$) and the IgG blank ($AU_{\text{IgG}}$), derived from the BLI measurements and recalculated using the extinction factor, from the total absorbance value. The residual protein concentration is then subsequently calculated via the BSA calibration.

To support this relationship, different sets of BSA/IgG mixtures were measured (Figure 1B). The experiment contained 45 measurements in total. The IgG concentration was set from 40 µg mL$^{-1}$ to 218 µg mL$^{-1}$, and 81 µg mL$^{-1}$ to 280 µg mL$^{-1}$ for BSA. The absorbance values ranged from 0.15 AU to 0.62 AU, respectively. The BSA concentration was recalculated after subtraction of the resulting absorbance value of a given IgG concentration from the total absorbance (calibrations used are depicted in **Figure 2**A). The slope of calculated and added concentrations of BSA was 1.04, representing a good recovery of the added BSA. The coefficient of variation (CV) had an average of 8%, an initial indicator for the error of this analysis.

Matrix effects were not observed. Different concentrations of BSA, from 65 µg mL$^{-1}$ to 130 µg mL$^{-1}$, were spiked into two host cell culture supernatants, from the beginning of fed-batch and from the harvest time point, respectively. The recovery was 94.6 ± 9.2% ($n = 18$).

Furthermore, the media and feed used exhibited the same absorbance value as the PBS buffer. As expected, smaller peptide molecules and single amino acids did not have any impact on the CBB absorbance.[23]

The experiments conducted demonstrated that the total absorbance can be separated into two absorbance attributes, which are linearly related (Equation (2)). As a result, the absorbance of a known substance, calculated via its extinction coefficient, can be subtracted from the total absorbance to obtain the concentration of remaining constituents.

### 3.2. RPC: Long-Term Assessment

The consistency of this method was tested in a long-term study of over two years by three different operators. For each assay, a set of standards was measured and a linear regression was performed. The limit of quantitation (LOQ) and limit of detection (LOD) were calculated using the standard deviations of the blank responses and were 70.9 µg mL$^{-1}$ and 23.4 µg mL$^{-1}$, respectively.

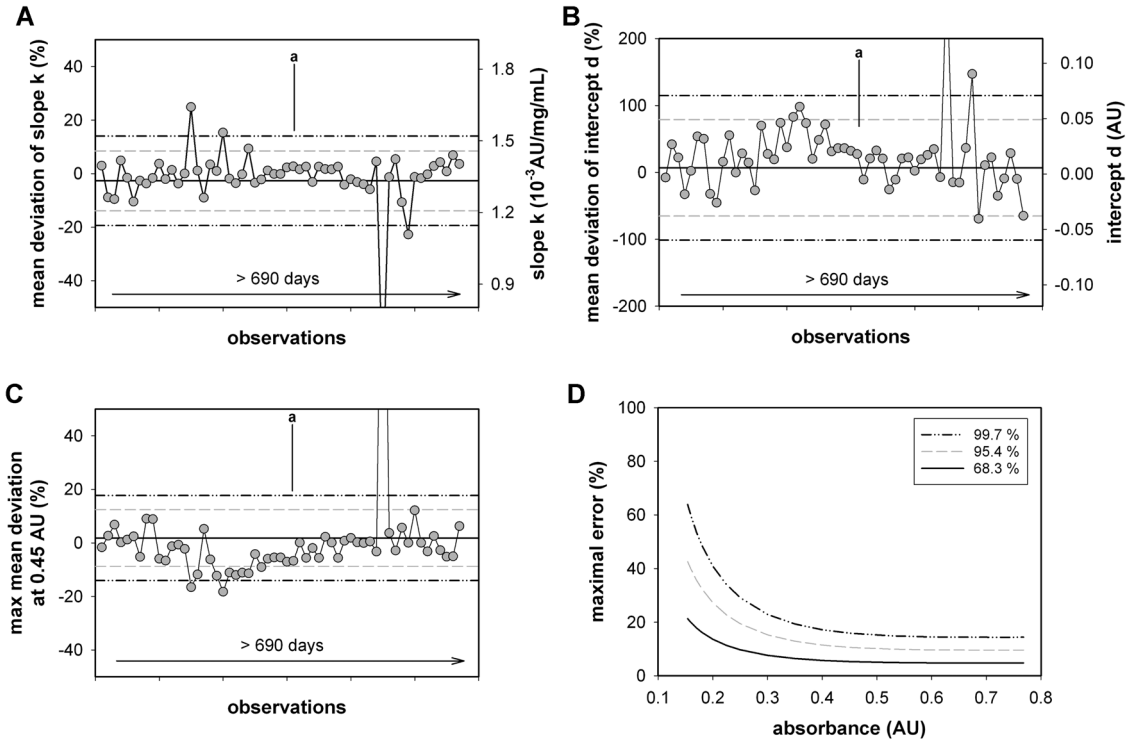


**Figure 2.** A) Obtained mean deviation from the slope $k$, B) the intercept $d$ derived from the BSA standard measurements, and C) the mean deviation to the target concentration at 0.45 AU, calculated according to Equation (3) during a time course of 690 days. The solid line represents the average value. The gray dashed line and the dashed dot line represent 95.4% and 99.7% of the sample population ($n = 10$), respectively. The mark "a" indicates where the operator had changed. D) Maximal error as a function of the measured absorbance, which could be obtained through the deviations of $k$ and $d$.

 

The mean deviations (see Equation (1)) of the resulting values of the slope $k$ and intercept $d$ were monitored throughout the study (Figure 2A,B). The first ten values were taken to calculate the average and standard deviation of those parameters. If $k$ or $d$ was outside of the value $\bar{x}\pm3\sigma$, 99.7% of the sample population was within, the assay was discarded. Consequently, the method was stable and robust over the time course. No obvious trends occurred that could indicate any altering effects of the standard or the CBB dye. Also, the change in the operator had no effect on the analysis performance.

While $k$ resulted in low variation, $d$ exhibited larger deviations; however, considering the absolute values it did not affect the measurements to a great extent. Therefore, the possible impact on the determination of the variances of $k$ and $d$ was evaluated. This was done by the addition of the absolute deviation of $k$ and $d$ to the linear function and then calculating the concentration for different absorbance values along the calibration range (Equation (3)). The resulting value was then substituted into Equation (1) to assess the mean deviation compared to the target concentration $x_{\text{target}}$:

$$\left(x_{\text{target}} + \Delta x\right) = \frac{y_{\text{target}} - (d+\Delta d)}{k + \Delta k} \quad (3)$$

For the limits of the chart plots, the first ten assays were again taken to gather a statistically meaningful population for determining the average and standard deviation. The resulting values can be considered as having maximal possible error that could occur if the stated calibration was invalid (Figure 2C,D).

For most of the calibration range, the error was below 20% (Figure 2D). The intercept $d$ affects the determination in the low-concentration region though the maximal possible error at higher absorbance values is dependent on the slope $k$. At low concentrations, higher variation had to be accepted. Therefore, when a larger quantity of protein is in the supernatant, particularly at a later stage of a process, the method is more accurate. At the beginning of a bioprocess or during the batch phase, RPC results with higher variances could be estimated.

Error propagation within this methodology can be obviated, since the antibody titer quantification via the BLI is a robust and reliable procedure.[27,28] The standard prediction error of this measurement was in the range of $\pm$9.096 µg (equivalent to $\pm$0.003 AU in the RPC method). It was apparent that the impact of the variance of antibody determination was very small and thus did not have a significant influence on RPC estimation.

### 3.3. Picogreen Method Evaluation and Long-Term Assessment

As a comparative method for cell lysis determination, DNA was quantified using the Picogreen assay.[3] The calibration range was established to be 52.5 ng mL$^{-1}$ to 840 ng mL$^{-1}$ (Figure 3 A). Both the ordinate and the $x$-axis were logarithmized to pass the constant variance and normal distribution test and, evidently, to establish a linear regression ($n = 10$). The LOD for this method was 9.4 ng mL$^{-1}$ and LOQ was 28.4 ng mL$^{-1}$.

Similar to the RPC method, mean deviations (see Equation (1)) from the slope $k$ and intercept $d$ were monitored over a time course of over 690 days (**Figure 3**B,C); both exhibited variation under 20%. The change in the operator had a greater impact on the parameter distribution, indicated by "a"; as such, a new calibration was necessary.

The impact on variations of $k$ and $d$ on the evaluation of the DNA concentration was recalculated (Equations (1) and (3)). Observation six, indicated by an arrow, was regarded as an outlier (Figure 3D).

With increasing fluorescence, maximal error decreases and will be less than 30%. DNA quantification using the Picogreen assay is highly sensitive[29] and thus susceptible to errors. Consequently, it is unremarkable that such deviations occurred during this long-term assessment. Data obtained from blank measurements substantiated these observations due to the fact that the CV was approximately 32%, which is a reasonable level of background variation.

Matrix and dilution effects were also occasionally apparent. DNA spiked into a mock supernatant demonstrated that the spiked DNA amount was more accurately estimated at a higher dilution factor. For the last five dilution steps, a recovery rate of 93.4 $\pm$ 13.4% was achieved. In contrast, DNA spiked into fresh media was not heavily influenced by the dilution. The achieved recovery rate was 110.1 $\pm$ 13.9%.

### 3.4. RPC and DNA as a Cell Lysis Marker

To compare both methods, the concentration range was transferred into the lysed cells per mL by assuming that a cell contained 315 pg of protein and 5.60 pg of DNA.[30] The working ranges for both methods were different. The RPC method covered a range from $2.6\times10^5$ to $1.7\times10^6$ lysed cells per mL, whereas the DNA method spanned a broader range from $9.4\times10^3$ to $1.5\times10^5$ lysed cells per mL. While DNA is more sensitive, RPC offers the advantage of being more accurate. The RPC showed a reasonable error level of below 20% over nearly the entire working range. Furthermore, the RPC longtime robustness, without repeated calibration effort, makes this tool useful for both research and industrial applications, as no additional calibration was required.

Furthermore, the characteristics of both methods could be easily monitored. The mean deviations of slope $k$ and intercept $d$ are practical and reasonable indicators.

### 3.5. Improved Process Characterization Based on Cell Lysis Monitoring

The developed RPC and DNA method was applied during a CHO shake flask study, where a $3^2$ full factorial experimental design was conducted. It was assumed that variations in the cell size throughout the course of the fed-batch cultivation had no impact on the protein content per cell. The two independent parameters included the glucose concentration in the feed phase and the process temperature. In total, 18 experiments were conducted and 180 samples measured. Increasing the glucose content in the feed had no influence on the VCC, HCPs, or the product titer. Therefore, the complete data set for

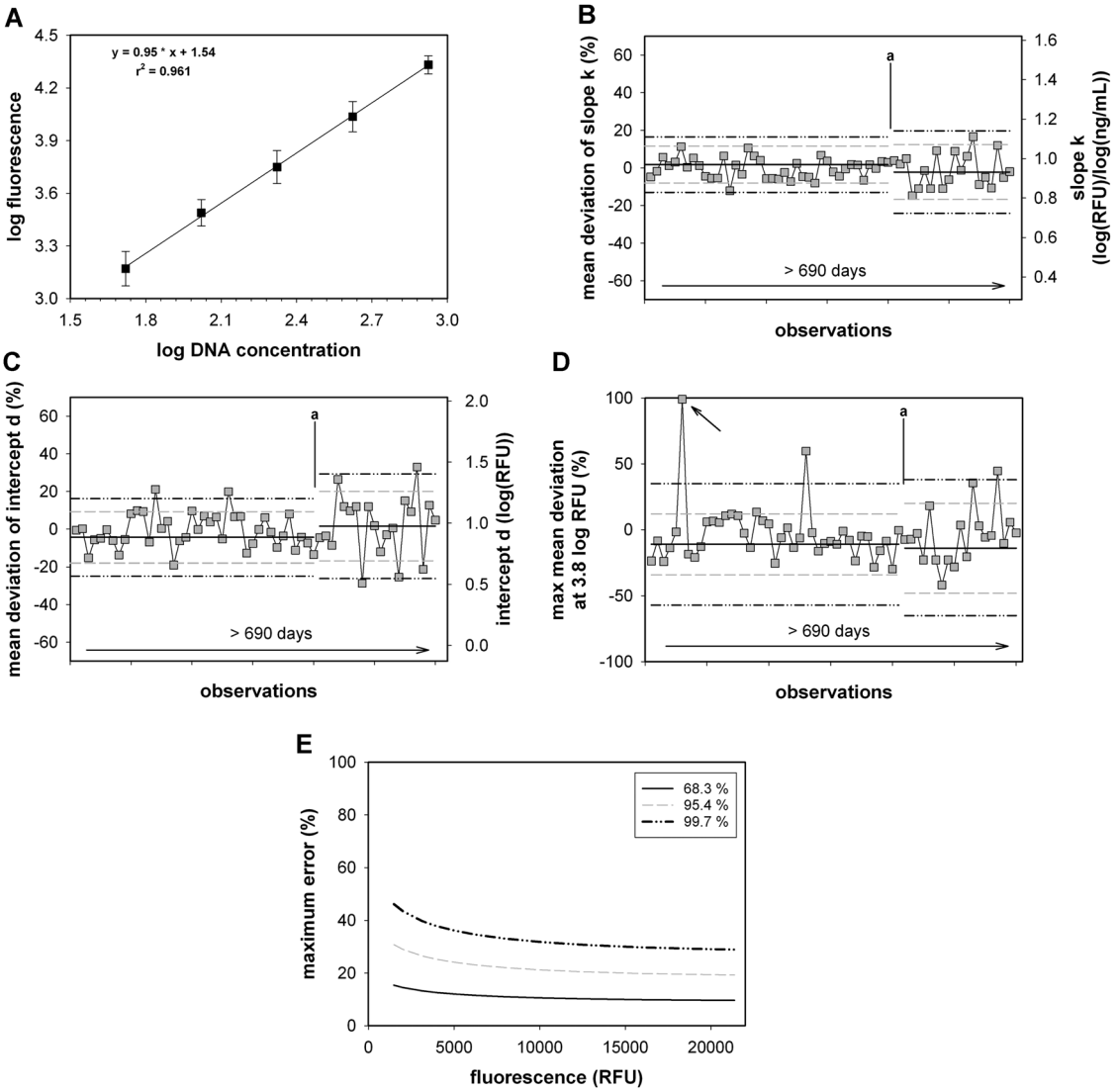


**Figure 3.** A) DNA concentration as a function of RFU. The first calibration set is depicted ($n = 10$). B) The mean deviation of the slope $k$, C) intercept $d$, and D) the mean deviation to the target concentration at 3.8 log RFU, calculated according to Equation (3), over a time course of 690 days. The mark "a" indicates when the operator changed and when a new calibration was performed. The solid line represents the average value. The gray dashed line and the dashed dot line represent 95.4% and 99.7% of the sample population ($n = 10$), respectively. E) The maximal error for the first calibration as a function of the measured fluorescence, which could be obtained through the deviations of $k$ and $d$. RFU, relative fluorescence units.

each particular temperature profile was summed up and averaged (**Figure 4**). The duration of the process was controlled via the viability of the cell culture (stopped at <70%).

Depending on the temperature, the fed-batch processes reached TCCs of between $1.2 \times 10^7$ cells per mL and $2.5 \times 10^7$ cells per mL, with product titers ranging from 400 µg mL$^{-1}$ to 600 µg mL$^{-1}$. Specific productivity $q_p$ decreased over time and achieved maximum values of approximately 12 pg cell$^{-1}$ d$^{-1}$. The processes at 31 °C lasted 1.6- and 1.3-fold longer compared to the experiments at 37 °C and 34 °C, respectively, until the stop criterion (viability <70%) was reached (Figure 4A,B). At lower temperatures, more cells were in the G1/G0 phase and the growth slowed or even stopped (Figure 4C,D), which is why temperature shifts are widely used for proliferation control.[31]

Apparently, cell lysis accounted for a maximum of 8.8% of the total produced biomass in the system (**Figure 5**A), whereas the HCP content reached values up to 500 µg mL$^{-1}$, corresponding to 50% of total protein in the supernatant for this model process. Despite this small fraction of lysed biomass, the resulting impurities were rather substantial.

Since dead and living cells can undergo cell lysis, the ITCD was calculated (Equation (4)), which we defined as

$$\mathrm{ITCD} = \int_{t_0}^{t_{\mathrm{end}}} \mathrm{TCC}\, \mathrm{d}t \tag{4}$$

This was plotted against the RPC (Figure 5B). The fed-batch process exhibited a constant specific protein release rate of $1.5 \times 10^{-7}$ µg/$X_{\mathrm{total}}$/h, which corresponds to a constant lysis rate

 

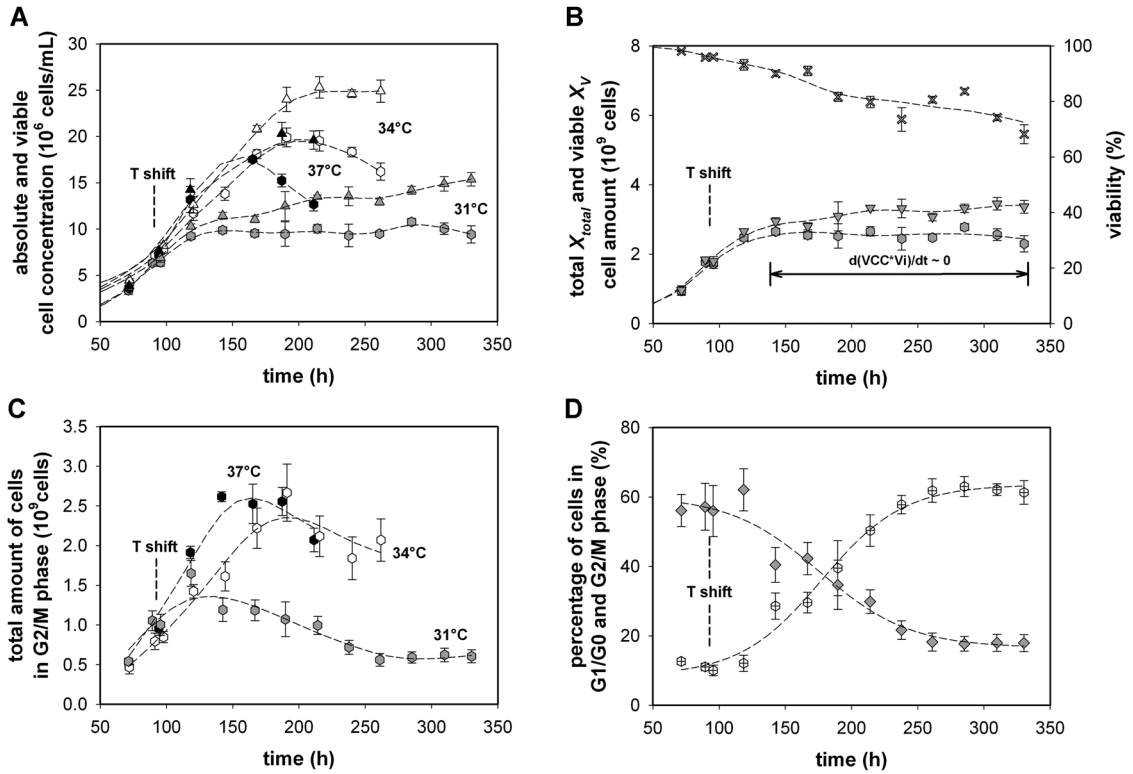


**Figure 4.** A) The absolute (37°C ▲, 34°C △, and 31°C ◭) and VCC (37°C ⬢, 34°C ⬡ and 31°C ⬢) amount over the time course of fed-batch processes performed at different temperatures. B) Total cell amount ($X_{total}$) ▽,viable cell amount ($X_v$) ⬢, and viability ✕ trend of the process at 31°C. The time period where the change in the viable biomass over time was zero is marked with an arrow. C) Total amount of cells remaining in the G2/M phase at 37°C ⬢, 34°C ⬡, and 31°C ⬢. D) Percentage of cells in G1/G0 ⊕ and G2/M ◆ phases over the time course for the fed-batch process at 31°C (measured by flow cytometry). The time point of the temperature shift is also depicted.

$k_{DL}$ of $4.6 \times 10^{-4}$ lysed cell concentration (LCC)/TCC/h, and is subsequently temperature-independent. It is proposed that the majority of lysis in this process is derived from dead cells since cell damage in bioprocesses is largely bubble-associated.[32]

The amount of DNA in cultivations at 31 °C was lower than those in processes at 34 °C and 37 °C cultivation temperature (Figure 5C). The two linear regressions exhibited different slopes, $k_{34+37\,°C}$ of 4.8 pg per cell and $k_{31\,°C}$ of 2.0 pg per cell, for the combined data set of 37 °C and 34 °C and for the process at 31 °C, respectively. In the process at 31 °C, substantially more cells were in the G1/G0 phase[31] (Figure 3C,D). Since the cells in the G1/G0 phase (*N*) have a different amount of DNA compared to the cells in the S G2/M phase (*N* to 2 *N*), the lysis of a G1/G0 cell releases a lower amount of DNA into the supernatant than an S G2/M cell. In this respect, it was remarkable that $k_2$ was approximately one half of $k_1$. However, the derived amount of DNA per cell was lower than expected.[30] Therefore, DNA would be inappropriate for cell lysis estimation in the type of experimental setup used in the present study.

### 3.6. RPC as a Key Process Indicator

In the best case, the cell culture supernatant should exclusively contain the target protein. This would provide the best starting conditions for ensuring high purification performance. Conventionally, viability or a death marker protein is used as a performance indicator and harvest criterion.[33] However, from the downstream perspective, cell viability is only relevant when the amount of RPC and DNA increases, which only occurs during cell lysis. This could also be of significant relevance for the yield, longevity, and overall performance of the subsequent protein purification strategies.[2,16] In general, reducing the soluble impurity level can simplify early-stage downstream processing.[34] It is known that certain HCP species affect the downstream process more than others. HCP constituents can associate with the monoclonal antibody (mAb) product or they might even co-elute due to noncharacteristic binding to the chromatography resin. Among others, clusterin, actin, or nidogen-1, are some of the most prominent proteins interacting with mAbs. Most of these sticky proteins are intracellular proteins.[17] Hence, cell lysis leads to an increased level of these proteins in the supernatant, which increases the probability of their association to the mAb and their sticking to the chromatography resins. Owing to the wash and cleaning in place (CIP) procedures of the protein A columns, HCP precipitates and deposits on the resin, which contributes to fouling. Moreover the diversity of HCP species also changes over the lifetime of the protein A resin, which can lead to clearance problems in the subsequent purification steps.[35]

In terms of purity, the ratio of RPC to mAb, and also other overexpressed active pharmaceutical ingredients, could be used to identify an optimal and a consistent stop criterion for a cell culture

 

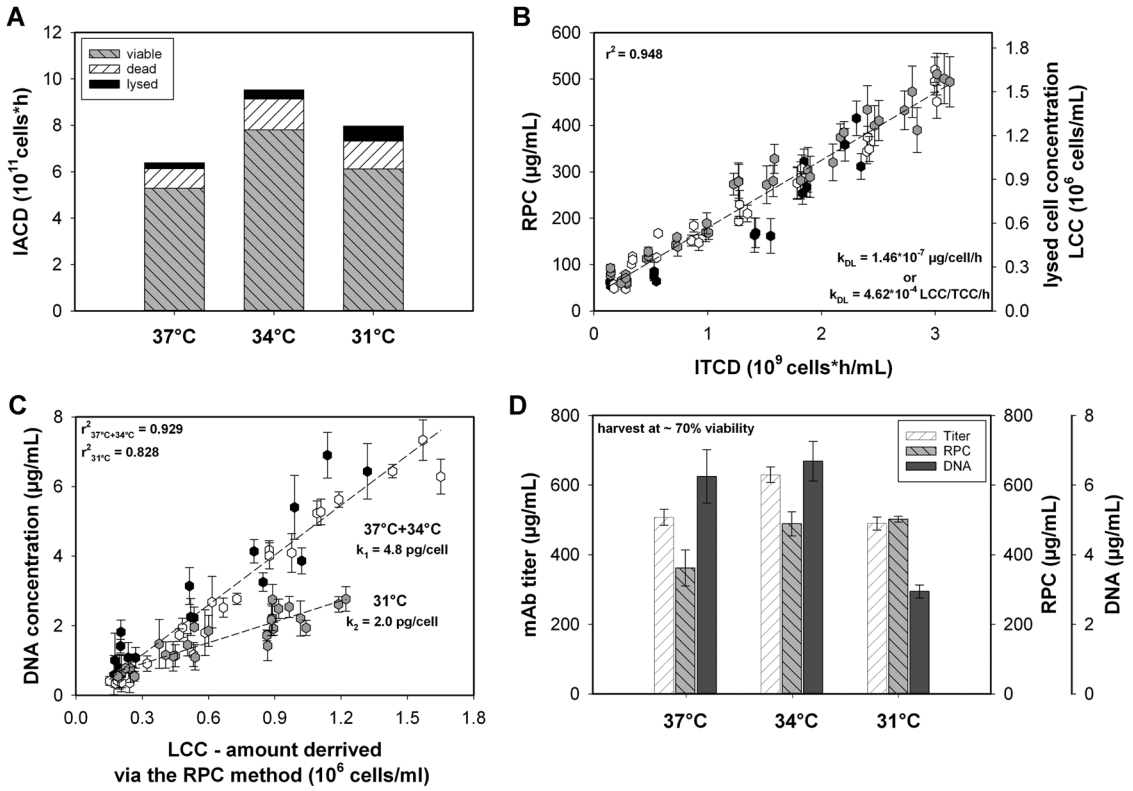


**Figure 5.** A) IACD at their corresponding process temperatures. B) RPC as a function of ITCD. C) DNA concentration as a function of lysed cells. The amount of lysed cells was determined using the RPC method (315 pg per cell). For (B) and (C), each data point depicts the average of a duplicate experiment at 37 °C ⬢, 34 °C ⬡, and 31 °C ⬢. D) mAb titer, DNA content, and RPC at harvest. IACD, integrated absolute cell densities; ITCD, integrated total cell density.

process. Although the fed-batches were all harvested with similar viability, the supernatant quality differed (Figure 5D). The process using the lowest temperature exhibited the worst ratio of impurities to the target protein, and could not accomplish similar ratios to the other two processes. The results clearly demonstrate that the RPC/mAb ratio could be an alternative process indicator for CHO cell cultures. It can give an appropriate impression of the impurity level in the supernatant. However, to understand the dynamics and the complexity of HCPs, a qualitative analysis must be further applied.[15,19,36]

## 4. Conclusions

Cell lysis is an important parameter to correctly characterize bioprocesses. Lysed cells have a substantial impact on the upstream and downstream performance. Information regarding the RPC is beneficial for establishing and maintaining a consistent process performance. Notably, RPC determination adds great value for further improvement to integrated bioprocesses as well as to the development of process models for process control purposes.

One particularly important aspect is that a producing CHO cell consists largely of proteins (>70%), whereas DNA remains a minority (1.4%). Therefore, changes to the protein spectrum will not have a great impact on the overall protein content, since the majority of the proteins are necessary for cell maintenance and protein production.[37] Indeed, HCP production can be very similar throughout the different growth phases.[1] We showed that the DNA content subsequently depends on the phase of the cell cycle. A cell in the S or G2/M phase contains more DNA than a cell in the G1 or G0 phase. Notably, the amount of cells at a certain cell stage will differ depending on the process conditions.

With this established methodology, the user has a very precise, fairly accurate, and robust tool for depicting the state of a cell culture bioprocess, apart from relying only on the viability of a cell population. The presented assay could be implemented as a high-throughput technique, as it can be performed in multiwell plate format and thus the use of pipetting robots may also be feasible. Furthermore, the method described in this study does not include light-sensitive or time-dependent steps; it is easy to implement and cost effective, and thus it could be applied to arbitrarily large experimental settings. The generated data are most suitable for establishing soft sensors and process models. Moreover, RPC[14] can now be monitored inexpensively and easily throughout the entire process, which makes it an interesting approach also for continuous processing.

## Acknowledgements

The authors would like to acknowledge the entire PAT-Plant project team, but especially Benjamin Bayer and Florian Bacher for their efforts in conducting the fed-batch experiments. They also thank the Austrian

 

Research Promotion Agency (FFG) and Bilfinger Industrietechnik Salzburg (Competence Headquarters, 849725) for their support.

## Conflict of Interest

The authors declare no conflict of interest.

## Keywords

Bradford assay, cell culture bioprocess, CHO, HCP determination, host cell protein

Received: December 6, 2018
Revised: April 7, 2019
Published online: May 17, 2019

[1] I. H. Yuk, J. Nishihara, D. Walker Jr, E. Huang, F. Gunawan, J. Subramanian, A. F. J. Pynn, X. C. Yu, J. Zhu-shimoni, M. Vanderlaan, D. C. Krawitz, E. Stage, C. Culture, D. N. A. Way, S. S. Francisco, *Biotechnol. Bioeng.* **2015**, *112*, 2068.
[2] M. Kornecki, F. Mestmäcker, S. Zobel-Roos, L. Heikaus de Figueiredo, H. Schlüter, J. Strube, *Antibodies* **2017**, *6*, 13.
[3] T. Klein, N. Heinzel, P. Kroll, M. Brunner, C. Herwig, L. Neutsch, *J. Biotechnol.* **2015**, *207*, 67.
[4] P. Kroll, K. Eilers, J. Fricke, C. Herwig, *Eng. Life Sci.* **2017**, *17*, 440.
[5] C. Legrand, J. M. Bour, C. Jacob, J. Capiaumont, A. Martial, A. Marc, M. Wudtke, G. Kretzmer, C. Demangel, D. Duval, J. Hache, *J. Biotechnol.* **1992**, *25*, 231.
[6] J. L. Goergen, A. Marc, J. M. Engasser, I. National, P. De Lorraine, *Cytotechnology* **1993**, *11*, 189.
[7] M. Allen, P. Millett, E. Dawes, N. Rushton, *Clin. Mater.* **1994**, *16*, 189.
[8] F. K.-M. Chan, K. Moriwaki, M. J. De rosa, *Methods Mol. Biol.* **2013**, *979*, 65.
[9] A. J. Racher, D. Looby, J. B. Griffiths, *Cytotechnology* **1990**, *3*, 301.
[10] P. Kroll, I. V. Stelzer, C. Herwig, *Biotechnol. Lett.* **2017**, *39*, 1667.
[11] J. M. Newton, D. Schofield, J. Vlahopoulou, Y. Zhou, *Biotechnol. Prog.* **2016**, *32*, 1069.
[12] J. M. Newton, J. Vlahopoulou, Y. Zhou, *Biochem. Eng. J.* **2017**, *121*, 38.
[13] A. S. Tait, C. E. M. Hogwood, C. M. Smales, D. G. Bracewell, *Biotechnol. Bioeng.* **2012**, *109*, 971.
[14] D. G. Bracewell, R. Francis, C. M. Smales, *Biotechnol. Bioeng.* **2015**, *112*, 1727.
[15] C. E. Hogwood, D. G. Bracewell, C. M. Smales, *Curr. Opin. Biotechnol.* **2014**, *30*, 153.
[16] M. Pathak, A. S. Rathore, K. Lintern, D. G. Bracewell, *Biotechnol. Prog.* **2018**, *34*, 412.
[17] N. E. Levy, K. N. Valente, K. H. Lee, A. M. Lenhoff, *Biotechnol. Bioeng.* **2016**, *113*, 1260.
[18] J. Zhu-Shimoni, C. Yu, J. Nishihara, R. M. Wong, F. Gunawan, M. Lin, D. Krawitz, P. Liu, W. Sandoval, M. Vanderlaan, *Biotechnol. Bioeng.* **2014**, *111*, 2367.
[19] C. H. Goey, D. Bell, C. Kontoravdi, *mAbs* **2018**, *10*, 476.
[20] K. Zboray, W. Sommeregger, E. Bogner, A. Gili, T. Sterovsky, K. Fauland, B. Grabner, P. Stiedl, H. P. Moll, A. Bauer, R. Kunert, E. Casanova, *Nucleic Acids Res.* **2015**, *43*, e102.
[21] J. Xu, J. S. Long, *Stata J.* **2005**, *5*, 537.
[22] H. Hefzi, K. S. Ang, M. Hanscho, A. Bordbar, D. Ruckerbauer, M. Lakshmanan, C. A. Orellana, D. Baycin-Hizal, Y. Huang, D. Ley, V. S. Martinez, S. Kyriakopoulos, N. E. Jiménez, D. C. Zielinski, L. E. Quek, T. Wulff, J. Arnsdorf, S. Li, J. S. Lee, G. Paglia, N. Loira, P. N. Spahn, L. E. Pedersen, J. M. Gutierrez, Z. A. King, A. M. Lund, H. Nagarajan, A. Thomas, A. M. Abdel-Haleem, J. Zanghellini, H. F. Kildegaard, B. G. Voldborg, Z. P. Gerdtzen, M. J. Betenbaugh, B. O. Palsson, M. R. Andersen et al., *Cell Syst.* **2016**, *3*, 434.
[23] M. R. de Moreno, J. F. Smith, R. V. Smith, *J. Pharm. Sci.* **1986**, *75*, 907.
[24] K. M. Carroll, D. M. Simpson, C. E. Eyers, C. G. Knight, P. Brownridge, W. B. Dunn, C. L. Winder, K. Lanthaler, P. Pir, N. Malys, D. B. Kell, S. G. Oliver, S. J. Gaskell, R. J. Beynon, *Mol. Cell. Proteomics* **2011**, *10*, 1.
[25] X. Pan, C. Dalm, R. H. Wijffels, D. E. Martens, *Appl. Microbiol. Biotechnol.* **2017**, *101*, 8101.
[26] A. H. Cawood, U. Potter, H. G. Dickinson, *J. Histochem. Cytochem.* **1978**, *26*, 645.
[27] R. Tobias, S. Kumaraswamy, *Forte Bio Appl. Note* **2013**, *14*, 1.
[28] K. N. Jonnalagadda, L. R. A. Markely, B. Guan, C. Alves, S. Prajapati, *Anal. Methods* **2016**, *8*, 7193.
[29] X. Li, Y. Wu, L. Zhang, Y. Cao, Y. Li, J. Li, L. Zhu, G. Wu, *Anal. Biochem.* **2014**, *451*, 18.
[30] A. Maccani, W. Ernst, R. Grabherr, *Cytometry, Part A* **2013**, *83A*, 893.
[31] N. Kumar, P. Gammell, M. Clynes, *Cytotechnology* **2007**, *53*, 33.
[32] W. Hu, C. Berdugo, J. J. Chalmers, *Cytotechnology* **2011**, *63*, 445.
[33] S. Albrecht, C. Kaisermayer, D. Reinhart, M. Ambrose, R. Kunert, A. Lindeberg, J. Bones, *Anal. Bioanal. Chem.* **2018**, *410*, 3197.
[34] C. E. M. Hogwood, A. S. Tait, N. Koloteva-Levine, D. G. Bracewell, C. M. Smales, *Biotechnol. Bioeng.* **2013**, *110*, 240.
[35] K. Lintern, M. Pathak, C. M. Smales, K. Howland, A. Rathore, D. G. Bracewell, *J. Chromatogr. A* **2016**, *1461*, 70.
[36] M. Nishita, S. Y. Park, T. Nishio, K. Kamizaki, Z. Wang, K. Tamada, T. Takumi, R. Hashimoto, H. Otani, G. J. Pazour, V. W. Hsu, Y. Minami, *Sci. Rep.* **2017**, *7*, 1.
[37] D. Baycin-Hizal, D. L. Tabb, R. Chaerkady, L. Chen, N. E. Lewis, H. Nagarajan, V. Sarkaria, A. Kumar, D. Wolozny, J. Colao, E. Jacobson, Y. Tian, R. N. O'Meally, S. S. Krag, R. N. Cole, B. O. Palsson, H. Zhang, M. Betenbaugh, *J Proteome Res.* **2012**, *11*, 5265.

 

Journal of Industrial Microbiology & Biotechnology (2019) 46:1167–1178
https://doi.org/10.1007/s10295-019-02202-5

SIMB
Society for Industrial Microbiology and Biotechnology

FERMENTATION, CELL CULTURE AND BIOENGINEERING - ORIGINAL PAPER

# Impact of mammalian cell culture conditions on monoclonal antibody charge heterogeneity: an accessory monitoring tool for process development

**Bernhard Sissolak[1] · Nico Lingg[2] · Wolfgang Sommeregger[3] · Gerald Striedner[1] · Karola Vorauer-Uhl[1]**

Received: 31 October 2018 / Accepted: 30 May 2019 / Published online: 7 June 2019


## Abstract

Recombinant monoclonal antibodies are predominantly produced in mammalian cell culture bioprocesses. Post-translational modifications affect the micro-heterogeneity of the product and thereby influence important quality attributes, such as stability, solubility, pharmacodynamics and pharmacokinetics. The analysis of the surface charge distribution of monoclonal antibodies provides aggregated information about these modifications. In this work, we established a direct injection pH gradient cation exchange chromatography method, which determines charge heterogeneity from cell culture supernatant without any purification steps. This tool was further applied to monitor processes that were performed under certain process conditions. Concretely, we were able to provide insights into charge variant formation during a fed-batch process of a Chinese hamster ovary cell culture, in turn producing a monoclonal antibody under varying temperatures and glucose feed strategies. Glucose concentration impacted the total emergence of acidic variants, whereas the variation of basic species was mainly dependent on process temperature. The formation rates of acidic species were described with a second-order reaction, where a temperature increase favored the conversion. This platform method will aid as a sophisticated optimization tool for mammalian cell culture processes. It provides a quality fingerprint for the produced mAb, which can be tested, compared to the desired target and confirmed early in the process chain.

**Keywords** Product quality · Recombinant mAbs · Charge heterogeneity determination · Mammalian cell culture · CHO

## Introduction

Recombinantly produced monoclonal antibodies (mAbs), as well as biosimilars, are key products in today's pharmaceutical industry [1, 2]. Post-translational product modifications induced by chemical and enzymatical intra- and extracellular mechanisms during the production process lead to micro-heterogeneity of mAbs, in turn affecting product characteristics (e.g., efficacy, safety, pharmacodynamics and pharmacokinetics) [3]. The recombinant cell line, the culture media and the process settings affect these quality attributes [4, 5]. During process development, it is important to ensure a reproducible, distinct and preferably homogenous pattern of the product. For the establishment of biosimilars, it is important to match the characteristics of the originator product [6]. The effects of various extra- and intracellular influences on different aspects of product quality have been evaluated in great detail. For instance, *N*-glycosylation is by far the best-studied quality attribute and there are several strategies available for glycosylation control [7].

One additional important measure of mAb heterogeneity is the distribution of surface charge variants. Due to numerous modifications, the net surface charge of mAbs can be altered [8–11]. Charge species with a lower isoelectric point (pI) than the main fraction of the product are defined as acidic variants and generated by sialylation, deamidation of asparagine and glutamine, glycation and other mechanisms. Glycation, for instance, is a non-enzymatic reaction where a reducing sugar molecule, most commonly glucose, is covalently bound to a reactive amino group [12]. Basic variants are defined as species with a higher pI than the main fraction

✉ Bernhard Sissolak
bernhard.sissolak@boku.ac.at

[1] Department of Biotechnology, University of Natural Resources and Life Sciences (BOKU), Vienna, Austria

[2] Austrian Centre of Industrial Biotechnology GmbH (ACIB), Vienna, Austria

[3] Bilfinger Industrietechnik Salzburg GmbH, Salzburg, Austria

and generated by incomplete C-terminal lysine clipping of the heavy chains, as well as by fragmentation and aggregation [13]. Several studies indicate that mAb variants can lead to varying biological responses [14–16]. For instance, it was shown that the basic variants exhibited an increased binding to the FC and the neonatal receptor, indicating an increased half-life [15]. Another study reported that only a few specific variants of the tested mAb had a statistical relevant impact on the cell proliferation assay [10]. Hence, to know and understand the mechanism behind the charge heterogeneity is of particular importance.

Common analytical methods for the determination of charge heterogeneities of mAbs are capillary isoelectric focusing (cIEF) and ion exchange chromatography (IEX) [17]. Both methods are widely used in various applications [18], but IEX methods, using a salt gradient elution, are recognized as the gold standard and routinely in use [19–22]. The major limitation of IEX is when using a salt buffer system to coerce the user to adapt it for every new kind of mAb. However, the use of pH gradients was shown to be product-independent [23] and recently, a cation exchange chromatography (CEX) method with a linear pH gradient for the determination of charge heterogeneity of mAbs was published [24]. This technique was shown to be robust, exhibit a high resolution [25], result in similar precisions compared to imaged cIEF [26] and be scalable for semi-preparative purposes [14, 15].

Monitoring and controlling of product quality are required for the whole production chain [27]. The successful application of process analytical technology (PAT) and quality by control (QbC) to bioprocesses [28] requires reliable and unbiased product quality data over the time course of a fermentation process. Samples taken from crude culture supernatants should be analyzable with a minimum of manipulation. In this respect, pre-purification of relevant samples would possibly falsify the results [29–31]. Moreover, the avoidance of purification steps reduces the workload, while the method becomes more applicable as a process-monitoring tool and allows for decision making early in the process chain.

In this work, we aimed to adjust the method developed by Lingg et al. [24] for the measurement of charge heterogeneity directly from cell culture supernatants without prior purification or additional sample manipulation. This approach offers the possibility to assess any quality changes already in the early stages of cell line, media and process development. Eventually, the derived data enable advanced process characterization and monitoring. In the first part of this manuscript, we explain the applicability of CEX separation for the analysis of crude culture supernatants and evaluate the influence of matrix effects. In the following, it is used as a process-monitoring tool for a model antibody, expressed in Chinese hamster ovary (CHO) cells, within an experimental setting, while varying glucose concentration in the feed media and cultivation temperature. Process relevant samples were analyzed by CEX to study the impact of these variations on mAb charge heterogeneity.

## Materials and methods

### Fed-batch experiments

A recombinant CHO monoclonal cell line, generated by the *Rosa26* bacterial artificial chromosome expression strategy [32], producing an antitumor necrosis factor (TNF) alpha IgG1, was used (Antibody Lab GmbH, Austria). The cell line originated from the host cell CHO-K1 (ATCC CCL-61), which was serum-free adapted for prior use. A working cell bank of the recombinant cell line with $5 \times 10^6$ cells per vial was used as the starting material for all experiments. The cells were thawed in chemically defined culture medium (Dynamis AGT, A26175, Thermo Fisher Scientific, USA) supplemented with 8 mM L-glutamine (25030081, Sigma Aldrich, Germany), 3 mL/L phenol red solution (RNBD642, Sigma Aldrich, Germany), 1:1000 anti-clumping agent (0010057DG, Thermo Fisher Scientific, USA) and 1 mg/mL G418 (10131027, Thermo Fisher Scientific, USA).

The culture was subsequently passaged three times (every 3–4 days) in the above-mentioned media without G418 and anti-clumping agent and used as the starting material for the inoculation of the batch with a starting cell density of $2.5 \times 10^5$ cells/mL. The fed-batch cultivations were performed in shake flask (#431147, Corning, USA) with a starting volume of 300 mL. As batch medium, the culture medium was additionally supplemented with 0.1% (v/v) Antifoam C (A8011, Sigma Aldrich, Germany) to represent typical large-scale cultivation conditions. Within the experimental setup, the parameters of temperature and glucose addition during the feed phase were changed. In this study, the feed (CHO CD EfficientFeed™ A AGT™ Kit, A1442002, Thermo Fischer Scientific, USA) was supplemented with 0.1% antifoam as well as additional 10, 20 or 30 g/L glucose, which will be referred to as Feed 1, Feed 2 and Feed 3, respectively. The pulse feeding started at day 3 and lasted until day 13. A linear feed rate was carried out with a total added feed volume of 33 vol% (v/v) with respect to the end volume. The process temperatures were changed at day 4–31 °C or 34 °C or remained constant at 37 °C.

An 11 mL sample was drawn each day for several offline analyses. The cultivations were terminated when the viability dropped below a threshold of 70%. All cultivations were conducted in a humidified $CO_2$ incubator (Heracell™ VIOs 160i, Thermo Scientific, USA) at 5% (v/v) $CO_2$ in ambient air, at the temperature defined in the experimental design

with an orbital shaker (MaxQ 2000 $CO_2$ Plus, Thermo Scientific, USA) at 200 rpm.

For the mock control fed-batch bioprocess, the host cell line was cultivated at a constant 37 °C with Feed 3 (+30 g/L glucose). The fed-batch was performed applying the same settings as mentioned above.

### All experiments were carried out in duplicates

For the LC–MS and the boronate affinity chromatography analysis, samples from a stirred tank reactor ($V = 15$ L) were used. The same procedure, cell line and parameters as stated above were utilized.

### Analytics

The total cell concentration (TCC) was determined by counting the cell nuclei using the particle counter Z2 (Beckman Coulter, USA). Therefore, an aliquot of the cell suspension was centrifuged for 10 min at 200*g* at room temperature. The cell pellet was resuspended in a 0.1 M citric acid monohydrate (C1909, Merck, Germany) and 2% (v/v) Trition X-100 (Merck, Germany) buffer. A minimum of 1 h later, an aliquot of the lysate was diluted with 9 mL of a 0.9% NaCl solution and measured.

Viability was measured by the trypan blue (K490, Amresco, USA) exclusion assay [33]. The viable cell concentration (VCC) was calculated by applying the viability to the TCC.

The product titer was determined by bio-layer interferometry (BLI) using Protein A tips (Octet System, QK, ForteBio, USA) as already described by [34].

The carbohydrates were measured via ion exclusion chromatography (HPX 87H, 300 × 7.8 mm, #1250140, BioRad, USA) on an Agilent 1200 series device (Agilent, USA). The column was tempered at 25 °C. The mobile phase was 5 mM sulfuric acid and the flow rate was 0.45 mL/min. The used detector was a refractive index detector tempered at 35 °C. The calibration range for D(+)-glucose was between 100 and 2000 mg/L. The chromatograms were evaluated with ChemStation software (Revision B.04.01, Agilent, USA).

Gel electrophoresis was performed with an Invitrogen NuPage™ 4–12% Bis–tris gel (NP0321BOX) in a Novex Mini-cell chamber (both Thermo Fisher Scientific, USA). A SeeBlue® Plus2 pre-stained protein standard (LC5925, Thermo Fisher Scientific, USA) was used for size comparison. The samples were applied with 4 × sample buffer (NuPAGE LDS, NP0007, Thermo Fisher Scientific, USA), while the used running buffer contained 0.3% (w/v) Tris, 1.5% (w/v) glycine and 0.1% (w/v) SDS. Gels were run at 150–200 V. Adalimumab (Humira™, AbbVie, USA) was used as a reference.

Protein A purification was done via a Proteus Protein A mini spin column (PUR 006, Bio-Rad, USA) according to the manual instructions.

Glycated mAb species were determined via boronate affinity chromatography (BAC) (0013066, Tosoh Bioscience, Japan). Solvent A consisted of 50 mM EPPS (E9502, Merck, Germany), 10 mM Tris (65837, Fluka, USA) and 200 mM NaCl (S7653, Merck, Germany), which were adjusted to a pH 8.7 with 10 M NaOH. Solvent B was 500 mM sorbitol (85529, Merck, Germany) in Mobile Phase A. Chromatography was performed according to a previously published study [35].

For the peptide analysis, the samples were digested in gel and analyzed via LC–MS as previously published [36–38].

### Charge heterogeneity determination

For the method, as previously described in two publications [24, 25], a weak cation exchange resin (Dionex ProPac WCX-10 4 × 250 mm, 088768, Thermo Fisher Scientific, USA) was utilized. Due to the fact that supernatants were directly applied, a guard column (4 × 50 mm) was also installed (054994, Thermo Fisher Scientific, USA). Two complex, four-component buffers were used to ensure a highly linear pH gradient. The compounds were 3-morpholino-2-hydroxypropanesulfonic acid (MOPSO, M8389), 4-(2-hydroxyethyl)piperazine-1-ethanesulfonic acid (HEPES, H3375)), *N*,*N*-bis(2-hydroxyethyl)glycine (Bicine, B3879,), 3(cyclohexylamino)-2-hydroxy-1-propanesulfonic acid (CAPSO, C2278) and 3-(cyclohexylamino)-1-propanesulfonic acid (CAPS, C2632, all Merck, Germany). To ensure elution was only based on the pH shift, sodium chloride (S7653, Merck, Germany) was added to Buffer A according to Table 1 to obtain constant conductivity. The pH was adjusted with sodium hydroxide (Merck, Germany). The two different buffer systems used are listed in Table 1.

In this study, supernatants were applied using a flow rate of 1.0 mL/min, while the injection volume was 100 µL. The

**Table 1** Running (A) and elution (B) buffer compositions used in the CEX method

| System | Buffer | HEPES | MOPSO | Bicine | CAPSO | CAPS | NaCl |
|---|---|---|---|---|---|---|---|
| pH 7–10.5 | A (mM) | 0.0 | 7.1 | 5.3 | 14.9 | 0.7 | 12.6 |
| | B (mM) | 0.0 | 14.6 | 4.9 | 1.4 | 7.1 | 0.0 |
| pH 8–10.5 | A (mM) | 5.5 | 0.0 | 4.2 | 9.5 | 0.8 | 6.3 |
| | B (mM) | 0.0 | 0.0 | 10.5 | 2.5 | 7.0 | 0.0 |

elution gradient for both buffer systems was set to 0.07 pH/min. The chromatograms were evaluated with ChemStation software. As a reference, the same adalimumab standard as stated above was used. Statistical analysis was performed with SigmaPlot 13.0 software.

## Results and discussion

### Assessment of the method's appropriateness concerning the cell culture matrix

Since the IEX method has already been thoroughly verified, this study is entirely focused on the adaptation for cell culture samples. Critical considerations were taken in terms of possible matrix effects and the qualitative evaluation of the resulting peak areas.

The recombinantly produced anti-TNF-alpha antibody was compared to a pharmaceutical adalimumab reference, which is a well-described mAb [21]. The reference standard analyzed by a CEX with a linear pH gradient exhibited a distinct peak distribution (see Fig. 1a). Due to the use of a strictly pH-dependent system, the charge variants were only separated according to their net surface charge, where acidic forms were eluted prior to the neutral and basic variants. Both buffer systems (pH 7–10.5 and pH 8–10.5) and different flow rates were tested in terms of their applicability for supernatants. The pH gradient itself was set to a constant slope of 0.07 pH/min. In conclusion, the pH 7 variant resulted in a better separation of the acidic species. It is obvious that the close proximity of the calculated pI of the mAb (8.60) and the starting pH conditions affect the separation profile of the acidic isoforms. The tested flow rates, between 0.5 and 1 mL/min, did not significantly affect the measurement's resolution characteristics. This confirms the

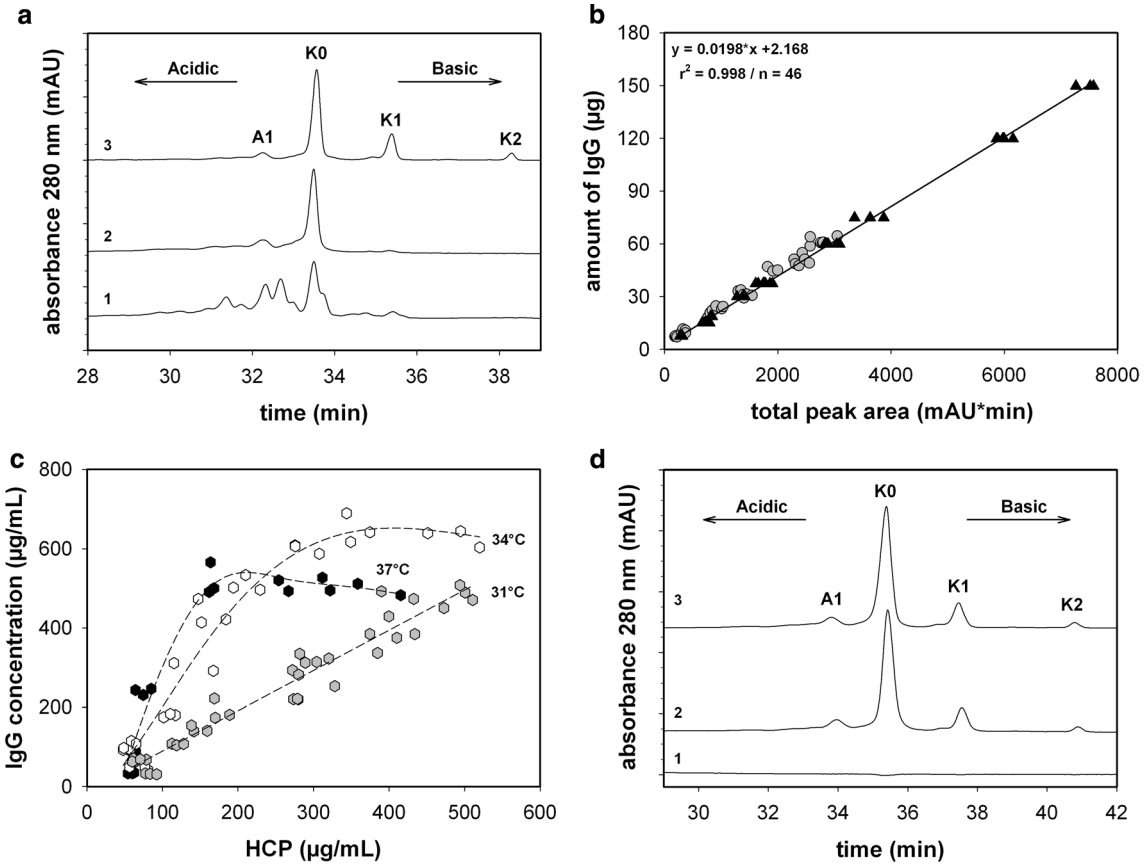


**Fig. 1** **a** HPLC-chromatogram of a recombinantly produced protein measured directly from the supernatant at harvest (1), the same sample but pre-purified via Protein A (2) and the adalimumab reference (3), using the pH 7 buffer system. **b** Amount of IgG as a function of the integrated total peak area for the shaker data [grey-filled circle] and control standards [filled triangle]. **c** Amount of host cell proteins (HCPs) and IgG of fed-batch experiments at 37 °C [filled hexagon], 34 °C [unfilled hexagon] and 31 °C [grey hexagon]. **d** CEX chromatogram of a mocking supernatant (1), a standard spiked into the same supernatant (2) and the standard (3). *K0* main variant, *K1* 1-lysine variant, *K2* 2-lysine variant, *A1* acidic variant without further characterization. Linear regression was performed on the adalimumab dataset

excellent mass transfer properties of the core shell particle-based stationary phase. Therefore, the pH 7 buffer system was chosen and the flow rate was set to 1 mL/min for the following studies. Due to the fact that the resolution was already sufficient, no attention was paid to optimize the running conditions any further.

Under these conditions, several samples and the reference standard in different matrices were analyzed as shown in Fig. 1. The most abundant variant was allocated to the main variant and marked as K0, where K0 represents the complete cleavage of the C-terminal lysine. In the basic region, two peaks were evident, which caused incomplete lysine clipping, enumerated as K1 and K2, where one or both lysine residues remained attached to the heavy chain C-termini [21]. In the acidic area, there was only one pronounced peak (A1) evident for the standard. The anti-TNF-alpha antibody produced in our process revealed a different chromatographic pattern. The main variant (K0) was identified at a similar retention time, while the basic and the acidic region exhibited more variants. These differences are not remarkable due to the fact that the reference standard was a purified API, while the anti-TNF-alpha antibody expressed in a certain cell line with a defined media was produced under variable process conditions and not purified at all.

During repeated test sequences, it became apparent that slight variabilities in the buffer system resulted in minor retention time shifts caused by these sensitive gradients (see Fig. 1a, d). Consequently, the reference material was analyzed each time when a new buffer was prepared, both to control the performance characteristic and to ensure correct integration. To make the set of data comparable, the retention time was normalized. This was done by dividing the retention time $t_i$ by the retention time of the main variant $t_{main}$ peak. Thereafter, peak area integration was performed within a $t_{normalized}$ of 0.76–1.23 for all analyses; in the following, this is referred to as the total peak area.

After the performance optimization, the reference standard and various samples were evaluated according different criteria. For the indication, whether or not the samples were affected by matrix proteins, both supernatant samples ($n=36$) and standards ($n=46$) were analyzed. The relationship between the total area and the amount of IgG, previously determined with BLI was assessed. The linear relationship of both indicated that the established performance was sufficient to obtain reliable data for standards and supernatants (see Fig. 1b).

Furthermore, for a comprehensive quantitative evaluation, it is important that the interprecision of the distribution is appropriate. The calculated coefficient of variation (CV) for the acidic, main and basic variants of the control standard ($n=15$) was below 10% for all variants (see Table 2). These results are in accordance with the comprehensively verified data published by Lingg et al. [25]. For demonstrating the charge distribution reproducibility of the recombinantly produced mAbs in supernatants, as fed-batch samples, which were collected at day 4, were analyzed. Day 4 was at the end of the batch phase assuming that the experiments were performed in a similar manner. All temperature shifts were performed after the batch phase. The acidic and main variant distribution exhibited a CV of 4% and 10%, respectively ($n=8$). The CV of the basic variant area was higher at 26%, caused by the low amount of this variant (see Table 2). Compared to the standard, the quantitative distribution of the fed-batch sample at day 4 was different. Acidic species were the most abundant variants, evidencing a possible impact of the chosen bioprocess conditions.

**Table 2** Charge heterogeneity distribution consistency of the control standards and supernatant samples determined by the described CEX method using the pH 7 buffer system

| Sample | Variant | Relative area $\pm\sigma$ (%) |
|---|---|---|
| Pharmaceutical standard ($n=15$) | Acidic | 16.2 ± 1.3 |
| | Main | 59.2 ± 1.6 |
| | Basic | 24.5 ± 0.8 |
| Fed-batch samples drawn at day 4 ($n=8$) | Acidic | 69.2 ± 3.0 |
| | Main | 24.6 ± 2.5 |
| | Basic | 6.6 ± 1.7 |

Although it can be shown that a linear relationship between the total area and the amount of IgG exists, the variable amount of HCPs could falsify the chromatographic results, for instance, in the later stages of the cell culture process, when the viability decreases and the cells start to lyse. The HCP population is highly heterogeneously composed, but the majority should exhibit a pI below 7 and a molecular weight lower than 150 kDa [39, 40]. The ratio of HCP to IgG titer ranged between 20 and 50% and was independent of the feeding strategy (see Fig. 1c). Co-elution of any proteins or antibody fragments was not observed. Silver-stained fractionated samples revealed only one pronounced band at around 150 kDa (data not shown). Additionally, in the mock control, where the HCP content was even higher (up to 700 µg/mL), no additional peak occurred within the elution period of the mAb. In this respect, only a slight baseline drift of around 0.2–0.4 milli-absorbance units was detectable, primarily indicating an effect of supernatant compositions, which is not caused by HCPs. Spiking experiments in the mock control supernatant confirmed the assumption that HCPs do not affect the elution pattern (see Fig. 1d). Therefore, the contribution of HCPs and the culture supernatant matrix to the measured charge variant distribution was considered as not significant. Co-elution of any other proteins or other cell culture components did not affect the quality of the obtained data.

In summary, the results indicate that the determination of mAb charge distribution directly from supernatants is practicable. It has also been shown that the method is reliable and reproducible.

## Process monitoring of cell culture processes

The optimized method was used to monitor mAb charge heterogeneity during a cell culture process to elucidate the influences of temperature and glucose concentration.

The batch phase exhibited similar trends in all measured variables for each experiment. The process temperatures had a significant impact on overall productivity, growth rates and viability of the cells (see Fig. 2). Such observations have already been described in several publications [41–44]. Reduced process temperature can, moreover, be used for the proliferation control of cell culture processes [45]. Even though glucose concentrations in the cultures varied from 2 to 15 g/L (Fig. 2d), depending on the feed and temperature, almost no impact on the monitored process variables could be detected. Only the osmolality could be partly linked to the glucose concentration in the supernatant, which ranged from 345 (high glucose) to 233 mOsm/kg (low glucose) (see Fig. 2d, e). Lactate production was only observed in the batch phase, while consumption took place during the remaining process (Fig. 2c), independent of the temperature and glucose profile. Interestingly, no difference in specific nutrient uptake and byproduct formation rates was determined, due neither to the elevated glucose level nor to the change in process temperature. $q_{gluc}$ was independent in respect of the feed or process temperature used (see Fig. 2f), with such behavior previously reported in other publications [46, 47]. The observation may be correlated with the fact that glucose uptake is not only dependent on the amount of glucose but also on amino acids such as leucine, lysine and serine [48].

To evaluate the impact of process variation on charge distribution, several fed-batch samples from day 4, followed by samples after the temperature shift until the harvest criteria with a viability of 70%, were applied to the CEX column ($n = 36$). In turn, it became obvious that variation in the process parameters, glucose concentration and temperature affected the charge variant distributions to a great extent (see Fig. 3). Since the glucose concentration had no apparent influence on cell metabolism, it was supposed to have affected the mAb charge distribution in an extracellular manner (see Fig. 3a, c, e, g). This is also evidenced by the fact that the K0 main proportion correlates linearly with the percentage of acidic species (Fig. 3a). The resulting basic species are in opposition to this observation due to the fact that they mostly derive from incomplete C-terminal lysine processing, which is a known intracellular process (see Fig. 3b, d, f).

Under these defined process conditions, the basic species were generally rare, which suggests that C-terminal lysine processing occurred almost completely. However, process temperature predominantly affected the basic variant formation. As the amount of basic species was independent of the amount of the main variant, no trend could be identified; only two cluster regions were obvious (Fig. 3b). However, three linear relationships between the total basic area and K0 peak area could be determined by separating the data into three distinct groups according to the applied temperature (Fig. 3d). Evidently, lowering the temperature resulted in imperfect C-terminal lysine processing. This temperature-based occurrence was in accordance with previously published data [49]. The expression levels and the specific activity of the enzyme carboxypeptidase (B and H), which is considered to play a major role in C-terminal lysine cleavage, is temperature dependent [50, 51]. Hence, the processing of C-terminal lysine clipping, an important quality attribute [16], can be influenced by process temperature and sufficiently monitored with this method. The extracellular glucose concentration had no impact at all on basic species variations (Fig. 3f). The dataset could only be divided into two distinct groups: a 37 °C + 34 °C and a 31 °C cluster. No correlation was evident. Thus, in conclusion, the accumulated amount of basic species was the result of an intracellular process and most probably regulated by the amount and activity of the carboxypeptidase.

The vast impact of glucose on the micro-heterogeneity of the mAb was evident. The highest main variant (K0) content was observed at 34 °C with Feed 1 (low glucose). At an elevated glucose concentration, the amount of K0 was significantly reduced. For instance, the process at 31 °C with Feed 3 (high glucose) resulted in the highest charge heterogeneity. Acidic variants were the most abundant variants and ranged from 60 to 90% of the total peak area. It was obvious that an increase in the acidic species was attended by a decrease in the main variant (see Fig. 3a). The process at 31 °C, however, exhibited a slight parallel shifted linear correlation, due to the increased amount of basic species. At 31 °C, the proportion of basic variants was, on average, 5% higher than in the case of the other processes, which resulted in a decreased offset value of around the same proportion. However, both correlations exhibited a similar slope (Fig. 3a). The acidic heterogeneity was mainly dependent on the feed used; thus, an increase in glucose in the supernatant resulted in an enriched fraction of acidic variants (see Fig. 3c, e). It was lowest at 34 °C and 37 °C when a low glucose feed was applied. An induction of mAb alteration effects, due to osmolality and differences in the elution pattern, as reported by Schmelzer and Miller [52], was not evident. Acidic variant formation was mainly provoked by two parameters: the increasing total amount of main variants and incremental glucose concentration in the supernatant. Interestingly,

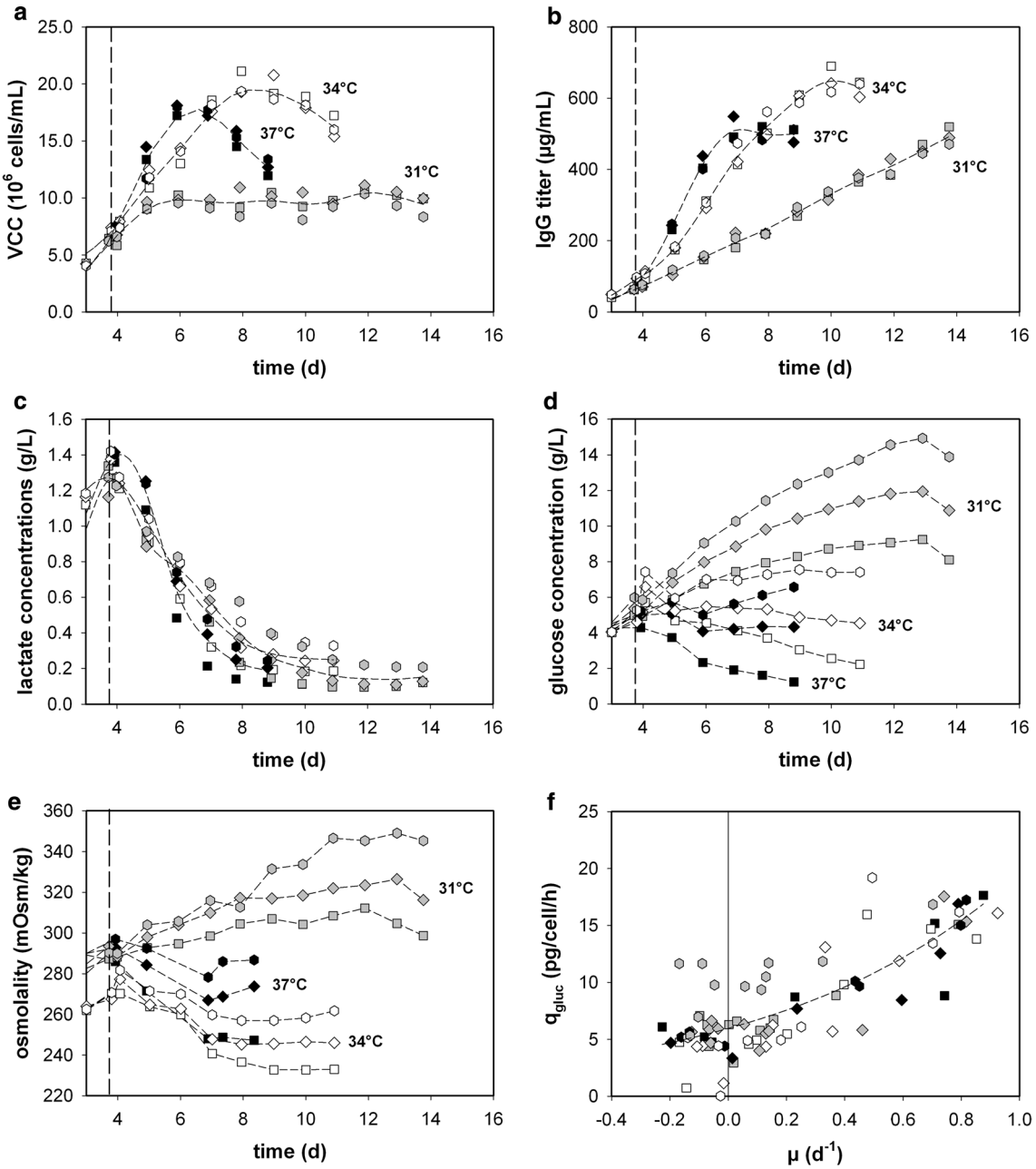


**Fig. 2** Fed-batch process parameters: **a** VCC, **b** protein titer, **c** lactate and **d** glucose concentration and **e** osmolality as a function of process time. **f** Specific glucose consumption ($q_{gluc}$) as a function of the growth rate ($\mu$). 37 °C + Feed 1 [filled square], 37 °C + Feed 2 [filled diamond], 37 °C + Feed 3 [filled hexagon], 34 °C + Feed 1 [unfilled square], 34 °C + Feed 2 [unfilled diamond], 34 °C + Feed 3 [unfilled hexagon], 31 °C + Feed 1 [grey square], 31 °C + Feed 2 [grey diamond], 31 °C + Feed 3 [grey hexagon]. Fed-batch process started at day 3. Vertical dashed line indicates temperature shift (≈day 4). Short dashed lines indicate trends

regarding the latter, a saturation plateau was reached. At glucose concentrations higher than 7 g/L, the ratio of the total acidic area to the K0 main peak area remained almost unaffected (Fig. 3e).

According to these results, three assumptions were made: first, during those bioprocesses, acidic variants mainly evolved from the main ones already present in the supernatant; second, considering that the different feeds had no influence on any major process parameter, among others, biomass and productivity, the glucose concentration in the supernatant directly influenced the formation of acidic variants; and, third, there was a predefined number of possible glucose-inducible acidic variants. Under the selected process conditions, glycation, the non-enzymatic attachment of a reactive glucose to a protein, was most likely a feasible cause of acidic peak formation. It has

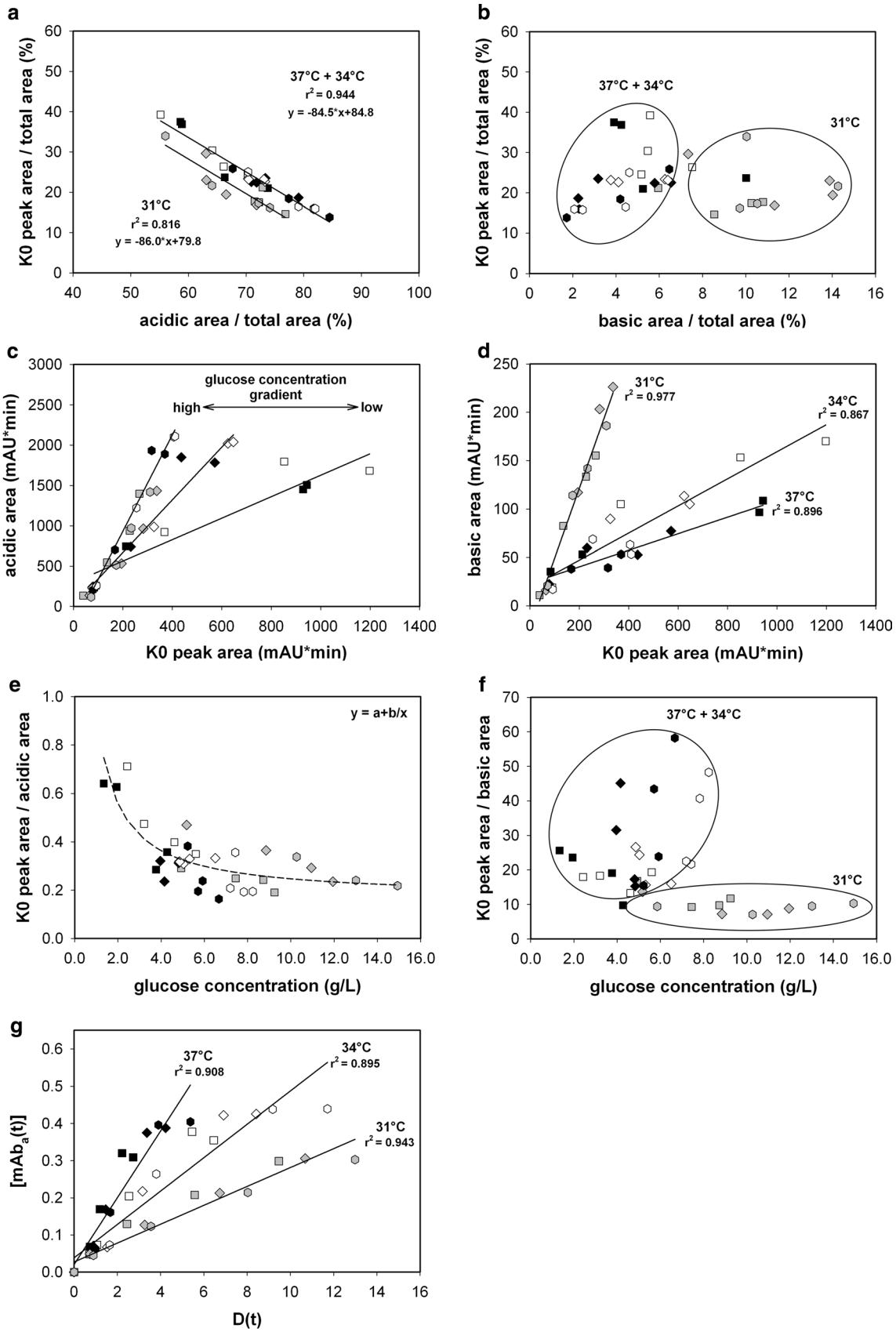
a
K0 peak area / total area (%)
acidic area / total area (%)
37°C + 34°C
r² = 0.944
y = -84.5*x+84.8
31°C
r² = 0.816
y = -86.0*x+79.8
b
K0 peak area / total area (%)
basic area / total area (%)
37°C + 34°C
31°C
c
acidic area (mAU*min)
K0 peak area (mAU*min)
glucose concentration gradient
high
low
d
basic area (mAU*min)
K0 peak area (mAU*min)
31°C
r² = 0.977
34°C
r² = 0.867
37°C
r² = 0.896
e
K0 peak area / acidic area
glucose concentration (g/L)
y = a+b/x
f
K0 peak area / basic area
glucose concentration (g/L)
37°C + 34°C
31°C
g
[mAb_a(t)]
D(t)
37°C
r² = 0.908
34°C
r² = 0.895
31°C
r² = 0.943

◂**Fig. 3** K0 main peak ratio as a function of the acidic (**a**) and basic variant (**b**) ratio. **c** Acidic area and **d** basic area as a function of the K0 main peak area. The ratio of the K0 peak area to the **e** acidic area and the **f** basic area as a function of glucose concentration. **g** Acidic peak area concentration at time point $t$ as a function of $D(t)$, that is, the product of newly built IgG concentration and glucose concentration integrated over time. 37 °C + Feed 1 [filled square], 37 °C + Feed 2 [filled diamond], 37 °C + Feed 3 [filled hexagon], 34 °C + Feed 1 [unfilled square], 34 °C + Feed 2 [unfilled diamond], 34 °C + Feed 3 [unfilled hexagon], 31 °C + Feed 1 [grey square], 31 °C + Feed 2 [grey diamond], 31 °C + Feed 3 [grey hexagon]

already been related to the protein content and the glucose concentration [12] and also seems to be substantiated by this study.

Due to that fact that acidic species, induced by glucose, were most likely extracellularly formed, a second-order reaction, as proposed for typical non-reversible glycation reaction [53], was constructed. Unlike Yuk et al. [53], we set up some constraints. First, only a certain amount of the antibody is susceptible to be transformed into an acidic species. Second, if one antibody is not transformed within the certain time period, then a transformation will not occur during the rest of the process. We defined the second-order reactions as follow (Eqs. 1–3):

$$[\Delta\mathrm{mAb}] + \left[\mathrm{glucose}\right] \rightarrow \left[\mathrm{mAb_{acidic}}\right] \tag{1}$$

Setting up the second-order reaction in its differential form, as well as integrating and rearranging, yielded:

$$\left[\mathrm{mAb_{acidic}}\right](t) = k \times D(t), \tag{2}$$

with

$$D(t) = \int_{t_0}^{t_i} [\Delta\mathrm{mAb}] \times \left[\mathrm{glucose}\right] \times \mathrm{d}t, \tag{3}$$

where $[\mathrm{mAb_{acidic}}](t)$ represents the concentration of the acidic variants at time point $t_i$, $k$ is the reaction constant and $D(t)$ is the integrated product at time point $t_i$ of the newly built IgG and the glucose concentration. If the second-order reaction assumption is true, the plotting of $[\mathrm{mAb_{acidic}}](t)$ against $D(t)$ should yield in a straight line with a slope of $k$ (Fig. 3g).

Evidently, the data are separated into three distinct groups, in respect of their applied process temperature. A linear regression was carried out. In conclusion, the reaction rate, and consequently the slopes of the representative lines, were dependent on the process temperature: 0.09, 0.04 and 0.03 $\frac{g_{\mathrm{acidic}} L}{g_{\mathrm{IgG}} g_{\mathrm{glucose}} d}$, for 37 °C, 34 °C and 31 °C, respectively. These findings are in agreement with published research data. Typical antibody alteration effects, which result in acidic variant formation, for instance, deamidation [54, 55] or glycation [56, 57], can be modulated by temperature [51].

Finally, it can be speculated that the glycosylation pattern may also contribute to the acidic charge heterogeneity (Fig. 4a). Nevertheless, this is not the case, because anti-TNF-alpha antibodies do not contain any sialic acids, while the proportion of high mannose types is similar to the reference material [13, 21]. Additionally, the BAC analysis indicated that a substantial proportion of the mAb was glycated (Fig. 4b). The reference material, when incubated in a high glucose solution, exhibited a peak at a similar retention time. Thus, in conclusion, it was determined that glycation was the main driver for the formation of variable amounts of acidic species under the adjusted process conditions.

To the best of our knowledge, this is the first study that provides insights into the formation of charge variants during a cell culture process without using any pre-purification steps. Evidently, within the chosen process conditions, the formation of variable acidic species is of dominant importance. To achieve an understanding of consistent product quality, appreciating the mechanism of charge variant formation is inevitable. Rapid determination of the charge distribution pattern can significantly facilitate process optimization. This can be useful for process development and control of antibody and biosimilar production. Medium composition effects, such as glucose concentration and physical variations (e.g., temperature), on the generation of charge variants can be analyzed accordingly; thus, product quality attributes can be determined very early on in the process chain. That said, when assigning the occurring variants to distinct post-translational modifications, a more detailed and thorough characterization is necessary. The chromatographic pattern alone does not imply the occurred modifications [58]. Combination with other methods, such as LC–MS or BAC, could help to significantly improve the understanding of the mechanism of peak formation.

## Conclusion

In this work, we established a process-monitoring tool for the determination of charge heterogeneity of mAbs directly from cell culture supernatants. This method is based on cation exchange chromatography using a linear, basic pH gradient, with which cell culture supernatant samples can be directly analyzed for mAb charge heterogeneity without the need for prior protein purification. This represents a potential powerful tool for process development, since changes in product quality due to changes in process parameters can be detected earlier. It also has potential to serve as an in-process control method for any mAb production process, which can offer invaluable process knowledge. Under the Quality by Design paradigm, this increase in knowledge about the relationship

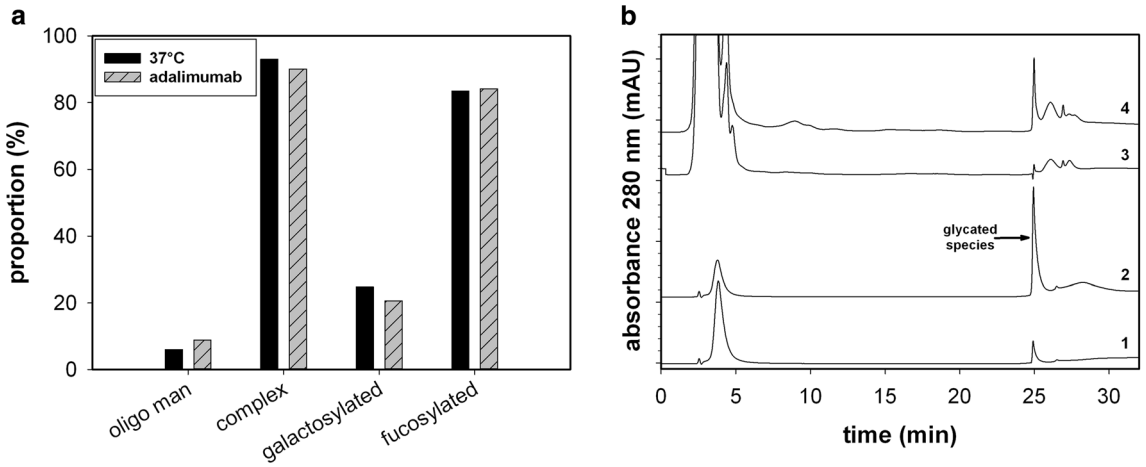


**Fig. 4** **a** Type of detected glycoforms for reference, for the recombinant produced mAb at 37 °C. **b** BAC chromatogram of the reference material (1), the reference incubated in 0.19 M glucose solution for 68 h at 37 °C (2), mocking supernatant from the host cell line (3), and a supernatant sample of a fed-batch process with a high number of acidic variants (≈90%) (4)

of product and quality parameters can lead to a more consistent product quality through improved process control.

We also present a case study, in which the process parameter glucose level and temperature where analyzed for their effect on product quality. We showed that target protein production was predominantly affected by the process temperature, whereas the acidic variant formation and thus the product quality were highly influenced by the glucose level in the cell environment. The formation of acidic variants could be conclusively linked to an extracellular mechanism. These observations confirm the importance of the control of glucose level to ensure consistent high-quality mAb output. The process temperature, however, remains important as well, since, next to the titer, it secondarily affected the rate of acidic peak formation as well as basic variant formation.

However, charge heterogeneity of a mAb can be an adequate fingerprinting technique to confirm the desired product quality attributes, already early in the process chain. Depending on the mAb, the method can be adapted to gain information in an even shorter period of time. In general, this method will add great value to process optimization.

**Acknowledgements** Open access funding provided by University of Natural Resources and Life Sciences Vienna (BOKU). We would like to thank Florian Strobl for the idea to perform this study, as well as Clemens Keinprecht, Katarina Kljajic and Gabi Lhota, along with the whole PAT-Plant project team, for their practical contribution to this work. The project was funded by the Austrian Research Promotion Agency (FFG) and Bilfinger Industrietechnik Salzburg (Competence Headquarters, 849725).

## Compliance with ethical standards

**Conflict of interest** The authors declare no commercial or financial conflicts of interest.



## References

1. Ecker DM, Jones SD, Levine HL (2015) The therapeutic monoclonal antibody market. MAbs 7(1):9–14
2. Udpa N, Million RP (2016) Monoclonal antibody biosimilars. Nat Rev Drug Discov 15(1):13–14
3. Kunert R, Reinhart D (2016) Advances in recombinant antibody manufacturing. Appl Microbiol Biotechnol 100(8):3451–3461
4. Rathore S et al (2015) Fermentanomics: relating quality attributes of a monoclonal antibody to cell culture process variables and raw materials using multivariate data analysis. Biotechnol Prog 31(6):1586–1599
5. Beyer M, Schuster A Jungbauer, Lingg N (2018) Microheterogeneity of recombinant antibodies: analytics and functional impact. Biotechnol J 13(1):1–26
6. Goncalves J, Araujo F, Cutolo M, Fonseca E (2016) Biosimilar monoclonal antibodies: preclinical and clinical development aspects. Clin Exp Rheumatol 34(4):698–705
7. Sha S, Agarabi C, Brorson K, Lee DY, Yoon S (2016) *N*-glycosylation design and control of therapeutic monoclonal antibodies. Trends Biotechnol 34(10):835–846
8. Nidhi K, Indrajeet S, Khushboo M, Gauri K, Sen DJ (2011) Hydrotropy: a promising tool for solubility enhancement: a review. Int J Drug Dev Res 3(2):26–33
9. Liu et al (2014) In vitro and in vivo modifications of recombinant and human IgG antibodies. MAbs 6(5):1145–1154
10. Singh SK, Narula G, Rathore AS (2016) Should charge variants of monoclonal antibody therapeutics be considered critical quality attributes? Electrophoresis 37(17–18):2338–2346
11. Jefferis R (2016) Posttranslational modifications and the immunogenicity of biotherapeutics. J Immunol Res 2016:1–15
12. Quan C et al (2008) A study in glycation of a therapeutic recombinant humanized monoclonal antibody: where it is, how it got

there, and how it affects charge-based behavior. Anal Biochem 373(2):179–191
13. Du Y, Walsh A, Ehrick R, Xu W, May K, Liu H (2012) Chromatographic analysis of the acidic and basic species of recombinant monoclonal antibodies. MAbs 4(5):578–585
14. Hintersteiner B, Lingg N, Janzek E, Mutschlechner O, Loibner H, Jungbauer A (2016) Microheterogeneity of therapeutic monoclonal antibodies is governed by changes in the surface charge of the protein. Biotechnol J 11(12):1617–1627
15. Hintersteiner B et al (2016) Charge heterogeneity: basic antibody charge variants with increased binding to Fc receptors. MAbs 8(8):1548–1560
16. van den Bremer ETJ et al (2015) Human IgG is produced in a pro-form that requires clipping of C-terminal lysines for maximal complement activation. MAbs 7(4):672–680
17. Fekete S, Gassner AL, Rudaz S, Schappler J, Guillarme D (2013) Analytical strategies for the characterization of therapeutic monoclonal antibodies. Trends Anal Chem 42:74–83
18. Wang F, Peklansky B, Anderson C, Wang Y, Rustandi RR (2012) Improved ion-exchanged HPLC method in mab using ph gradient and its comparison with cIEF. J Liq Chromatogr Relat Technol 35(9):1259–1269
19. Fekete S, Beck A, Veuthey JL, Guillarme D (2015) Ion-exchange chromatography for the characterization of biopharmaceuticals. J Pharm Biomed Anal 113:43–55
20. Joshi V, Kumar V, Rathore AS (2015) Rapid analysis of charge variants of monoclonal antibodies using non-linear salt gradient in cation-exchange high performance liquid chromatography. J Chromatogr A 1406:175–185
21. Tebbey PW, Varga A, Naill M, Clewell J, Venema J (2015) Consistency of quality attributes for the glycosylated monoclonal antibody Humira® (adalimumab). MAbs 7(5):805–811
22. Wagner-Rousset E et al (2017) Development of a fast workflow to screen the charge variants of therapeutic antibodies. J Chromatogr A 1498:147–154
23. Farnan D, Moreno GT (2009) Multiproduct high-resolution monoclonal antibody charge variant separations by pH gradient ion-exchange chromatography. Anal Chem 81(21):8846–8857
24. Lingg N, Tan E, Hintersteiner B, Bardor M, Jungbauer A (2013) Highly linear pH gradients for analyzing monoclonal antibody charge heterogeneity in the alkaline range. J Chromatogr A 1319:65–71
25. Lingg N, Berndtsson M, Hintersteiner B, Schuster M, Bardor M, Jungbauer A (2014) Highly linear pH gradients for analyzing monoclonal antibody charge heterogeneity in the alkaline range: validation of the method parameters. J Chromatogr A 1373:124–130
26. Michels DA, Tu AW, McElroy W, Voehringer D, Salas-Solano O (2012) Charge heterogeneity of monoclonal antibodies by multiplexed imaged capillary isoelectric focusing immunoassay with chemiluminescence detection. Anal Chem 84(12):5380–5386
27. Van Beers MMC, Bardor M (2012) Minimizing immunogenicity of biopharmaceuticals by controlling critical quality attributes of proteins. Biotechnol J 7(12):1473–1484
28. Sommeregger W, Sissolak B, Kandra K, von Stosch M, Mayer M, Striedner G (2017) Quality by control: towards model predictive control of mammalian cell culture bioprocesses. Biotechnol J 12(7):1–7
29. Cohn EJ et al (1946) Preparation and properties of serum and plasma proteins. IV. A system for the separation into fractions of the protein and lipoprotein components of biological tissues and fluids. J Am Chem Soc 68(3):459–475
30. Bergmann-Leitner ES, Mease RM, Duncan EH, Khan F, Waitumbi J, Angov E (2008) Evaluation of immunoglobulin purification methods and their impact on quality and yield of antigen-specific antibodies. Malar J 7(1):129
31. Gagnon P, Nian R (2016) Conformational plasticity of IgG during protein A affinity chromatography. J Chromatogr A 1433:98–105
32. Zboray K et al (2015) Heterologous protein production using euchromatin-containing expression vectors in mammalian cells. Nucleic Acids Res 43(16):e102
33. Strober W (2001) Trypan blue exclusion test of cell viability. Curr Protoc Immunol Appendix 3B:1–2
34. Reinhart D, Damjanovic L, Kaisermayer C, Kunert R (2015) Benchmarking of commercially available CHO cell culture media for antibody production. Appl Microbiol Biotechnol 99(11):4645–4657
35. Zhang B, Mathewson S, Chen H (2009) Two-dimensional liquid chromatographic methods to examine phenylboronate interactions with recombinant antibodies. J Chromatogr A 1216:5676–5686
36. Gruber C, Altmann F (2015) Site-specific glycosylation profiling using liquid chromatography-tandem mass spectrometry (LC-MS). In: Castilho A (ed) Glyco-engineering. Humana Press, New York, pp 407–415
37. Loos C, Gruber F, Altmann U, Mehofer F, Hensel Grandits M (2014) Expression and glycoengineering of functionally active heteromultimeric IgM in plants. PNAS 111(17):6263–6268
38. Stadlmann J, Pabst M, Kolarich D, Kunert R, Altmann F (2008) Analysis of immunoglobulin glycosylation by LC-ESI-MS of glycopeptides and oligosaccharides. Proteomics 8(14):2858–2871
39. Jin M, Szapiel N, Zhang J, Hickey J, Ghose S (2010) Profiling of host cell proteins by two-dimensional difference gel electrophoresis (2D-DIGE): implications for downstream process development. Biotechnol Bioeng 105(2):306–316
40. Tcheliessnig L, Konrath J, Bates R, Jungbauer A (2013) Host cell protein analysis in therapeutic protein bioprocessing—methods and applications. Biotechnol J 8(June):655–670
41. Moore et al (1997) Effects of temperature shift on cell cycle, apoptosis and nucleotide pools in CHO cell batch cultues. Cytotechnology 23(1–3):47–54
42. Furukawa K, Ohsuye K (1999) Enhancement of productivity of recombinant alpha-amidating enzyme by low temperature culture. Cytotechnology 31(1–2):85–94
43. Yoon SK, Song JY, Lee GM (2003) Effect of low culture temperature on specific productivity, transcription level, and heterogeneity of erythropoietin in Chinese hamster ovary cells. Biotechnol Bioeng 82(3):289–298
44. Trummer E et al (2006) Process parameter shifting: Part I. Effect of DOT, pH, and temperature on the performance of Epo-Fc expressing CHO cells cultivated in controlled batch bioreactors. Biotechnol Bioeng 94(6):1033–1044
45. Kumar N, Gammell P, Clynes M (2007) Proliferation control strategies to improve productivity and survival during CHO based production culture: a summary of recent methods employed and the effects of proliferation control in product secreting CHO cell lines. Cytotechnology 53(1–3):33–46
46. Vergara M et al (2014) Differential effect of culture temperature and specific growth rate on CHO cell behavior in chemostat culture. PLoS One 9(4):1–6
47. Fan Y et al (2015) Amino acid and glucose metabolism in fed-batch CHO cell culture affects antibody production and glycosylation. Biotechnol Bioeng 112(3):521–535
48. Sellick et al (2011) Metabolite profiling of recombinant CHO cells: designing tailored feeding regimes that enhance recombinant antibody production. Biotechnol Bioeng 108(12):3025–3031
49. Chung S et al (2018) Industrial bioprocessing perspectives on managing therapeutic protein charge variant profiles. Biotechnol Bioeng 115(7):1646–1665
50. Bradley G, Yamauchi F (1996) Ostrich (*Struthio camelus*) Carboxy Pmifkdbn, kinetic properties am3 of the pancreatic enzyme. Science (80-.) 28(5):521–529

51. Zhang X et al (2015) Culture temperature modulates monoclonal antibody charge variation distribution in Chinese hamster ovary cell cultures. Biotechnol Lett 37(11):2151–2157
52. Schmelzer E, Miller WM (2002) Hyperosmotic stress and elevated $pCO_2$ alter monoclonal antibody charge distribution and monosaccharide content. Biotechnol Prog 18(2):346–353
53. Yuk H et al (2011) Controlling glycation of recombinant antibody in fed-batch cell cultures. Biotechnol Bioeng 108(11):2600–2610
54. An Y, Zhang Y, Mueller HM, Shameem M, Chen X (2014) A new tool for monoclonal antibody analysis application of IdeS proteolysis in IgG domain-specific characterization. MAbs 6(4):879–893
55. Tang H et al (2018) Insights into the generation of monoclonal antibody acidic charge variants during Chinese hamster ovary cell cultures. Appl Microbiol Biotechnol 102(3):1203–1214
56. Lee S, Krishnanchettiar S, Lateef SS, Gupta S (2007) Analyses of the in vitro non-enzymatic glycation of peptides/proteins by matrix-assisted laser desorption/ionization mass spectrometry. Int J Mass Spectrom 260(1):67–74
57. Berning WK, Quan C, Zhang YT (2017) Glycation of antibodies: Modification, methods and potential effects on biological functions. MAbs 9(4):586–594
58. Ponniah G, Nowak C, Neill A, Liu H (2017) Characterization of charge variants of a monoclonal antibody using weak anion exchange chromatography at subunit levels. Anal Biochem 520:49–57

Received: 18 April 2019 | Revised: 28 May 2019 | Accepted: 6 June 2019

DOI: 10.1002/btpr.2864

RESEARCH ARTICLE

BIOTECHNOLOGY PROGRESS

# Lectin bio-layer interferometry for assessing product quality of Fc- glycosylated immunoglobulin G

Jakob Wallner[1] | Bernhard Sissolak[2] | Wolfgang Sommeregger[2] | Nico Lingg[1] | Gerald Striedner[1] | Karola Vorauer-Uhl[1]

[1]Department of Biotechnology, University of Natural Resources and Life Sciences, Vienna, Austria

[2]Research and Development, Bilfinger Industrietechnik Salzburg GmbH, Salzburg, Austria

**Correspondence**
Jakob Wallner, Department of Biotechnology, University of Natural Resources and Life Sciences, Muthgasse 11, A-1190 Vienna, Austria.
Email: jakob.wallner@boku.ac.at

**Funding information**
Österreichische Forschungsförderungsgesellschaft, Grant/Award Number: 849725

## Abstract

Glycosylation, as the most prominent posttranslational modification, is recognized as an important quality attribute of monoclonal antibodies affected by various bioprocess parameters and cellular physiology. A method of lectin-based bio-layer interferometry (LBLI) to relatively rank galactosylation and fucosylation levels was developed. For this purpose, Fc-glycosylated immunoglobulin G (IgG) was recombinantly produced with varying bioprocess conditions in 15 L bioreactor and accumulated IgG was harvested. The reliability, the robustness and the applicability of LBLI to different samples has been proven. Data obtained from LC–MS analysis served as reference and were compared to the LBLI results. The introduced method is based on non-fluidic bio-layer interferometry (BLI), which becomes recently a standard tool for determining biomolecular interactions in a label-free, real-time and high-throughput manner. For the intended purpose, biotinylated lectins were immobilized on disposable optical fiber streptavidin (SA) biosensor tips. *Aleuria aurantia* lectin (AAL) was used to detect the core fucose and *Ricinus communis* agglutinin 120 (RCA120) to determine galactosylation levels. In our case study it could be shown that fucosylation was not affected by variations in glucose feed concentration and cultivation temperature. However, the galactosylation could be correlated with the ratio of mean specific productivity ($q_P$) and ammonium ($q_{NH4+}$) but was unrelated to the ratio of mean $q_P$ and the specific glucose consumption ($q_{gluc}$). This presented method strengthens the applicability of the BLI platform, which already enables measurement of several product related characteristics, such as product quantity as well as kinetic rates ($k_d$,$k_{on}$) and affinity constants ($k_D$) analysis.

**KEYWORDS**
bio-layer interferometry, CHO cell culture, fucosylation, galactosylation, glycosylation

## 1 | INTRODUCTION

Monoclonal antibodies (mAbs) continue to dominate biopharmaceutical approvals and constitute about 40% of biotherapeutics that are available on the market and thus form a major class of molecules produced and developed by the biopharmaceutical industry.[1] Product quality and quantity are important measures in antibody discovery and in process development. These requirements are driven by numerous influential factors such as process performance and cell physiology. The complexity of such a multifactorial system makes it

Jakob Wallner and Bernhard Sissolak contributed equally to this work.

difficult to identify the parameters with relevant influence on product quality. Thus, direct control of product quality in the individual bioprocess, a central goal of the quality by design approach, is severely limited.[2] Consequently, it is crucial to get a deeper understanding of the biological system, the process, the product and the interdependencies amongst each other.

In respect of product quality, the glycosylation is among others, a relevant characteristic, which can profoundly affect protein stability and the functions, which are relevant to their therapeutic application. Recently, the correlation between the glycoform profiles and the safety and efficacy of a drug, in particular, has achieved significant attention of researchers worldwide.[3] The glycan structure is affected by the enzymatic machinery of the host cell, transit time in the Golgi bodies, environmental factors and the availability within the sugar nucleotide pool.[4-6] With respect to process conditions, several publications have shown that the osmolality level (in combination with pH),[7] availability of glucose,[8,9] ammonium production rates[10] or dissolved CO2 level[7,11] can lead to alternations in glycosylation patterns. In order to study such mechanisms in more detail and to measure product quantity and relevant quality parameter, appropriate analytical assays are required.

Several techniques already exist to measure those quality specifications. The most commonly applied technique for the complete structural elucidation of glycoprotein oligosaccharides is the application of a combination of chemical, enzymatic, and chromatographic techniques combined with mass spectrometry.[12,13] Another promising approach is the application of lectin-binding assays.[14] Lectins are glycan-binding proteins that selectively recognize glycan epitopes of glycoproteins, which enables the specific monitoring of oligosaccharide structures. The interactions of lectins with glycan structures can be measured via the bio-layer interferometry (BLI), a well-established biosensor technology.[15] The BLI technology is performed in an open shaking micro-well plate format without any micro-fluidics and using disposable optical fiber biosensors. The physical principle of this technique is based on the correlation of the spectral shift $\Delta\lambda$ with a change in thickness (nm) on the biosensor surface. The platform also allows the measurement of biomolecular interactions, enabling full kinetic measurements and facilitates the quantitation of biomolecules.[16] Accordingly, several product quality characteristics and the product quantity can be determined on a single platform.

A recent study showed the applicability of the BLI platform as a high-throughput technique for determining the sialylation of mAbs.[17] This was done by measuring the binding rate of *Maackia amurensis* lectin II (MALII) to (a-2,3)-linked sialic acids of highly sialylated proteins bound in a native state to Protein A sensors. However, all oligosaccharides, except (a-2,3)-linked sialic acids are normally hidden located within the folded structure of immunoglobulin G (IgG) and are not accessible to related lectins. This induces the necessity for reduction of the disulfide bonds, which lead to the opening of the tertiary and quaternary protein structure of IgG, and enables lectins to bind to oligosaccharides attached in the Fc component.[18,19] In the present

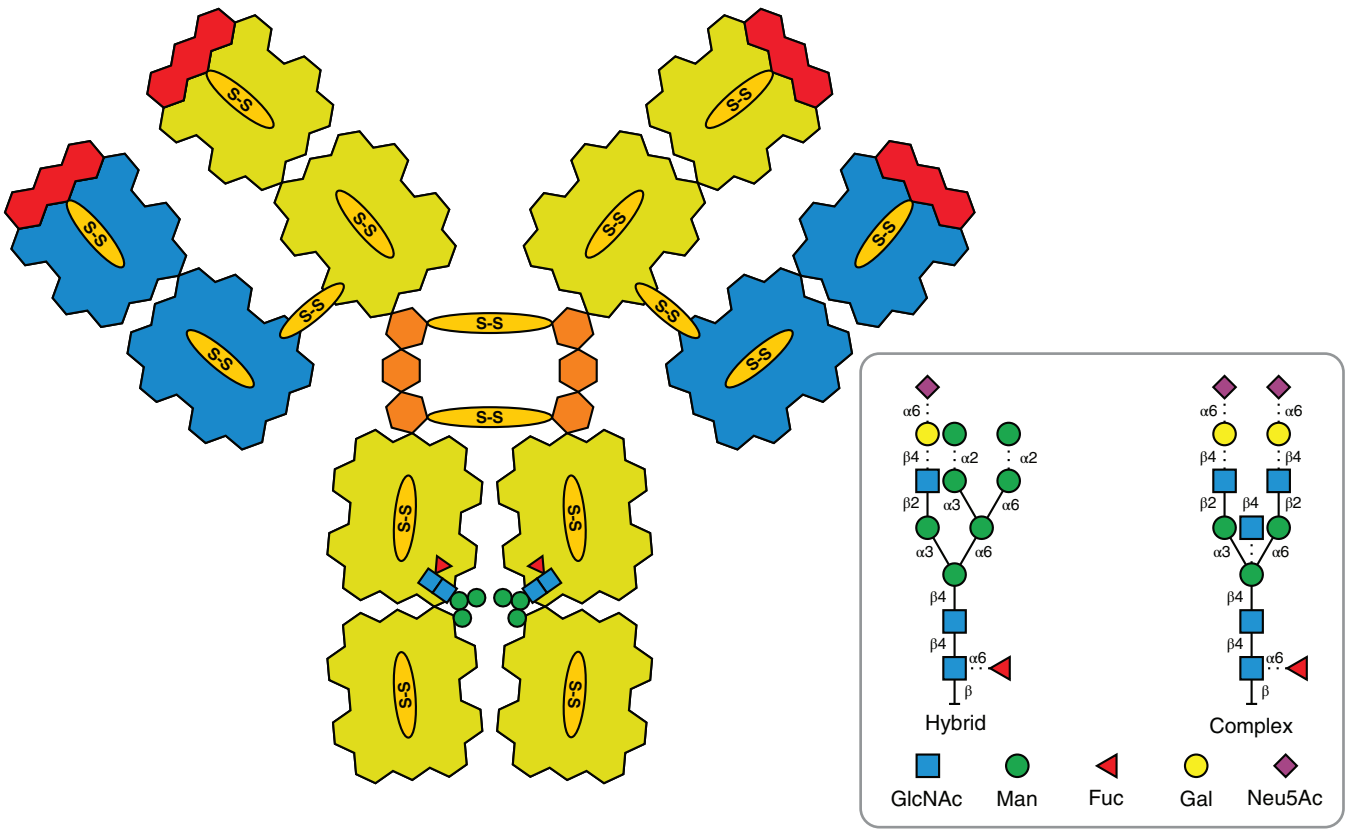


**FIGURE 1** IgG antibody and N-glycan structures. Schematic representation of a glycoprotein IgG (mAbs contains only Fc glycosylation). The disulfide bonds stabilizing the tertiary and quaternary protein structure are also shown

study a non-sialylated antitumor necrosis factor (anti-TNF-α) IgG1 (Figure 1) recombinantly produced in Chinese hamster ovary (CHO) cells in a 15 L pilot scale fed-batch process under varying conditions was used as a model protein. For this study the mAB was purified from the harvest of 13 fed batch cultivation runs t with variations in feed media glucose concentration and cultivation temperature.

*Ricinus communis* agglutinin 120 (RCA120) and *Aleuria aurantia* lectin (AAL) were used to determine the terminal galactose and core fucose content of the pre-purified IgG.[14] The resulting galactosylation and fucosylation levels were compared with results obtained by the well-established analysis technique using MS detection.[20] Since the harvest samples represent the accumulated product of the entire bioprocess, the glycosylation was further related to the overall process performance. To the best of our knowledge this study presents for the first time application of the BLI platform to determine the galactosylation and fucosylation levels of CHO culture samples.

## 2 | MATERIAL AND METHODS

### 2.1 | Bioprocess set up

As a model protein Fc-glycosylated anti-TNF-α IgG1 was used, produced by a recombinant monoclonal CHO cell line (Antibody Lab GmbH, Austria). Generation of the cell line was conducted by applying the Rosa26 bacterial artificial chromosome (BAC) expression strategy to a serum-free adapted host cell line derived from CHO-K1 (ATCC CCL-61).[21]

A vial of the working cell bank ($5 \times 10^6$ cells) was thawed in a chemically defined culture medium (Dynamis AGT, A26175, Thermo Fisher Scientific) supplemented with 8 mM L-glutamine (25030081, Sigma Aldrich, Germany), 3 mL/L phenol red solution (RNBD642, Sigma Aldrich, Germany), 1:1000 Anti Clumping Agent (0010057DG, Thermo Fisher Scientific) and 1 mg/mL G418 (G8168, Sigma Aldrich, Germany).

Every three to 4 days the cells were passaged with the aforementioned media but without anti-clumping agent and G418. Cultivation was performed in a humidified incubator (HeracellTM VIOs 160i, Thermo Scientific) at 37°C, 5% vol/vol $CO_2$ and 200 rpm (MaxQ 2000 $CO_2$ Plus, Thermo Scientific).

With the fourth passage the cells were transferred into the 15 L bioreactor (LabQube, Bilfinger Industrietechnik GmbH, Austria) with a seeding concentration of $2.5 \times 10^5$ cells/mL and a starting volume of 10 L. The batch phase was kept identical for every experiment. The experimental setup included the variation of temperature, at 31, 34, and 37°C, in addition to variation in the amount of glucose (G7021, Sigma Aldrich, Germany), with the addition of 10, 20, or 30 g/L of glucose, and aspartate concentration with additions of 0 or 7 g/L aspartate, in the feed phase (CHO CD EfficientFeed A, A1442001, Thermo Fisher Scientific). Additionally, the feed medium was also supplemented with 0.1% antifoam (A8011, Sigma Aldrich, Germany) to maintain a constant antifoam concentration during the process. A constant feed rate of 418 g/d was used during the feed-phase.

The process was controlled via process air mass flow (PA) and stirrer speed to maintain the dissolved oxygen level (DO) above 30% and $CO_2$ mass flow to keep the pH constant at 7.0. The total gas-flow range was kept within 0.01–0.1 vvm.

The experimental setup used is displayed in Table 1.

**TABLE 1** Experimental design of the fed-batch processes

| Run number | Shift 1 | Shift 2 | Shift 3 | Shift 4 |
|---|---|---|---|---|
| 1 | 36.3°C/F3 (72 hr) | | | |
| 2 | 36.3°C/F3 (72 hr) | | | |
| 3 | 37°C/F3 (72 hr) | 37°C/F1 (192 hr) | | |
| 4 | 34°C/F1 (72 hr) | | | |
| 5 | 34°C/F2 (72 hr) | | | |
| 6 | 34°C/F2 (72 hr) | | | |
| 7 | 34°C/F2 (72 hr) | | | |
| 8 | 34°C/F2 (72 hr) | | | |
| 9 | 34°C/F2 (72 hr) | 37°C/F2 (120 hr) | 34°C/F1 (192 hr) | 31°C/F1 (240 hr) |
| 10 | 31°C/F2 (72 hr) | 34°C/F2 (120 hr) | 37°C/F3 (192 hr) | 34°C/F3 (240 hr) |
| 11 | 34°C/F1 (72 hr)r | 31°C/F1 (120 hr) | 31°C/F2 (192 hr) | 34°C/F2 (240 hr) |
| 12 | 37°C/F2 (72 hr) | 34°C/F3 (120 hr) | 31°C/F2 (192 hr) | 34°C/F1 (240 hr) |
| 13 | 34°C/F3 (72 hr) | 37°C/F2 (120 hr) | 31°C/F2 (192 hr) | 37°C/F3 (240 hr) |

*Note:* Experiments are presented by the time point (hours [hr]), type of shift, temperature or feed change. F1, F2, and F3 represent the additional glucose concentration in the feed, consisting of 10, 20, and 30 g/L, respectively.

### 2.2 | Off-line analyses

The total cell concentration (TCC) was determined by counting the cell nuclei using a Z2 particle counter (Beckman Coulter). Therefore, an appropriate amount of cell suspension was centrifuged at 180g for 10 min. The cell pellet was subsequently resuspended in a 0.1 M citric acid monohydrate and 2% (vol/vol) Triton X-100 buffer to lyse the cells for a minimum of 1 hr before measurement. Sample dilution was performed using a 0.9% NaCl solution.

Culture viability was assessed using a haemocytometer and trypan blue exclusion. The viable cell concentration (VCC) was determined by multiplying viability with the TCC.

Glucose was determined via ion exclusion chromatography (HPX 87H, 300 × 7.8 mm, #1250140, BioRad) using an Agilent 1,200 series (Agilent) at 25°C. The mobile phase consisted of 5 mM sulphuric acid

and the flowrate was set to 0.45 mL/min and measured via a Refractive Index Detector (35°C). The calibration range for D(+)-glucose was 100–2000 mg/L. The chromatograms were evaluated using Chemstation software (revision B.04.01, Agilent).

Ammonium was measured via an ion selective electrode (ISE, GZ-27512-00, Cole-Parmer). Therefore, the cell suspension was centrifuged at 180 rpm for 10 min and two times 3 mL of the supernatant were stored at −20°C. Before each measurement the ISE was filled with the reference solution (0.1 M $NH_4Cl$, GZ-27503-71, Cole Palmer) and calibrated (from 1 to 100 mM, GZ-27503-00, Cole Palmer). The 60 µL of 10 M sodium hydroxide solution (221,465, Merck, Germany) were added to each sample and the solution was vortexed, shortly before measurement.

Osmolality was measured by using a freezing point osmometer (Osmomat 030-D, Gonotec, Germany). Thawed samples of the cell broth supernatant were measured in duplicates.

The product titre was determined by BLI using Protein A tips (Octet System, QK, ForteBio).[22]

## 2.3 | Lectin assay

### 2.3.1 | Immunoglobulin G purification

The mAb was purified from clarified supernatants using Protein A affinity chromatography. The experiments were performed on an Äkta Pure system (GE Healthcare). A POROS A 20, 2.1 × 30 mm column was used for the stationary phase (Thermo Scientific). The column was equilibrated with phosphate buffered saline (PBS), pH 7.4 for 25 column volumes (CV). The column was loaded with 2 mL clarified supernatant at a residence time of 0.1 min (except for sample ID 160714 and 180,202 where only 1.5 mL was available). After sample application the column was washed with PBS for 20 CV. The mAb was eluted with 100 mM glycine pH 3.0 in a 10 CV step gradient elution and the collected fractions were immediately neutralized with 1 M Tris HCl pH 8.0. The column was cleaned with 6 M guanidine HCl, 50 mM Tris, pH 8.0 solution for two CV and immediately re-equilibrated with PBS. The outlet was monitored by measuring UV absorbance at 280 nm to detect eluting antibody. Due to tailing of the elution, only the main portion of the peak was collected, resulting in a loss of ~5% in the tail.

### 2.3.2 | Reduction of disulphide bonds

Purified IgG was diluted with PBS to a concentration of 100 µg/mL (± 5 µg/mL), as determined by absorbance at 280 nm, using ε 1.43.[23] Nine volumes of the diluted IgG sample were mixed with one volume of 2-mercaptoethanol (1 M in PBS) Sigma (Vienna, Austria) and incubated for 2 hr at 37°C. To block thiol-groups, one volume of 0.2 M iodoacetamide Sigma (Vienna, Austria) was added to the reduced sample (final concentration 0.1 M). Incubation was performed overnight, in the dark and at room temperature.[19]

### 2.3.3 | Bio-layer interferometry for analysis of galactose and fucose content on IgG

Octet Red96e (ForteBio, Menlo Park, CA) was used for lectin/carbohydrate binding studies. Typical assay performance is shown in Figure 2a. Samples were diluted in black 96-well plates (Nunc F96 MicroWellTMPlates, ThermoFisher Scientific, Langenselbold, Germany). Puffer (Sample diluent) contained PBS, 0,005% P20, Sigma (Vienna, Austria) and 0.1 mg/mL BSA. The total working volume for each step was 210 µL per well and the rpm setting for each baseline, loading, and association was 1,000 rpm. The test was performed at 25°C. Prior to each assay, streptavidin (SA) biosensor tips (ForteBio, Menlo Park, CA) were pre-wetted in 210 µL sample diluent for at least 10 min followed by equilibration with sample diluent for 60 s. Afterward, SA biosensor tips were non-covalently loaded with biotinylated *Ricinus communis* agglutinin I (RCA I) or biotinylated AAL, both obtained from Vector Labs, UK, in a sample diluent concentration of 0.83 µg/ for 120 s, followed by an additional equilibration step (60 s) with sample diluent. Prior to analysis, reduced samples were diluted three times in sample diluent, yielding an IgG concentration of 15 µg/mL (± 5 µg/mL). Association was carried out for 600 s. All measurements were performed in triplicate. Raw data,

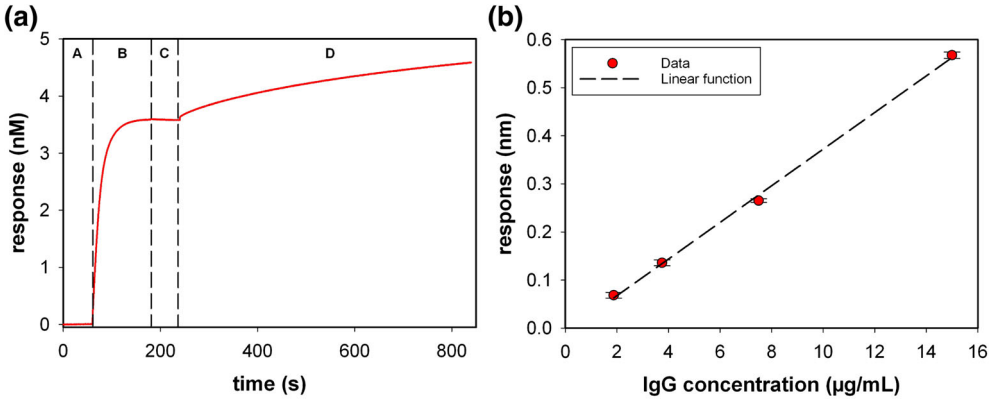


**FIGURE 2** (a) Sensorgram of a typical test performance, including baseline steps (A, C), lectin loading (B) and association of reduced immunoglobulin G (D). (b) Dose–response curve of IgG by serial dilution of one reduced sample (run 12), diluted to 15, 7.5, 3.75, and 1.875 µg/mL in sample diluent. RCA120 lectin was immobilized on streptavidin sensor tips prior IgG association. The linear signal curve resulted in an equation of y = 0.0381 × −0.0084 and in a correlation coefficient of 0.9986

obtained with the Octet Software (Version 11.0, Menlo Park, CA) were exported to Excel spreadsheets (Version 2003, Microsoft, Redmond, WA). Raw data of the IgG association response were aligned to the individual association step. The individual specific response R at a defined time t (Rt) for each concentration was calculated as an average of three independent measurements. The reproducibility of (Rt) was determined with $n = 8$. The responses at 600 s (Rt) of the harvest 13 fed-batch experiments were compared with the outcomes of mass spectrometry measurements, using linear regression analysis. The computations were performed using Mathematica (Version 11.3 of 2018, Wolfram Research Inc., Urbana-Champaign, IL). The statistical analysis was based on 95% significance. The quantitation limit (LOQ) for IgG association was assumed by measuring the minimum concentration at which the analyte can be reliably quantified. A typical signal-to-noise ratio is 10:1. The baseline noise was determined during the initial 60 s PBS buffer step ($n = 8$).

### 2.3.4 | Monosaccharide analysis performed with mass spectrometry

The samples were digested in gel. The proteins were S-alkylated with iodoacetamide and digested with trypsin (Promega). The digested samples were loaded on a BioBasic C18 column (BioBasic-18, 150 × 0.32 mm, 5 μm, Thermo Scientific) using 65 mM ammonium formiate buffer as the aqueous solvent. A gradient from 5% B (B: 100% ACCN) to 32% B in 35 min was applied, followed by a 15-min gradient from 32 to 75% B that facilitates the elution of large peptides, at a flow rate of 6 μL/min. Detection was performed with QTOF MS (Bruker maXis 4G) equipped with the standard ESI source in positive ion, DDA mode (i.e., switching to MSMS mode for eluting peaks). MS-scans were recorded (range: 150–2,200 Da) and the three highest peaks were selected for fragmentation. Instrument calibration was performed using ESI calibration mixture (Agilent). Manual glycopeptide searches were made using DataAnalysis 4.0 (Bruker). For the quantification of the different glycoforms the peak areas of the extracted ion chromatograms (EICs) of the first four isotopic peaks were summed, using the quantification software Quant Analysis (Bruker). Note that MS of glycopetides only allows identifying the composition of the glycan and as a consequence only one possible isomer is annotated.[20,24]

## 3 | RESULTS AND DISCUSSION

### 3.1 | Development of an appropriate bio-layer interferometry method for the determination of galactose and fucose

Selected IgG samples of defined bioprocesses were purified using Protein A affinity chromatography to remove potential inferring host cell proteins. For this approach, in principle also other procedures (e.g., immunoprecipitation, etc.) could be applied as long as the glycosylation of IgGs is not affected. After the purification procedure, IgG was diluted to a concentration of 100 μg/mL determined by absorbance at 280 nm. In a first step lectin binding to non-reduced IgG was tested. As expected, binding of non-reduced IgG to the immobilized lectins could not be achieved (see Figure S1). These results are in excellent agreement with published data and provide additional evidence that reduction of IgG is a prerequisite to obtain freely accessible carbohydrate structures attached to the Fc part of the IgG.[18,19,25] Consequently, IgG was reduced with β-mercaptoethanol followed by carboxymethylation of cysteines with iodoacetamide to avoid reformation of the disulphide linkages.[26] For the BLI assay, the lectin and the IgG concentration was adjusted to gain an optimized test performance as described in the materials and methods section. Finally, SA biosensor tips were captured to saturation with biotinylated lectins (data not shown). An additional equilibration step with buffer was applied to remove the excess of biotinylated lectins and to obtain a constant loading baseline. The equilibration time was 60 s to achieve a sufficient baseline signal. Moreover, the lectin-coated SA biosensor tips were incubated with the purified, reduced IgG to measure the corresponding association profiles. In preliminary experiments, different IgG concentrations were tested and finally optimized. After reduction the samples contained 0.1 M β-mercaptoethanol and 0.1 M iodoacidamid. During the test optimization it became evident that these concentrations are already too high to accurately associate the IgG to the lectins. A simple threefold dilution step with sample diluent was sufficient to obtain reliable signals. Nonspecific interactions of the reduced IgG with the biosensor were eliminated by introducing 0.005% P20 and 0.1 mg/mL BSA to the sample diluent. No unspecific interaction of samples with uncoated SA biosensor tips occurred, which confirms the selectivity of the procedure. Finally, a standardized IgG concentration of 15 μg/mL was used. Dose–response linearity was demonstrated with a serial dilution experiment (Figure 2b). Therefore, one sample (No 12) was diluted to 15, 7.5, 3.75, and 1.875 μg/mL in sample diluent, attached to the pre-coated AAL lectin sensor and measured. A linear signal curve resulted in a correlation coefficient of 0.9986. The coefficient of variation for triplicate determinations of each concentration was <10%. The assay sequence begins with the equilibration of the SA biosensor tips with the PBS buffer in order to measure the baseline signal for calculation of the LOQ, which is defined as the lowest concentration at which the analyte can not only be reliably detected but at which some predefined goals for bias and imprecision are met. To obtain LOQ datasets for the evaluation of significant/reliable measurements, the average baseline noise of SA biosensor tips in PBS was determined and the LOQ assumed to be a signal-to-noise ratio of 10:1.[27] The baseline noise of the initial 60 s was 0.004 nm ($n = 8$). Thus, the LOQ was calculated as 0.04 nm. From the dose–response linearity measurements, as explained above, it was found that the mean $R_t$ of the lowest used IgG concentrations (1.875 μg/mL) toward the pre-coated RCA120 lectin sensor was 0.068. Prior reduction IgG was diluted to a concentration of 100 μg/mL. However, dose–response linearity experiments and estimation of LOQ demonstrate that significant lower initial IgG concentration can be applied. For both, galactose and fucose, it could be demonstrated that the lectin-BLI (LBLI) is a promising tool when the accessibility of the protected sugar moieties can be achieved.

### 3.2 | Determination of fucosylation of IgG in different mammalian cell culture processes

In a next step the LBLI method was compared to a widely used standard approach for determining glycan structures. Therefore, the selected 13 harvest samples were purified and glycosylation levels were measured via LC–MS and the LBLI method as described above (data is shown in Table S1). In general, the fucosylated forms of the harvest product were constant within the experimental setup. With both methods a similar fucosylation level (Figure 3a) was determined. The level range was found to be 82.3 ± 1.2% with respect to the LC–MS analysis. The new established LBLI method obtained a mean value of $R_T$ 1.11 ± 0.09 nm. A regression analysis in order to compare both methods was not feasible due to the constant output.

### 3.3 | Determination of galactosylation of immunoglobulin G in different mammalian cell culture processes

Significant variations were observed for the galactosylation of the mAb. They ranged from approximately 16.5–33.1% calculated by LC–MS and 0.24–0.70 nm RT for the LBLI analysis (Table S1 and Figure 3b). A linear relationship between the LC–MS and the LBLI responses was observed. Specifically, a function of r = a + b*p with a = −0.277 nm (confidence limits: −0.428–0.126) and a significantly positive parameter b = 0.031 nm (confidence limits: 0.023–0.038) was obtained. Hence, higher LBLI-responses corresponded to higher proportions of galactosylation (Figure 3b). It follows that with the LBLI tool the galactosylation levels can be successfully measured and data obtained from LC–MS analysis were equal compared to the LBLI results.

### 3.4 | Process parameters affecting glycosylation

The product is continuously secreted into the supernatant. The finally determined glycosylation pattern, represents the accumulated profile from the entire production process. Connecting the overall process performance with the glycosylation can already provide an appropriate picture about certain impacts. However, for a comprehensive understanding of the impact of process and cellular dynamics on glycosylation, straightforward techniques that enable the analysis of samples throughout the process, will be beneficial.

Since, fucosylation levels stayed constant in all samples of the test case we merely focused on the evaluation of the galactosylation. According to recent studies[10,28-30] glucose and ammonium can be environmental key factors in context of mAb galactosylation.

Since the IgG is accumulated during the process in the supernatant, the average production ($NH4^+$) and consumption (glucose) rate for the entire process should, presupposed that there is an impact, may reflect the overall variance of the glycosylation pattern. The rates $\bar{q}_n$ were calculated according to Equation (1). However, in the experimental runs different product titres were achieved, which means that different amounts of protein were available and susceptible to post-translational modification. Accordingly, the rates $\bar{q}_{NH4^+}$ and $\bar{q}_{gluc}$ were set into a relationship with the specific protein production rate $\bar{q}_p$, which was also calculated according to Equation (1).

$$\bar{q}_n = \frac{\sum_{t_0}^{t_{harvest}} n_{t+1} - n_t + n_{feed}}{\sum_{t_0}^{t_{harvest}} \frac{X_{v,t+1} - X_{v,t}}{\mu_t}}, \quad (1)$$

*n* represents the glucose, ammonium or mAb, respectively, $X_v$ the amount of viable cells and μ the growth rate to a given time point. The variable $n_{feed}$ represents the amount of substrate feed into the system. Hence, for mAb and ammonium this term becomes zero.

The results obtained from different experimental setups indicate that the average specific glucose uptake rate does not correlate with the galactosylation content (Figure 4a). This finding may be attributed to the fact that glucose concentrations were never limiting throughout the processes. Reduced glucose level can negatively influence the galactosylation index due to a reduced availability of uridindiphsophate

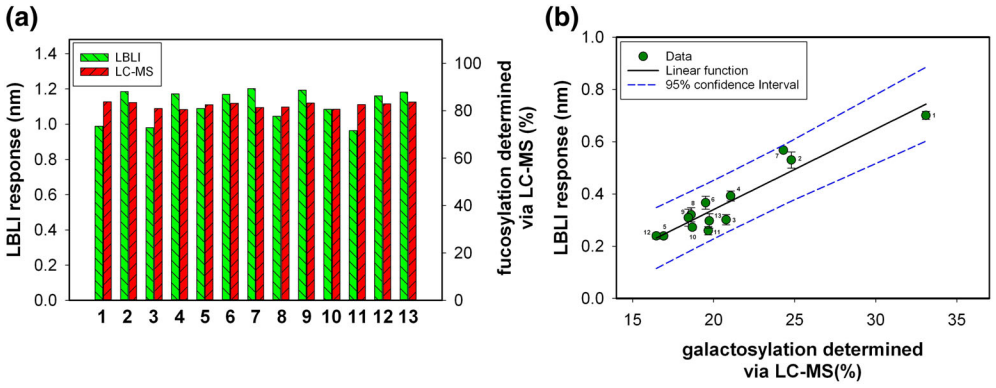


**FIGURE 3** (a) The proportion of fucosylated glycoforms determined via LC–MS and the responses of the lectin based BLI (LBLI) assay in nm depicted for all runs. (b) Linear regression analysis of all 13 CHO cell culture fed batch runs performed in 15 L pilot scale. The responses in [nm] of LBLI assay were compared with obtained galactosylated glycoforms in (%) of LC–MS measurements. Dots and error bars represent the mean Rt values and standard deviation of LBLI triplicate measurements, and the corresponding results from a single LC–MS run (without *SD*). The regression line and its single confidence band (dashed line) are plotted. The linear regression line resulted in the equation of y = 0.0309 × −0.277 and a correlation coefficient of 0.8925

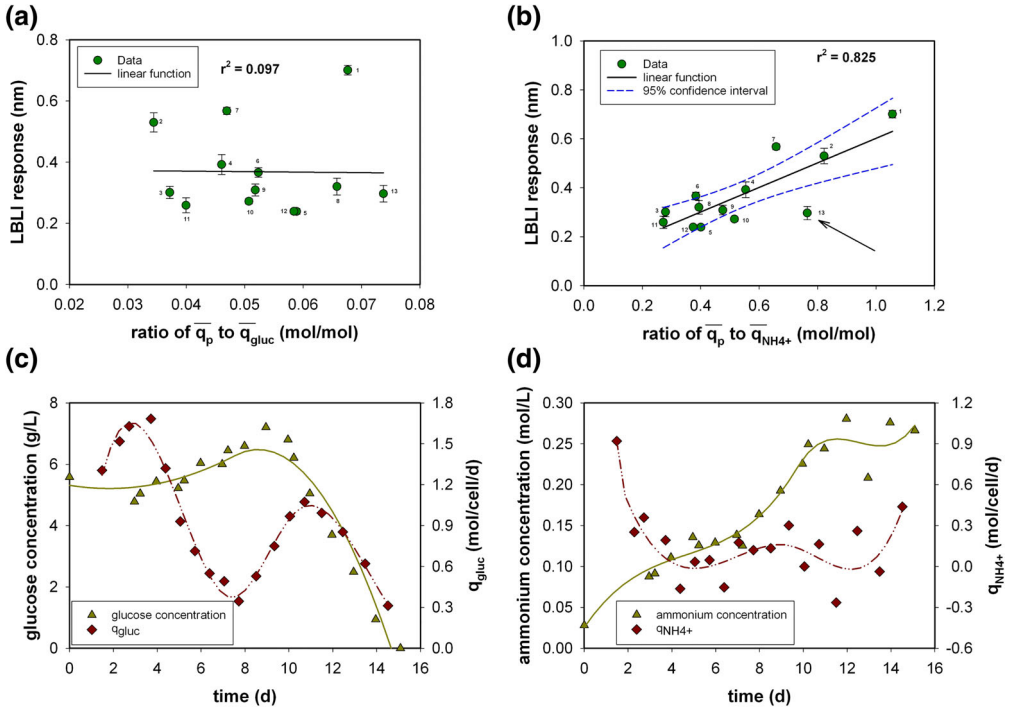


**FIGURE 4** The impact of the ratios $q_P$ to $q_{gluc}$ (a) and to $q_{NH4+}$ (b) on the LBLI response or respectively the galactosylation proportion of the mAb. The regression lines and coefficients are depicted. (b) Regression line depicted was performed without the outlier. The arrow indicates the outlier. The confidence band (dashed line) are plotted. Example trends of process run 12 for (c) glucose concentration and the respective specific rate and (d) ammonium concentration and the respective specific rate

(UDP) sugars and decrease the galactosylation index.[8,9] This observation points to the fact that other additional factors might influence the galactosylation.

In this respect, the ratio of mean $q_p$ to $q_{NH4+}$ was calculated (Figure 4b). A linear relationship with the galactosylation levels of the mAb could be determined. The less ammonium per mAb produced, the more galactosylation occured. A regression analysis performed with all runs resulted in the equation of $y = 0.502 \times x + 0.100$ with a regression coefficient of 0.660. In conclusion our results indicate that the ammonium production impacts the galactosylation profile. This finding is in agreement with the already known fact that high ammonium concentrations can increase the internal pH of the Golgi bodies and subsequently promote the inhibition of the enzymes required for the oligosaccharide processing. Galactosylation and sialylation of mAbs are mainly influenced by this regulation.[3,29] This result suggests that the production of ammonium per product is a crucial parameter.

In this study we assumed that the rates were constant for an entire process run. Due to this simplification certain dynamics and correlations might be undetectable. For instance, the availability of glucose, due to glucose depletion or a low glucose uptake rate, might have had an influence on the galactosylation level (Figure 4c). It also remains unclear if the ammonium production rate or the ammonium concentration in the supernatant was the real cause for the determined glycosylation pattern (Figure 4d). A clear understanding of the dynamics can only be achieved if the whole process progression is taken into consideration. In principle the presented LBLI method is capable of high throughput analysis. In this respect, the protein purification step still remains a bottleneck for this analysis. Therefore, future research will focus on different high throughput (HT) protein purification procedures to reduce the work load and to be capable to identify such process dynamics.

## 4 | CONCLUSION

The glycosylation is a relevant key quality attribute for monoclonal antibodies. It can be affected by many different factors, such as the expression system, process conditions, or media composition and feed protocols and thereof vary from batch to batch.[3] In this study we showed that the developed LBLI method, verified with data resulted from LC–MS, is feasible to determine the Fc fucosylation and galactosylation of an anti-TNF alpha antibody. Samples containing mAbs with varying glycosylation profiles were used to show the method applicability. By both applied analytical techniques it could be shown that fucosylation remained constant within the experimental design, while galactose varied. Based on the monitored glucose and ammonium levels it could deduce that a low ratio of $q_p$ to $q_{NH4+}$ resulted finally in a reduced galactosylation level in harvest samples. To gain more insight into the very complex process dynamics individual, additional in-process measurements and intra-cellular analysis would be necessary.

The application of HTX-BLI-based instruments in the 32-channel mode and 384 well plates enables 32 individual glycoanalytic measurements to be performed in less than 15 min. Antibodies either captured by Protein A or complementary methods prior reduction under standardized conditions, allows the identification of protected glycan structures within the protein in an efficient manner. This is a huge advantage compared to conventional techniques, where determination of glycosylation patterns are still accompanied with a high

workload, expenditures costs and usually requires an advantage expertise.[31] For the future, the LBLI method and the in general the BLI platform offer a simple and inexpensive high throughput (HT) technique for the analysis of several important product related parameters such as the product titer, the antibody antigen binding kinetics and the glycosylation pattern. Although, in research very often different techniques and equipment are used, in R&D and production the use of only one machinery is definitely advantageous to fulfill all the regulatory needs and the future goals of automatization. The presented technique will accelerate cell line, media and process development but also will be important as a process monitoring tool. To transfer the proposed platform to industrial application, automatization of protein capture need to be established to overcome this bottle neck for future analysis. Currently, different HT purification systems are under examination with the aim to complete the proposed platform.

## ACKNOWLEDGMENTS

We would like to acknowledge the entire PatPlant research group for their effort in conducting those experiments. We also thank the Austrian Research promotion Agency (FFG) and Bilfinger Industrietechnik Salzburg (Competence Headquarters, 849725) for their support. Furthermore, we thank Assoc. Prof. Kühleitner and Assoc. Prof. Brunner (Institute of Mathematics, University of Natural Resources and Life Sciences) for helpful discussions. The BLI equipment was kindly provided by the EQ-BOKU VIBT GmbH and the BOKU Core Facility for Biomolecular and Cellular Analysis.

## CONFLICT OF INTEREST

The authors declare no commercial or financial conflict of interest.

## ORCID

*Bernhard Sissolak* https://orcid.org/0000-0002-5267-5005

## REFERENCES

1. Xu X, Nagarajan H, Lewis NE, et al. The genomic sequence of the Chinese hamster ovary (CHO)-K1 cell line. *Nat Biotechnol*. 2011;29(8):735-741. https://doi.org/10.1038/nbt.1932.
2. Sommeregger W, Sissolak B, Kandra K, von Stosch M, Mayer M, Striedner G. Quality by control: towards model predictive control of mammalian cell culture bioprocesses. *Biotechnol J*. 2017;12:1600546. https://doi.org/10.1002/biot.201600546.
3. Batra J, Rathore AS. Glycosylation of monoclonal antibody products: current status and future prospects. *Biotechnol Prog*. 2016;32(5):1091-1102. https://doi.org/10.1002/btpr.2366.
4. Raju TS. Terminal sugars of fc glycans influence antibody effector functions of IgGs. *Curr Opin Immunol*. 2008;20:471-478. https://doi.org/10.1016/j.coi.2008.06.007.
5. Jefferis R. Glycosylation as a strategy to improve antibody-based therapeutics. *Nat Rev Drug Discov*. 2009;8:226-234. https://doi.org/10.1038/nrd2804.
6. Hossler P, Khattak SF, Li ZJ. Optimal and consistent protein glycosylation in mammalian cell culture. *Glycobiology*. 2009;19(9):936-949. https://doi.org/10.1093/glycob/cwp079.
7. Schmelzer AE, Miller WM. Hyperosmotic stress and elevated pCO2 alter monoclonal antibody charge distribution and monosaccharide content. *Biotechnol Prog*. 2002;18(2):346-353. https://doi.org/10.1021/bp010187d.
8. Liu B, Spearman M, Doering J, Lattová E, Perreault H, Butler M. The availability of glucose to CHO cells affects the intracellular lipid-linked oligosaccharide distribution, site occupancy and the N-glycosylation profile of a monoclonal antibody. *J Biotechnol*. 2014;170:17-27. https://doi.org/10.1016/j.jbiotec.2013.11.007.
9. Villacrés C, Tayi VS, Lattová E, Perreault H, Butler M. Low glucose depletes glycan precursors, reduces site occupancy and galactosylation of a monoclonal antibody in CHO cell culture. *Biotechnol J*. 2015;10(7):1051-1066. https://doi.org/10.1002/biot.201400662.
10. Chen P, Harcum SW. Effects of elevated ammonium on glycosylation gene expression in CHO cells. *Metab Eng*. 2006;8(2):123-132. https://doi.org/10.1016/j.ymben.2005.10.002.
11. Brunner M, Fricke J, Kroll P, Herwig C. Investigation of the interactions of critical scale-up parameters (pH, pO2and pCO2) on CHO batch performance and critical quality attributes. *Bioprocess Biosyst Eng*. 2017;40(2):251-263. https://doi.org/10.1007/s00449-016-1693-7.
12. Mariño K, Bones J, Kattla JJ, Rudd PM. A systematic approach to protein glycosylation analysis: a path through the maze. *Nat Chem Biol*. 2010;6(10):713-723. https://doi.org/10.1038/nchembio.437.
13. Beyer B, Schuster M, Jungbauer A, Lingg N. Microheterogeneity of recombinant antibodies: analytics and functional impact. *Biotechnol J*. 2018;13(1):1-26. https://doi.org/10.1002/biot.201700476.
14. Zhang L, Luo S, Zhang B. The use of lectin microarray for assessing glycosylation of therapeutic proteins. *MAbs*. 2016;8(3):524-535. https://doi.org/10.1080/19420862.2016.1149662.
15. Wallner J, Lhota G, Jeschek D, Mader A, Vorauer-uhl K. Journal of pharmaceutical and biomedical analysis application of bio-layer interferometry for the analysis of protein / liposome interactions. *J Pharm Biomed Anal*. 2013;72:150-154. https://doi.org/10.1016/j.jpba.2012.10.008.
16. Wallner J, Lhota G, Schosserer M, Vorauer-Uhl K. An approach for liposome immobilization using sterically stabilized micelles (SSMs) as a precursor for bio-layer interferometry-based interaction studies. *Colloids Surf B Biointerfaces*. 2017;154:186-194. https://doi.org/10.1016/j.colsurfb.2017.03.015.
17. Jonnalagadda KN, Markely LRA, Guan B, Alves C, Prajapati S. Analytical methods high-throughput sialylation measurement using lectins on an octet platform for clone screening. *Anal Methods*. 2016;8(18):7193-7198. https://doi.org/10.1039/C6AY01703G.
18. Dalziel M, McFarlane I, Axford JS. Lectin analysis of human immunoglobulin G N-glycan sialylation. *Glycoconj J*. 1999;16(12):801-807.
19. Liljeblad M, Lundblad A, Påhlsson P. Analysis of agalacto-IgG in rheumatoid arthritis using surface plasmon resonance. *Glycoconj J*. 2000;17(5):323-329.
20. Gruber C, Altmann F. Site-specific glycosylation profiling using liquid chromatography-tandem mass spectrometry (LC-MS). In: Castilho A, ed. *Glyco-engineering*. New York, NY: Humana Press; 2015:407-415. https://doi.org/10.1007/978-1-4939-2760-9_27.
21. Zboray K, Sommeregger W, Bogner E, et al. Heterologous protein production using euchromatin-containing expression vectors in mammalian cells. *Nucleic Acids Res*. 2015;43(16):e102. https://doi.org/10.1093/nar/gkv475.
22. Reinhart D, Damjanovic L, Kaisermayer C, Kunert R. Benchmarking of commercially available CHO cell culture media for antibody production. *Appl Microbiol Biotechnol*. 2015;99(11):4645-4657. https://doi.org/10.1007/s00253-015-6514-4.
23. Tan K. Current protocols in immunology. John E. Coligan, Ada M. Kruisbeek David H. Margulies, Ethan M. Shevach and Warrren

Strober (eds). John Wiley and Sons: new York US$240 (loose-leaf binder) (1991). *Cell Biochem Funct*. 1991;9(4):295-295. https://doi.org/10.1002/cbf.290090416.
24. Loos A, Gruber C, Altmann F, Mehofer U, Hensel F, Grandits M. Expression and glycoengineering of functionally active heteromultimeric IgM in. *Plan Theory*. 2014;21(7):6263-6268. https://doi.org/10.1073/pnas.1320544111.
25. Sumar N, Bodman KB, Rademacher TW, et al. Analysis of glycosylation changes in IgG using lectins. *J Immunol Methods*. 1990;131(1):127-136.
26. Aitken A, Learmonth M. Carboxymethylation of cysteine using Iodoacetamide/ Iodoacetic acid. *Protein protocols handbook, the*. New Jersey: Humana Press; 2002:455-456. https://doi.org/10.1385/1-59259-169-8:455.
27. Armbruster DA, Pry T. Limit of blank, limit of detection and limit of quantitation. *Clin Biochem Rev*. 2008;29 Suppl 1(Suppl 1):S49-S52.
28. Hong JK, Cho SM, Yoon SK. Substitution of glutamine by glutamate enhances production and galactosylation of recombinant IgG in Chinese hamster ovary cells. *Appl Microbiol Biotechnol*. 2010;88(4):869-876. https://doi.org/10.1007/s00253-010-2790-1.
29. Aghamohseni H, Ohadi K, Spearman M, et al. Effects of nutrient levels and average culture pH on the glycosylation pattern of camelid-humanized monoclonal antibody. *J Biotechnol*. 2014;186:98-109. https://doi.org/10.1016/j.jbiotec.2014.05.024.
30. Allen M, Millett P, Dawes E, Rushton N. Lactate dehydrogenase activity as a rapid and sensitive test for the quantification of cell numbers in vitro. *Clin Mater*. 1994;16(4):189-194. https://doi.org/10.1016/0267-6605(94)90116-3.
31. Huffman JE, Pučić-Baković M, Klarić L, et al. Comparative performance of four methods for high-throughput glycosylation analysis of immunoglobulin G in genetic and epidemiological research. *Mol Cell Proteomics*. 2014;13(6):1598-1610. https://doi.org/10.1074/mcp.m113.037465.

## SUPPORTING INFORMATION

Additional supporting information may be found online in the Supporting Information section at the end of this article.

**How to cite this article:** Wallner J, Sissolak B, Sommeregger W, Lingg N, Striedner G, Vorauer-Uhl K. Lectin bio-layer interferometry for assessing product quality of Fc-glycosylated immunoglobulin G. *Biotechnol Progress*. 2019;35:e2864. https://doi.org/10.1002/btpr.2864